The Effects of DJ-1 and A20 Family Members on Inflammation and Oxidative Response

Richard Sean McNally

A dissertation submitted to the faculty of the University of North Carolina at Chapel Hill in partial fulfillment of the requirements for the degree of Doctor of Philosophy in the Department of Microbiology and Immunology.

Chapel Hill

2010

Approved by:

Advisor: Dr. Jenny P.-Y. Ting, Ph.D.

Dr. Blossom Damania, Ph.D.

Dr. Nancy Raab-Traub, Ph.D.

Dr. Steven Bachenheimer, Ph.D.

Dr. Cam Patterson, M.D.

ABSTRACT

R. Sean McNally: The Effects of DJ-1 and A20 Family Members on Inflammation and Oxidative Response

(Under the direction of Jenny P.-Y. Ting)

Dysregulation of the balance between cell survival and cell death is seen in the loss of dopaminergic neurons in Parkinson's disease and the inappropriate cell survival in cancer. Changes in DJ-1 expression are associated with both Parkinson's disease and cancer suggesting an important role of DJ-1 in this balance. Our lab has reported that DJ-1 positively regulates the antioxidant response transcription factor Nrf2 protecting cells from ROS and toxic insults. Although this work revealed a mechanism for DJ-1's effect on cell survival, we could not find a direct role of DJ-1 as DJ-1 did not bind any proteins in the Nrf2 pathway. Using Q-TOF mass spectrometry, we found that BBS1, CLCF1, MTREF, and Cezanne interact with DJ-1. We focused our attention on the de-ubiquitinating enzyme Cezanne due to its known inhibition of the cancer-associated transcription factor NF-κB. We confirmed the interaction between DJ-1 and Cezanne and found that it inhibits Cezanne's de-ubiquitinating activity. Using shRNA against DJ-1 and Cezanne, we found that DJ-1 positively regulates NF-κB nuclear localization and promotes cell survival while Cezanne has reciprocal effects. Using microarray, we identified *IL-8* and *ICAM-1* as downstream targets of DJ-1 and Cezanne's effects on NF-κB. This finding was

confirmed at the RNA and protein levels using real-time PCR, ELISA, and immunoblot. Finally, we identified the presence of this pathway in a primary cell type. This work is the first to identify a link between DJ-1 and NF-κB representing a novel mechanism by which DJ-1 can control cell survival. During this research, we also identified a putative mechanism of crosstalk between the Nrf2 and NF-κB pathways as two well known inhibitors of these pathways, Keap1 and A20, were found to interact. Unfortunately, the consequences of the Keap1/A20 interaction have not been elucidated due to the complex interplay between the Nrf2 and NF-κB pathways. Taken as a whole, this work reports that DJ-1 is one of the few proteins or stimuli known to enhance cell survival through the activation of both Nrf2 and NF-κB while also identifying a novel mechanism of crosstalk between these pathways with implications in both Parkinson's disease and cancer.

DEDICATION

This dissertation is dedicated to my friends and family. My family has always pushed me to reach my potential – even against my will during those lazy high school years. My friends, scientists and non-scientists alike, remain a constant source of inspiration due to their hard work and their willingness to put up with me through thick and thin. Which, for those who know me, is no small feat.

ACKNOWLEDGEMENTS

I would like to acknowledge Dr. Jenny Ting for her guidance throughout my graduate education and for giving me an opportunity to work in her lab. Many people in the Ting lab have contributed to this work in one way or another including Dr. Willie June Brickey, who helped with microarray analysis, and Dr. Beckley Davis. Dr. Davis, as both a friend and supervisor, has contributed to this work through his scientific advice and seemingly infinite patience. Former members in the lab, specifically Dr. Casey Clements, laid the ground work and produced reagents that made this work possible. Thanks are also in order to Dr. Tak Mak and Dr. Averil Ma who provided mice, cell lines, and A20 reagents. I would also like to thank my committee members including Dr. Steven Bachenheimer, Dr. Blossom Damania, Dr. Nancy Raab-Traub, and Dr. Cam Patterson for their suggestions which have helped shape this work. Finally, I would like to acknowledge the Lineberger Comprehensive Cancer Center, the UNC University Cancer Research Fund, and the UNC Cancer Cell Biology Training Grant (5T32CA071341-15) for funding.

TABLE OF CONTENTS

Page

LIST OF TABLES

LIST OF FIGURES

LIST OF ABBREVIATIONS

ARE – Anti-oxidant response element

BBS1 - Bardet–Biedl syndrome 1

CBP - cAMP response element-binding protein

CLCF1 - Cardiotrophin-like cytokine factor 1

CXCR1 - CXC chemokine receptor 1

DJ-1 – Don Juan 1

DNA - Deoxyribonucleic acid

DTT – Dithiothreitol

ELISA - Enzyme-linked immunosorbent assay

ERK - Extracellular signal-regulated kinase

GAPDH - Glyceraldehyde 3-phosphate dehydrogenase

H_2O_2 – hydrogen peroxide

HA – Hemagglutinin

HO-1 – Hemoxygenase 1

HRP – Horseradish peroxidase

IAP – Inhibitor of apoptosis

IB – Immunoblot

ICAM-1 – Intercellular adhesion molecule 1

IκB – Inhibitor of kappa B

IKK - IκB kinase

IL-8 – Interleukin 8

IP – Immunoprecipitation

MEF – Mouse embryonic fibroblast

MEK - Mitogen-activated protein kinase/extracellular signal-regulated kinase kinase

MPTP - 1-methyl-4-phenyl-1,2,3,6-tetrahydropyridine

MTREF - Mitochondrial transcription termination factor

Nrf2 - Nuclear factor (erythroid-derived 2)-like 2

NF-κB - Nuclear factor kappa-light-chain-enhancer of activated B cells

NQO1 - NAD(P)H dehydrogenase (quinone 1)

NSCLC – Non-small cell lung carcinoma

PCR – Polymerase chain reaction

PD – Parkinson's Disease

PSF - Protein-associated splicing factor

Q-TOF MS - quadrupole time of flight mass spectrometry

RIP - Receptor interacting protein

RNA - Ribonucleic acid

ROS – reactive oxygen species

RT-PCR – Reverse transcriptase polymerase chain reaction

shRNA – short hairpin ribonucleic acid

tBHQ – tert-butylhydroquinone

TNFα – Tumor necrosis factor alpha

TRAF - TNF receptor associated factor

TRXR1 – Thioredoxin reductase 1

Chapter I

INTRODUCTION

This dissertation is centered on the activity and downstream effects of the protein DJ-1. The importance of DJ-1 is highlighted by its association with both cancer and Parkinson's disease. While its molecular activity is still largely unknown, DJ-1 has been described to enhance cell survival through multiple pathways. It is this effect on cell survival that is currently thought to account for DJ-1's association with human diseases. This work identifies a novel pathway by which DJ-1 enhances cell survival and therefore continues the elucidation of the activity of DJ-1 as well as its effects in human disease.

1.1 Cell Survival – A key aspect of human disease

The balance between cell survival and cell death is pivotal to normal cellular physiology. Disruption of this balance can lead to numerous disease processes. Increased cell survival, especially in the context of DNA damage, can allow mutations to go unchecked leading to cancer. Decreased cell survival, due to an increase in sensitivity to toxins and cellular stress, can lead to the death of dopaminergic neurons as seen in Parkinson's disease. Due to the importance of this balance, many different pathways have evolved to tightly control cell survival. While numerous pathways have been shown to have a role in regulating the balance between cellular life and death, continued research identifying new pathways or connecting known pathways is necessary to fully elucidate this complex system.

1.2 DJ-1 promotes cell survival in human cancer

The name DJ-1 was first coined in 1997 by a group characterizing its ability to transform mouse NIH3T3 fibroblast cells. They showed that while DJ-1 weakly transformed cells on its own, it did so synergistically in combination with H-Ras or c-Myc (1). Identification of the Park7 locus mapped DJ-1 to chromosome 1p36.2-1p36.3, a hot spot for chromosomal abnormalities in human non-Hodgkin's lymphoma, leiomyoma, acute myeloid leukemia, astrocytoma, neuroblastoma, adenoma, and adenocarcinoma (2). DJ-1 is overexpressed in multiple human cancers including lung, ovarian, clear cell renal cell, pancreatic, and hepatocellular carcinoma (3-6). This increase in DJ-1 expression has been shown to be predictive of negative patient outcomes and poor prognosis in both breast cancer and esophageal squamous cell carcinoma (7, 8).

Our lab has focused on the role of DJ-1 in non-small cell lung carcinoma (NSCLC). Lung cancer is the number one cause of cancer-related mortality. It is estimated that over 215,000 new cases were diagnosed in 2008 in the United States alone (9). Risk factors include smoking, asbestos or radon exposure, and family history of lung cancer. While the incidence of lung cancer has actually decreased in the United States, most likely due to the decline in smoking, recent increases in smoking in other parts of the world may be preceding a global increase in lung cancer diagnoses.

There are two main types of lung cancer – small cell and non-small cell lung carcinoma (NSCLC). Approximately 85% of all lung cancers are of the NSCLC-type

(10). NSCLCs can be further divided into large cell carcinomas, adenocarcinomas, and squamous cell carcinomas. Location of the tumor can help narrow down the NSCLC subtype as adenocarcinomas and squamous cell carcinomas tend to grow on the lung periphery or near the major airways respectively. To confirm the subtype of NSCLC, a biopsy is needed for histological analysis. These biopsies can be taken during bronchoscopy or by fine needle aspiration. By histology, large cell carcinomas consist of anaplastic cells with large vesticular nuclei, adenocarcinoma cells take a cuboid to columnar shape with the presence of mucin, and squamous cell carcinomas are comprised of differentiated squamous cells with keratin pearls.

The symptoms of NSCLC at presentation are typically vague including persistent cough, coughing up blood, wheezing, shortness of breath, and unexplained weight loss. The first indication of a NSCLC is typically an abnormal opacity on chest x-ray. Once a mass is identified, MRI or CT is used to confirm the presence of a mass as well as to more accurately determine the size. Additional imaging studies including positron emission tomography (PET) and bone scans may then be used to help determine extent of the disease. PET scans use a radiotracer to identify changes in blood flow, oxygen use, and glucose metabolism. As these characteristics are different in tumor masses and cancer cells, this study can locate even small numbers of cancer cells in local lymph nodes or other organs. Bone scans are similar to PET scans except a bone-specific radiotracer is used. These studies can identity metastases that originated from the lung tumor and are used to determine the cancer stage. Lung cancer staging is on a 0-IV scale based on the spread of the carcinoma to local lymph nodes, invasion into adjacent tissues, and

metastasis to distant lymph nodes and other organs. This staging is used to plan treatment and also yields data on the patient's prognosis.

NSCLC has an average 5 year survival of 15% (11). A patient's chance of survival is based on the stage of disease at presentation, NSCLC subtype, and treatment regimen. Currently, surgery is the best chance for a long term cure. Removal of a segment or lobe of the lung or removal of an entire lung may be required to ensure complete removal of the tumor. After surgery, adjuvant chemotherapy has also been shown to have a modest effect in NSCLC although it is not typically as chemosensitive as SCLC. Unfortunately, 70% of NSCLC patients present with locally invasive or metastatic disease and are contraindicated for immediate surgery (11). For these patients, chemotherapy with or without radiation may be used prior to surgery to shrink the tumor or, in late stage patients, as a standalone, palliative care option. The most common NSCLC chemotherapy regimen is a combination of a platinum-based DNA crosslinking agent, such as carboplatin or cisplatin, and a microtubule stabilizer, such as taxol or docetaxel.

In 1997, our group identified tumor-specific taxol-responsive elements in the IL-8 promoter (12). These taxol-responsive elements were found to be active in a subset of NSCLC cell lines including squamous cell H157 and adenocarcinoma H1437 cells as treatment of these cell lines with taxol induced IL-8 secretion (13). This IL-8 secretion is not a general characteristic of NSCLC cell lines as IL-8 was not induced in the alveolar H358 or adenocarcinoma A549 cell lines. The largest induction of IL-8 release occurred in the H157 squamous cell carcinoma cell line so it was chosen for further study. A time course of taxol-induced IL-8 secretion

indicated that IL-8 was induced from 3 to 18 hours peaking at 6 hours. This increase in IL-8 protein secretion was preceded by an increase in IL-8 mRNA starting at 30 minutes post taxol treatment and peaking at 4 hours. This induction of IL-8 transcription was for the taxol-induced IL-8 secretion as inhibition of RNA polymerase II with actinomycin D blocked IL-8 secretion. The IL-8 secretion is dependent on NF-κB and MEK in H157 cells as it was blocked by adenovirus containing the IκB super-repressor and the MEK inhibitor U0126 respectively (13). As MEK is a positive regulator of the pro-survival kinase ERK, this work led our group to hypothesize that this taxol-induced activation of MEK would activate ERK leading to increased cell survival. Therefore, inhibition of MEK should increase the efficacy of taxol in H157 cells.

Later that year, our lab published a paper to confirm that hypothesis. First, our group reported that ERK was phosphorylated, and thus activated, by taxol treatment in a dose dependent manner (14). Next they showed that the combined treatment of taxol and U0126 induced synergistic cell killing in H157 cells as compared to each of the treatments alone. This taxol and U0126 synergy was also confirmed in the BT474 breast carcinoma cell line confirming that this effect is not specific for the H157 lung cancer line. This cell death phenotype is not specific to the U0126 MEK inhibitor as MEK inhibition by PD98059 or overexpression of dominant negative MEK yielded similar results.

To gain information on the downstream effectors important for the cell death seen in taxol/U0126 combination treatment, our group identified proteins whose expression was specifically affected by this combination treatment using 2D gels.

2D gels analysis on samples untreated, treated with taxol or U0126, or treated with both taxol and U0126 identified two proteins to be specifically downregulated in the combination treatment group. These proteins were identified by mass spectrometry as RhoGDIα and DJ-1 (3). Overexpression of DJ-1 protected H157 cells from taxol and U0126-induced cell death suggesting a pro-survival role of DJ-1 in this NSCLC cell type. Finally, overexpression of DJ-1 was identified in 6 out of 7 NSCLC tumor samples as compared to the healthy margins using real-time PCR suggesting a role of DJ-1 in human disease. This finding was later verified by a second group who reported heightened expression of DJ-1 in squamous cell and adenocarcinoma NSCLC tumor samples (15).

The mechanism of action of DJ-1 in cancer pathogenesis has not been fully elucidated. Although DJ-1 is thought to play a role in PD pathogenesis, its effect on the ubiquitination of misfolded and unfolded proteins as well as its chaperone activity towards α-synuclein are not known to play a role in cancer. Current literature suggests that it is DJ-1's regulation of transcription and intracellular signaling that affects cancer pathogenesis, which will be reviewed in section 1.8. In short, DJ-1 inhibits p53 and JNK-mediated apoptosis, stimulates cell survival through Akt and ERK, and induces the Nrf2-dependent detoxification pathway. Taken together, overexpression of DJ-1 in cancer cells would thus inhibit apoptosis and stimulate survival in cancer cells even in the presence of toxic compounds and cellular stress conferring a survival advantage to the cancer cells as compared to cells with normal DJ-1 levels.

1.3 DJ-1, a genetic cause of Parkinson's disease

In 1817, James Parkinson wrote a monograph entitled *An Essay on the Shaking Palsy*. In this essay, he described six patients with decreased muscular strength, tremors, and a propensity to hunch forward at the torso. It quickly became clear that James had described a new syndrome which was termed Parkinson's disease (PD). PD is a common progressive neurological disorder. It is characterized by bradykinesia, muscular rigidity, resting tremors, and postural instability. Incidence rises sharply with age with a median age of onset of 60 years and a lifetime risk of 1.5% (16, 17) . Due to the age range of the typical PD patient, many patients go undiagnosed attributing the symptoms simply to old age. Once diagnosed, there are patients with confirmed symptoms of PD going back a decade or more. The inclusion criteria for a diagnosis of PD are bradykinesia in the presence of muscular rigidity, 4-6 Hz resting tremor, or postural instability not caused by other known balance or visual dysfunction (18). Exclusion criteria range from a history of repeated head trauma to exposure to certain neurotoxins. The diagnosis can typically be made through a careful history and thorough neurological exam.

Parkinson's disease is caused by the loss of dopaminergic neurons in the central nervous system. While loss of dopaminergic neurons in the substantia nigra is a hallmark of PD, neuronal cell loss occurs in other structures including the locus coeruleus, raphe nuclei, dorsal nuclei of the vagus, and structures of the brain stem. Histologically, PD patient samples have decreased dopaminergic neurons. The remaining neurons commonly contain Lewy bodies, protein aggregates consisting

mainly of α-synuclein (19). While associated with PD, Lewy bodies can also be found in certain forms of dementia and a diagnosis of PD can be made in their absence.

Parkinson's disease is progressive and incurable, but a number of treatments can be used to decrease symptoms and to increase patient quality of life. The most efficacious therapy is L-dopa. L-dopa is an inactive form of dopamine that is activated in the central nervous system. It effectively increases the reduced levels of dopamine in the brain of PD patients thus ameliorating symptoms. In the human body, L-dopa can be deactivated by dopa decarboxylases (DDC) or carechol-O-methyl transferase (COMT). By using DDC or COMT inhibitors in combination with L-dopa, the half life of L-dopa can be increased, elongating the duration of L-dopa's effects (20). Patients with early stage disease or who are under 55 can be treated using dopamine agonists or selective type B monoamine oxidase inhibitors, although the mechanism of action of the latter is poorly understood. While effective, these therapies are usually replaced with L-dopa treatment as disease progresses. L-dopa treatment is typically well tolerated. Unfortunately, some patients have motor side effects like chorea, athetosis, and dystonia during initial treatment and many patients may develop these side effects as their PD progresses. This tightening of the therapeutic window of L-dopa over the treatment period highlights the need to identify novel pathways to target in PD.

In severely affected patients in whom L-dopa is not tolerated or ineffective, surgical intervention is an option. There are two main types of surgery used in PD (18). First, portions of the brain responsible for abnormal chemical release or

electrical impulse can be targeted using ablation, deep brain stimulation (DBS), or pallidotomy. In ablation, the target brain tissue is physically destroyed while in the more common DBS procedure an electrode is implanted that inactivates the targeted tissue. Pallidotomy is used to address specific symptoms. In this procedure, fine probes are used to both measure electrical activity and to deliver electrical charges. The effect of the electrical charges on a specific portion of the brain is evaluated by the patient who is awake during the procedure. Once a precise portion of the brain is identified as the offending tissue, it is ablated. Second, dopamine-producing neurons can be transplanted into the brain of PD patients in a process termed fetal mesencephalic dopamine cell implantation (21). In this procedure, dopaminergic neurons are harvested from fetal tissue and placed in the substantia nigra of the PD patient. While this method is not effective for all patients, certain patients have had improvement in symptoms for more than 10 years. As a relatively new procedure, the protocol for fetal grafts is still being optimized and holds promise of a possible long term cure for PD patients.

Most cases of PD are termed idiopathic, with no known cause. It is currently thought that these cases are caused by a combination of genetic factors and long-term exposure to varying toxins. Less than 10% of cases can be attributed to a direct genetic cause. Mutations in the genes for Parkin, PINK1, ATP13A2, α-synuclein, LRRK-2, GBA, and DJ-1 are all linked to PD (22-27). *Park7*, the gene that encodes for DJ-1, was linked to PD during a study of an isolated family in the southwest region of the Netherlands (28). The pedigree of this family had four occurrences of consanguinity within seven generations leading to autosomal

recessive, early onset PD in four individuals. The symptoms of this form of PD were similar to idiopathic PD characterized by bradykinesia, rigidity, postural instability, dystonia, hyperreflexia, asymmetric onset, and anxiety. Linkage analysis identified the disease locus as ≥ 25cM from the *Park6* locus, the gene that encodes PINK1. The new disease locus was termed *Park7*. This link was confirmed by another group shortly after using an independent dataset with two families from Italy and another from the Netherlands (29). Bonifati *et al.* went on to show that DJ-1 was deleted in the Dutch family while a leucine to proline substitution at residue 166 (L166P) was found in the Italian families (30).

Models using *Park7*$^{-/-}$ mice and mouse derived cells studying the effects of DJ-1 in the nervous system have been used to confirm a role of DJ-1 in PD pathogenesis. The first use of murine *Park7*$^{-/-}$ cells was in 2004. Martinat *et al.* used ES cells in which DJ-1 was disrupted by retroviral insertion between exons 6 and 7 using gene trap (31). These cells had decreased cell viability with H_2O_2 treatment as compared to wild type ES cells. This phenotype could be rescued by overexpression of wild type but not L166P mutant DJ-1. Differentiation of these ES cells into dopaminergic neurons increased cell death in *Park7*$^{-/-}$ neurons with 6-OHDA treatment, a neurotoxin that selectively kills dopaminergic neurons.

The first work to publish on *Park7*$^{-/-}$ mice was by Goldberg *et al.* in 2005 (32). In these mice, exon 2 was replaced by a neomycin cassette. While in-frame ATG codons existed in exons 3, 5, 6, and 7, they argued that these amino-terminal truncations would be inactive. No gross abnormalities, effects on fertility, or spontaneous development of PD-like symptoms were seen in the *Park7*$^{-/-}$ mice.

Analysis of brain samples yielded normal numbers of dopaminergic neurons and no Lewy bodies. While *Park7*$^{-/-}$ did not affect baseline neuronal survival, *Park7*$^{-/-}$ neurons release decreased dopamine in the evoked dopamine overflow model that they attributed to increased dopamine uptake by the *Park7*$^{-/-}$ neurons as compared to wild type. This decrease in dopamine levels correlated with a decrease in locomotion in an open field paradigm, a model known to be influenced by dopamine. These findings lead Goldberg *et al.* to hypothesize that DJ-1 causes PD not through the modulation of cell death but by regulating dopamine uptake. This hypothesis is bolstered by more recent papers, such as the work by Chandran *et al.*, showing no deficit of dopamine-producing neurons in *Park7*$^{-/-}$ mice (33).

As advanced age plays a role in the pathogenesis of PD, two groups investigated neuronal survival in aged *Park7*$^{-/-}$ mice First, Chen *et al.*, using 5-11 month old *Park7*$^{-/-}$ mice targeted for the first 5 DJ-1 exons, found no change in dopaminergic neuron cell number (34). Using specific brain sections, they evaluated the release and uptake of dopamine within four different brain structures – the dorsal and ventral caudate putamen and the nucleus accumbens core and shell. They found an increase in dopamine uptake specifically in the dorsal caudate putamen, similar to the findings of Goldberg *et al*. Strangely, a concurrent increase in dopamine release in this structure overcame the increased uptake leading to an overall increase in dopamine, which was contradictory to previous research. Second, Yamaguchi *et al.* similarly saw no neuronal degeneration in aged *Park7*$^{-/-}$ mice (35). Using 24-27 month old mice, they first repeated the behavioral assessment used by Goldberg *et al.* Similar to previous work, there was a decrease

in horizontal locomotion in a field test of *Park7*$^{-/-}$ mice. While this datum would suggest a decrease in dopamine levels, normal dopaminergic neuron number and dopamine levels were seen in the substantia nigra, striatum, and locus coeruleus. Although behavioral studies suggest a decrease in dopamine levels, these studies, taken together, show normal dopaminergic neuron number in multiple brain structures of *Park7*$^{-/-}$ mice with DJ-1 playing a disputed role in dopamine uptake.

While the absence of DJ-1 does not cause spontaneous PD-like symptoms over the natural lifespan of mice, models using neurotoxin and oxidative stress inducing agents have shown a role of DJ-1 in dopaminergic neuron survival. Using cortical neurons from *Park7*$^{+/+}$, *Park7*$^{+/-}$, and *Park7*$^{-/-}$ embryos, Kim *et al.* found a decrease in cell survival with H_2O_2 treatment in the absence of DJ-1 with an intermediate phenotype for the heterozygous cells *in vitro* (36). This phenotype was rescued in the *Park7*$^{-/-}$ neurons by overexpression of DJ-1. Using dopaminergic neurons identified using tyrosine hydroxylase staining, they found decreased cell survival without DJ-1 *in vitro* with treatment of rotenone, a lipophilic insecticide shown to cause dopaminergic neuronal cell death and a PD-like disease in rats. This effect is specific as DJ-1 expression had no effect on cell death caused by camptothecin or staurosporin. In *in vivo* assays, they used MPTP, a lipophilic neurotoxin. Being lipophilic, MPTP crosses the blood brain barrier where it is activated by MAO-B into MPP+. MPP+ interferes with complex I of the electron transport chain causing the buildup of ROS and eventually cell death. Its specificity for dopaminergic neurons is attributed to its entry into cells via the dopamine uptake system. *Park7*$^{-/-}$ mice have decreased TH+ neurons in the substantia nigra pars

compacta, decreased innervation of the striatum, and a larger decrease in dopamine levels as compared to control in the MPTP injection model. As the increased MPTP toxicity could be attributed to increased MPTP uptake through the dopamine uptake pathway, they also reported similar levels of MPTP in the substantia nigra in wild type and knockout mice. Finally, they showed that the neuron cell loss caused by MPTP could be inhibited by intracranial injection of DJ-1 adenovirus. These findings were later confirmed in a rat model of PD in which the neurotoxin 6-OHDA was injected intracranially to kill dopaminergic neurons and cause a PD-like disease (37). In these rats, injection of recombinant DJ-1 was found to protect nigral dopaminergic neurons from 6-OHDA-induced cell death, while injection of recombinant L166P DJ-1 did not lend any protection to these cells.

The protection of dopaminergic neurons from MPTP conferred by DJ-1 is at least partially mediated by the pro-survival kinase Akt. Aleyasin *et al.* found that phosphorylated, and thus activated, Akt was decreased in *Park7*$^{-/-}$ cortical neurons (38). Using these cells and a small molecule inhibitor of Akt, they found that Akt and DJ-1-mediated protection from H_2O_2-induced cortical neuron cell death required expression of both proteins *in vitro*. Finally, using adenoviral-mediated overexpression of Akt in *Park7*$^{+/+}$ and *Park7*$^{-/-}$ mice in the MPTP model, DJ-1 expression was found to be required for Akt-induced neuronal cell survival *in vivo*. This requirement for DJ-1 may be due to DJ-1's ability to inhibit PTEN, a known inhibitor of Akt, but future *in vivo* models will be necessary to confirm that hypothesis. While these *in vivo* studies confirm a role of DJ-1 in neurotoxin and

oxidative stress agents in PD-associated neuronal cell death, there is no mechanism as to how DJ-1 mechanistically accomplishes this effect.

There are three main hypotheses as to how DJ-1 affects neuronal cell survival in PD. First, DJ-1 increases cell survival through the management of misfolded or unfolded proteins. Xiong *et al.* reported that DJ-1 interacts with Parkin and PINK1 (39). This protein complex, termed the PPD complex, was shown to have ubiquitin E3 ligase activity that promotes the ubiquitination and degradation of unfolded or misfolded protein targets of Parkin, such as Parkin itself and synphilin-1. While not tested, this effect of DJ-1 on Parkin activity may extend to α-synuclein, a known target of Parkin (40). If this is the case, absence of DJ-1 may decrease Parkin activity, leading to α-synuclein accumulation, Lewy body formation, and cell death. This hypothesis is bolstered by the genetic association of both Parkin and PINK1 with PD as well as the presence of Lewy bodies in the dopaminergic neurons (22, 23). It does not, however, explain why this pathway specifically affects dopaminergic neurons. Second, DJ-1 acts as a chaperone to α-synuclein, the major component of Lewy bodies (41). Shendelman *et al.* found that DJ-1 was capable of suppressing the heat-induced aggregation of citrate synthase and glutathione S-transferase *in vitro* (41). This effect of DJ-1 is abolished in the presence of the reducing agent DTT and enhanced with H_2O_2 treatment suggesting that the DJ-1 chaperone activity is modified by oxidation of either DJ-1 or the target protein (42). This chaperone activity of DJ-1 has also been shown to extend to α-synuclein in a cell free system as recombinant α-synuclein protofibrils and fibrils were decreased in the presence of recombinant DJ-1 but not L166P mutant DJ-1 (41). In

neuroblastoma cells, overexpression of DJ-1 decreases the aggregation of α-synuclein in response to $FeCl_2$ treatment, while L166P DJ-1 increased this aggregation. Finally, insoluble α-synuclein aggregates were increased in *Park7*$^{-/-}$ ES cells as compared to wild type ES cells. While causation has not been confirmed, it has been hypothesized that the aggregation of α-synuclein plays a role in neuronal cell death in PD. By solubilizing α-synuclein, DJ-1 could decrease α-synuclein aggregation thus preventing neuronal cell death. While this hypothesis is plausible, Lewy bodies are not always present in PD patients nor are they known to be a specific hallmark of DJ-1-associated PD. Third, DJ-1 protects dopaminergic neurons from environmental insults through signaling and transcriptional modulation. Neurons lacking DJ-1 are more susceptible to cell death induced by oxidative stress, MPTP, rotenone, and dopamine itself (36, 43, 44). Protection from dopamine toxicity is of particular interest as it would explain why this neuronal cell death is so specific to dopaminergic neurons. The role of DJ-1 in signaling and transcription are described in detail in section 1.8, but in short cells without DJ-1 have increased pro-apoptotic signals, decreased pro-survival signals, and decreased detoxification potential leading to cell death. These three hypotheses on the action of DJ-1 in PD are not necessarily mutually exclusive and DJ-1's true function may certainly lie in a combination of two or more of these possibilities.

1.4 Molecular overview, Crystal Structure, and Post-translational Modification of DJ-1

DJ-1 is a protein of approximately 23 kilodaltons encoded by the *Park7* gene on the short arm of chromosome 1 (28). High levels of DJ-1 are found in a wide variety of cell types, and it is thought to be ubiquitously expressed (Fig. 1.1). This expression profile suggests a critical role of DJ-1 in cellular physiology. While mainly found as a homodimer in the cytoplasm of untreated cells, DJ-1 is known to have functions tied to both nuclear and mitochondrial localization (45, 46). Overall, DJ-1 protects cells from toxins and cellular stress leading to increased cell survival. This effect on cell survival is thought to account for its association with cancer and Parkinson's disease in humans. While the exact molecular mechanism by which DJ-1 enacts this effect has remained elusive, hypothesized activities range from protease to chaperone activity. Known downstream effects of DJ-1 activity include modulation of multiple intracellular signaling molecules and transcription factors including Akt, Jnk, p53, ERK, and Nrf2 (15, 47-50).

The DJ-1 crystal structure was elucidated by three groups that published in close succession (51-53). DJ-1 takes a flavodoxin-like Rossmann-fold consisting of three layers – a set of six parallel β-sheets flanked on either side by eight α-helices (Fig. 1.2A). All three groups crystallized DJ-1 as a dimer (Fig. 1.2B). This homodimer is likely the standard form of DJ-1 in solution and *in vivo* as DJ-1 runs at exactly twice the expected molecular weight in native gels. The L166 residue, mutation of which is associated with Parkinson's disease in humans, is found on the interface between the dimerized DJ-1 molecules. Mutation of L166 residue disrupts

the local tertiary structure, inhibiting homodimerization, and causing the ubiquitination and degradation of DJ-1 via the proteosome (54). A triad of putative catalytic residues, similar to the triad of a cysteine protease, consisting of cysteine 106, glutamate 18, and histidine 126 is present, but the residues are in an unfavorable conformation for proton transfer (Fig. 1.2C) (53).

DJ-1 can be modified through oxidation and SUMOylation. During crystallization, it was found that the conserved putative catalytic C106 residue was particularly sensitive to radiation-induced structural changes (Fig 1.2D). This residue was of particular interest as this cysteine is perfectly conserved in all homologues of DJ-1. Oxidation of DJ-1 at this residue occurs in response to H_2O_2, paraquat, and endotoxin (55-57). This oxidative potential led researchers to hypothesize that DJ-1 either acts as an oxidative scavenger or sensor. Taira *et al.* hypothesized that DJ-1 protects against oxidative stress by directly scavenging free radicals, but the lack of DJ-1 antioxidant enzymatic activity or machinery to replenish non-oxidized DJ-1 for this purpose makes this conclusion unlikely (58, 59). It is more likely that DJ-1 uses oxidization at the C106 residue to sense the oxidative environment of the cell. The effect of DJ-1 oxidation on its activity has been the subject of numerous, and sometimes conflicting, reports. While the mechanism by which oxidation of DJ-1 affects DJ-1's molecular function remains elusive, there is a general consensus that oxidation of DJ-1 enhances its pro-survival activity.

In 2004, Canet-Aviles *et al.* showed that mutation of the DJ-1 C106 residue abolished its ability to protect neuroblastoma cells from MPTP-induced cell death (46). They also reported a difference in subcellular localization of DJ-1 with C106

mutation. Using paraquat to induce oxidative stress, DJ-1 was found to re-localize to the outer mitochondrial membrane while C106A mutant DJ-1 remained localized mainly in the cytoplasm. This led them to hypothesize that oxidation of the C106 residue and re-localization was necessary for DJ-1's pro-survival function. Waak *et al.* also showed that oxidation of DJ-1 enhanced its ability to protect cells from stress. Their work focused on the effect of oxidation on the interaction of DJ-1 and apoptosis signaling kinase 1 (ASK1). As its name suggests, ASK1 initiates apoptosis. During cellular stress, ASK1 dimerizes and activates downstream JNK1 leading to apoptosis. DJ-1 binds to ASK1 disrupting ASK1 dimerization and thus activation (60). This DJ-1/ASK1 interaction is enhanced with H_2O_2 treatment as shown by co-immunoprecipitation experiments (61). As expected, they found that stable expression of C106A mutant DJ-1 did not confer protection to *Park7*$^{-/-}$ MEFs treated with H_2O_2 while wild type DJ-1 overexpression protected the cells. This body of work suggests an important role of oxidation on DJ-1's function. Although oxidation at the C106 residue is thought to enhance DJ-1's cytoprotection, more studies are needed to find the effect of C106 oxidation on DJ-1's putative molecular functions.

DJ-1 is also modified by conjugation with small ubiquitin-like modifier (SUMO). SUMO is a post-translational modification that is activated and conjugated to proteins at lysine residues in a process similar to ubiquitination. SUMOylation of a target protein can modulate interaction, localization, activity, and stability of proteins. As a binding partner of a protein in the PIAS family of SUMO E3 ligases, DJ-1 was speculated to be SUMOylated (62). Shinbo *et al.* verified this putative SUMOylation

of DJ-1 (63). In that paper, DJ-1 is reported to be SUMOylated at the K130 residue and that mutation of the K130 or L166 residue leads to improper conjugation of DJ-1 with SUMO-1. They also showed that the K130 residue, and thus SUMOylation of DJ-1, was necessary for DJ-1 to transform cells in combination with H-Ras and to protect cells from UV irradiation. Although research on the effect of SUMOlyation of DJ-1 is meager, this initial work suggests that SUMOylation of DJ-1 positively regulates DJ-1 activity.

1.5 DJ-1 Superfamily – Clues to the Molecular Function of DJ-1

DJ-1 is a member of the DJ-1/ThiJ/PfpI superfamily (Fig.1.3). This superfamily includes hundreds of members including proteins from numerous vertebrates, invertebrates, plants, and prokaryotes. DJ-1 orthologs in vertebrates cluster within a single group with 80-100% identity suggesting a conserved function (Fig. 1.4). Invertebrates actually contain two DJ-1 paralogs which retain approximately 40% identity with the human coding sequence. Although plants contain DJ-1 homologues, vertebrate and invertebrate DJ-1 is actually more closely related to bacterial ThiJ genes (64).

A number of bacterial proteins contain ThiJ domains. These proteins have varying functions as protein chaperones (65), catalases (66), proteases (67), and kinases (68). The prototypic member of this group is the kinase ThiJ. ThiJ functions in the biosynthesis of thiamine in *E. coli.* Thiamine is a cofactor for two enzyme complexes of the citric acid cycle, pyruvate dehydrogenase and alpha-ketoglutarate

dehydrogenase. Thiamine is produced by many prokaryotes and several species of plants, but this biosynthesis pathway is not intact in human or other animals. Due to this, thiamine is an essential vitamin in humans and thiamine deficiency leads to beriberi, a disease of the neurological and cardiovascular systems. The fact that the thiamine biosynthesis pathway is non-functional in humans combined with the lack of ThiJ-like kinase activity in human DJ-1 suggests that eukaryotic DJ-1 has lost this activity and has converged on another function (53).

The PfpI subfamily consists mainly of intracellular proteases (69). The major structural hallmark of a cysteine/serine protease is a triad of catalytic residues consisting of a cysteine or serine, glutamate, and histidine in close three dimensional approximation to allow proton transfer during protein cleavage. While DJ-1 has these residues (Cys106, Glu18, His126), the placement of the residues is unfavorable for protease activity leading to weak or no protease activity of DJ-1 depending on the assay and substrate (53, 70). Research into DJ-1 as a protease has continued as a group recently published that full length DJ-1 is a zymogen, requiring carboxy-terminal cleavage to be activated (71). Removal of the final 15 amino acids of DJ-1 moved the catalytic triad of DJ-1 into a more favorable conformation. Fluorescent protease activity assays with BODIPY FL-labeled casein identified pronounced proteolytic activity of the truncated DJ-1. They went on to show that this protease activity is inhibited by oxidation at the C106 residue. Finally, they reported that the truncated form of DJ-1 was more effective than full length DJ-1 in the inhibition of rotenone-induced cell death.

Since the elucidation of the crystal structure of DJ-1, it has been known that DJ-1 possesses an extra carboxy-terminal alpha helix not seen in the related PfpI family of proteases. It is therefore logical that removal of this alpha helix may reveal hidden protease activity of DJ-1. The major flaw of this work lies in the fact that they do not satisfactorily show that this truncated form of DJ-1 actually exists in human cells. Most of the work is done in overexpression or cell free systems. The only data provided to suggest that DJ-1 is cleaved at the C-terminus endogenously is a lower molecular weight band by immunoblot. This band could be accounted for by amino-terminal cleavage, cleavage of DJ-1 at the caspase 6 site at residue 149, or oxidation specific cleavage of DJ-1 at residue 157 - all of which may in fact show impaired protease activity (72, 73). Therefore, further research will be required to see if this activity is functionally important or if artificial truncation of DJ-1 is simply activating a lost function not seen endogenously.

Other minor prokaryotic DJ-1 superfamily members include protein chaperones and transcriptional regulators. Comparison of the crystal structures of DJ-1 and heat shock protein 31 (Hsp31) of *E. coli* found a conserved domain between the two proteins suggesting a protein chaperone function of DJ-1 (65). While seemingly in direct conflict with its putative protease activity, two groups have shown chaperone activity of DJ-1 towards α-synuclein, a target with implications in PD (41, 74). The DJ-1/ThiJ/PfpI superfamily also includes the AraC family of transcriptional activators (75). Proteins within this family homodimerize and directly bind DNA leading to transcriptional activation mediated by RNA polymerase II. These proteins are known to play a role in sugar catabolism, virulence, and

response to stress. While similarities can be seen between the AraC proteins and DJ-1, such as their structures and modulation of the cellular stress response, a direct effect of DJ-1 on transcription through DNA binding seems unlikely as DJ-1 is not known to bind DNA. Taken as a whole, DJ-1 homologue analysis yields clues but not a definitive answer as to the molecular function of DJ-1 due to the vast array of different functions exhibited within the DJ-1 superfamily.

1.6 Association of DJ-1 homologues and male fertility

Sequence analysis identified a homologue in rats termed contraception associated protein 1 (CAP1) (76, 77). Wagenfeld *et al.* showed that CAP1 was present in the epididymal fluid of rats rendered infertile by treatment with oral ornidazole while CAP1 was absent in the fluid of fertile, vehicle treated rats. This role in fertility is preserved in DJ-1 as fertility experiments in mice showed that depletion of DJ-1 in mouse semen using anti-DJ-1 serum decreased sperm fertility (78). While the mechanism by which DJ-1 affects fertility has not been extensively studied, two groups have described a connection between DJ-1 and the androgen receptor. First, DJ-1 was shown to positively regulate the androgen receptor through the inhibition of PIASxα binding (45). Second, DJ-1 was found to bind to and inhibit DJ-1-binding protein (DJBP), which negatively regulates the androgen receptor through recruitment of the histone deacetylase complex (62). DJ-1 may therefore boost fertility by inducing androgen receptor expression. It is important to

note that while DJ-1 depletion in the semen may decrease fertility, *Park7*$^{-/-}$ mice do not have overt fertility issues.

1.7 Discovery of DJ-1 as a RNA binding protein

While the first to name the protein, Nagakubo *et al.* was not the first group to ascribe a function to DJ-1. In 1993, Nachaliel *et al.* identified a cAMP-regulated RNA-binding protein (RBP) (79). RBP was later found to be a complex comprised of two major subunits – RNA binding subunits (RBS) and regulatory subunits (RS) (76). Analysis of the RS cDNA sequence showed near identity to the published DJ-1 cDNA sequence. The reason DJ-1 was termed RS was because this work did not find a direct interaction between DJ-1 and RNA, but Van der Brug *et al.* recently reported that DJ-1 directly binds RNA (80). Their first confirmation was completed by immunoprecipitating DJ-1 from M17 neuroblastoma cells, isolating RNA from the immunoprecipitation samples, and running the RNA on microarray. When compared to an IgG immunoprecipitation control, DJ-1 pulled down distinct RNA species including mitochondrial genes, genes involved in glutathione metabolism, and members of the PTEN/PI3K cascade. Next they confirmed the interaction of DJ-1 with specific transcripts by immunoprecipitation of DJ-1 coupled with RT-PCR. To verify RNA binding by DJ-1 *in vivo*, they immunoprecipitated DJ-1 from brain samples of *Park7*$^{+/+}$ mice using *Park7*$^{-/-}$ mice as a control. RNA was isolated from the immunoprecipitation samples and qRT-PCR was used to verify the presence of 6 transcripts in the DJ-1 containing samples as compared to the control. This work is

the first to identity DJ-1 as a direct RNA binding protein. It is of particular interest as it allows one function of DJ-1 to affect multiple cellular pathways. Unfortunately, the consequence of DJ-1 binding on the target RNA transcripts is not investigated in this paper. Therefore, DJ-1 may be altering RNA half-life, translation, or having no effect at all requiring future research on the subject.

1.8 Signaling and Transcriptional Modulation by DJ-1

DJ-1 has widespread effects on the transcriptome especially during times of cellular stress. Its role in PD and cancer pathogenesis can be, at least partially, attributed to its effects on transcription and intracellular signaling. Overall DJ-1 has a pro-survival effect mediated through three major mechanisms - inhibition of pro-apoptotic pathways, stimulation of pro-survival pathways, and induction of detoxification pathways.

DJ-1 inhibits four pro-apoptotic pathways. First, DJ-1 inhibits p53-mediated transcription and apoptosis. During the cell cycle, DNA damage causes cell cycle arrest allowing the cell to either repair the damage or undergo apoptotic cell death. One of the transcription factors that controls this checkpoint is p53. When genomic damage is too great, activation of p53-mediated transcription leads to the induction of apoptosis through downstream mediators such as Bax (81). DJ-1 overexpression decreased Bax transcript and protein levels in A549 squamous cell NSCLC cells (48). This effect was dependent on p53 as Bax expression was not changed in p53-null H1299 cells and the effect of DJ-1 on Bax could be inhibited by PFT-α, a known

p53 inhibitor. DJ-1 repressed p53-mediated transcription and cell death through direct binding of p53 and inhibition of its transcriptional activity. Second, DJ-1 inhibits pro-apoptotic JNK1 signaling (47). During UV irradiation, activation of Mekk1 leads to the induction of JNK1 signaling. The consequence of this JNK1 signaling in neurons, which includes c-Jun-mediated transcription, is apoptosis (82). Mo *et al.* found that DJ-1 binds to and sequesters Mekk1 in the cytoplasm thus inhibiting Mekk1 activity. This pathway allows DJ-1 to decrease JNK1 activity and c-Jun-mediated transcription and inhibit apoptosis. Third, DJ-1 inhibits ASK1. ASK1 induces apoptosis in response to oxidative and genotoxic stress. Inactive ASK1 is found bound to thioredoxin in the cytoplasm (83). During cellular stress, ASK1 is released allowing it to activate via auto-phosphorylation. This activated ASK1 then phosphorylates multiple MAP kinase kinases (MKKs) causing the downstream activation of JNK1 and p38 leading to apoptosis. DJ-1 binds to and inactivates ASK1 blocking JNK1 and p38-mediated pro-apoptotic signals thus promoting cell survival (84). Fourth, DJ-1 inhibits protein-associated splicing factor (PSF). PSF, when activated, silences transcription in neurons leading to neuronal cell death. DJ-1 binds to and inhibits PSF blocking the pro-apoptotic effect of PSF and stimulating cell survival (85). Inhibition of these four pro-apoptotic pathways allows cells overexpressing DJ-1 to avoid apoptosis in the face of significant DNA damage and cellular stress.

DJ-1 induces both the ERK and Akt pro-survival pathways. ERK, a kinase downstream of Ras, increases cell survival through the phosphorylation and activation of target transcription factors such as ELK-1 and STAT3. ERK is activated

via phosphorylation by the kinase MEK. Phosphorylation of MEK and ERK was increased by overexpression of DJ-1 in the MN9D dopaminergic neuron cell line (49). This effect was important for DJ-1's role in promoting cell survival as overexpression of DJ-1 did not protect these cells from H_2O_2-induced cell death in the presence of MEK inhibitors. DJ-1 also induces Akt activity, a pro-survival kinase downstream of PI3K. Akt acts as a pro-survival signal by inactivating, via phosphorylation, the pro-apoptotic proteins Bad, capase 9, and the forkhead transcription factor family (86-88). One of the mechanisms by which Akt is regulated is through inhibition by PTEN, a tumor suppressor commonly mutated in human cancers (89). Kim *et al.* identified DJ-1 as an antagonist of PTEN function in a gain-of-function screen in *Drosophila* (15). Using an overexpression system, they showed that this pathway is conserved in humans as DJ-1 blocks PTEN-induced cell death. Next, they showed that DJ-1's ability to protect cells from staurosporine-induced cell death requires PTEN as overexpression of DJ-1 does not confer protection in *Pten*$^{-/-}$ cells. Finally, Akt phosphorylation was proportional to DJ-1 expression as DJ-1 overexpression and knockdown led to increased and decreased Akt phosphorylation respectively. Therefore, DJ-1 stimulates cell survival by inhibition of PTEN, activation of Akt, and blocking Bad, caspase 9, and the forkhead transcription factor pro-apoptotic signaling. The importance of this pathway was recently confirmed *in vivo* in a MPTP injection PD model system that reported that DJ-1 expression is required for Akt-mediated protection of dopaminergic neurons in the striatum (38).

DJ-1 confers a survival advantage to cells by upregulating hypoxic and oxidative stress response pathways such as HIF1 and Nrf2. In 2009, Vasseur *et al.* reported that DJ-1 positively regulates the transcription factor HIF1 (90). HIF1 allows cells to respond to and survive hypoxic conditions and the associated cellular stress. When activated in response to hypoxic conditions, HIF1 leads to the transcription of multiple downstream targets such as hemoxygenase 1 and vascular endothelial growth factor 1 (91). These activated genes protect the cell from hypoxia-induced cell death and stimulate angiogenesis to restore normal oxygen levels. This pathway is especially important in solid tumors as the central portion of these tumors is thought to be hypoxic due to the local blood supply not meeting the increased cell mass and metabolism of the tumor. By inducing HIF1, DJ-1 may allow cancer cells to adapt to and survive the harsh tumor microenvironment.

In 2005, Zhou *et al.* reported that DJ-1 protects cells from oxidative stress by increasing the synthesis of glutathione, a molecule known to detoxify excess oxygen radicals (74). They showed that this increase in glutathione was due to an increase in glutamate cysteine ligase, a positive regulator of glutathione, but did not identify a mechanism for this increase in glutamate cysteine ligase expression. In 2006, our lab published that DJ-1 regulates the glutathione pathway by positively regulating the activity of the transcription factor Nrf2, a master regulator of the antioxidant response (see Appendix A). Under non-oxidative conditions, Nrf2 is found in the cytoplasm bound to its cytoplasmic inhibitor, Keap1 (92) (Fig. 1.5). Keap1 targets Nrf2 for ubiquitination and degradation by the proteosome in a cullin3-dependent manner (93, 94). Therefore, Nrf2 is inhibited by both cytoplasmic sequestration and

baseline degradation. In oxidative conditions, Nrf2 is released from Keap1 and translocates to the nucleus. In the nucleus, Nrf2 binds small Maf proteins and recruits co-activators such as CBP (95, 96). This protein complex then binds to antioxidant response elements (AREs) leading to the transcription of numerous downstream targets including small molecule antioxidants, antioxidant proteins, and detoxification enzymes such as glutathione, superoxide dismutase, and NADPH quinine oxidoredutase 1 (NQO1) respectively (97, 98).

Comparing cells treated with control siRNA and DJ-1 siRNA using microarray, we found that NQO1 expression was decreased in the presence of DJ-1 siRNA (50). As NQO1 is a target of Nrf2, we searched sequences upstream of the other microarray hits and identified 7 genes with putative ARE sites suggesting a role of DJ-1 in the regulation of Nrf2. First, we showed that siRNA-mediated knockdown of DJ-1 decreased Nrf2 protein levels. Using cyclohexamide to inhibit translation, we found that this decrease in Nrf2 protein levels was due to a decrease in Nrf2 protein half-life in the absence of DJ-1. Using luciferase, we also reported that knockdown of DJ-1 leads to a decrease in Nrf2 activity. To address the mechanism, we analyzed the interaction of Nrf2 and Keap1, the key step in Nrf2 regulation. We found that overexpression of DJ-1 decreased the interaction of Nrf2 and Keap1 as seen by co-immunoprecipitation. While DJ-1 positively regulates Nrf2 through disruption of the Nrf2/Keap1 interaction, we did not find the direct mechanism by which DJ-1 enacts this effect. Finally, these data were confirmed in a primary cell type to ensure that this pathway was not specific to the NSCLC cell type used.

This thesis has identified a positive regulatory role of DJ-1 on the transcription factor NF-κB. While DJ-1 is already associated with an array of transcription factors (Fig. 1.6), this work is the first to link DJ-1 to NF-κB, a well known pro-survival factor with ties to cancer pathogenesis and profound importance in immune responses. We will also describe the mechanism of this positive regulation as well as changes to specific gene targets of NF-κB and cell survival.

1.9 NF-kB, a cancer-associated transcription factor

The NF-κB transcription family is made up of five members including NF-κB1 (p105/p50), NF-κB2 (p100/p52), RELA (p65), cREL, and RELB. All five have a highly conserved REL domain allowing the proteins to form homodimer and heterodimer combinations as well as bind specific DNA sequences termed κB sites. NF-κB transcription factors function in two related pathways – canonical and non-canonical (99, 100). In the canonical pathway, NF-κB1 p105 is found bound to p65/RELA in the cytoplasm. This heterodimer is activated through the processing of p105 to p50 (101). The p50/p65 active dimer is sequestered in the cytoplasm by IκB, thus inhibiting its activity (102). This IκB inhibition is held until the pathway is activated. Many signals can activate the canonical pathway including endotoxin, growth factors, and pro-inflammatory cytokines such as TNFα. When TNFα binds to its receptor, it sets off a cascade of intracellular signaling (Fig. 1.7). First, positive regulators of NF-κB activity, such as RIP1 and TRAF6 are recruited to the intracellular portion of the TNFα receptor (103, 104). Once activated, these

molecules induce the IKK complex. This complex, comprised of the IKKα and IKKβ catalytic subunits and IKKγ regulatory subunit, phosphorylates IκB targeting it for degradation (105). This releases IκB's inhibition of the p50/p65 dimer allowing the dimer to translocate to the nucleus, bind κB sites, and induce transcription of a myriad of gene targets.

The non-canonical pathway is activated in a specific subset of cells, including lymphocytes, in response to lymphotoxin β and CD40L. Prior activation of the canonical pathway is required to first stimulate the expression of NF-κB2/p100. This inactive p100 is bound to RELB in the cytoplasm. Activation of this pathway induces NF-κB-inducing kinase (NIK) which in turn phosphorylates and activates an IKKα homodimer (106). This leads to the phosphorylation and processing of p100 to p52 producing an active p52/RELB dimer (107). The active dimer translocates to the nucleus where it induces transcription through direct DNA binding.

While typically associated with the activation of immune cells, NF-κB plays a direct role in cell survival. Targets of NF-κB include cell cycle proteins and pro-survival proteins including prominent oncogenes such as cyclin D, Bcl-2, and inhibitors of apoptosis (IAPs) (108-110). Through the action of these targets, NF-κB promotes cell survival and proliferation. It is, therefore, not surprising that a number of human cancers have been found to have aberrant activation of the NF-κB pathway. The first tie between NF-κB and cancer was through the protein v-Rel (111). V-Rel is a viral homologue of the REL proteins in Rev-T retrovirus. This virus, through v-Rel, is capable of causing avian reticuloendothelial lymphomatosis.

This work paved the way for numerous studies researching the role of NF-κB in cancer pathogenesis.

NF-κB/RELs have been found to be aberrantly activated in breast, head and neck, esophagus, cervix, prostate, colon, pancreas, and lung carcinomas (112, 113). Direct alteration of NF-κB or IκB activity by changes in expression or mutation is known to occur in particular cancers, such as Hodgkin's lymphoma, but this is atypical (114). More commonly, cancer-associated activation of NF-κB is seen secondary to an activation or overexpression of upstream receptors, growth factors, cytokines, or kinases. This activation confers protection to cancer cells by blocking apoptosis and stimulating cell survival through NF-κB's downstream targets. Some of these targets are proteins with roles in immunity, such as IL-8 and ICAM-1, the subject of this thesis (115, 116).

IL-8 and ICAM-1 function to promote angiogenesis and cell adhesion respectively (117, 118). Together they play an important role in the recruitment and extravasation of neutrophils from the blood into tissues during inflammation (119, 120). As mediators of the innate immune response, these proteins seem like unlikely candidates for overexpression in cancer. One would expect that increased immune surveillance due to the recruitment of immune cells would be disadvantageous, but both IL-8 and ICAM-1 have been found to be expressed at high levels in several human cancers.

IL-8 expression is associated with cancer progression, invasion, angiogenesis, and metastasis (121-127). Secreted human IL-8 acts through binding

to its receptor CXCR1 (128). Activation through this receptor induces NF-κB promoting both cell survival and the continued secretion of IL-8 (129). This pathway constitutes a pro-survival positive feedback loop and may affect cell survival, especially in tumor cells that secrete IL-8 in response to taxol and other chemotherapeutics (13). Certain tumors depend on this IL-8 signaling as blockade of IL-8 binding to its receptor causes a decrease in tumor size, tumor growth, and promotes cancer cell apoptosis (130). Secretion of IL-8 by tumors may also promote tumor growth and metastasis in solid tumors by stimulating angiogenesis. Increased blood flow to solid tumors increases oxygen and nutrient delivery optimizing growth while the increased vascularity allows tumor cells to gain access to the blood stream and metastasize to distant sites.

ICAM-1 is overexpressed in multiple human cancers as well (131-133). While it has not been associated with effects on cancer cell survival, ICAM-1 has been linked to both tumor progression and metastasis (127, 134, 135). The mechanism by which ICAM-1 affects these cancer characteristics has not been fully elucidated, but melanoma research suggests that ICAM-1 works in concert with IL-8 to promote metastasis (127). In a model proposed by Dong *et al.,* IL-8 recruits neutrophils to the tumor site. These activated neutrophils then upregulate β_2-integrins during extravasation. Interaction between these integrins on the neutrophils and ICAM-1 on the melanoma cells effectively tethers the cells together. Then when the neutrophil returns to the circulation, it carries the melanoma cell with it thus promoting metastasis. As aberrant NF-κB activation can contribute to cancer

development, there are many pathways that have evolved to regulate NF-κB. One such pathway involves the NF-κB-inhibiting ubiquitin editing enzyme A20.

1.10 The A20 family of NF-κB-inhibiting de-ubiquitinating enzymes

A20, originally termed TNFα induced protein 3 (TNFAIP3), was initially identified as a transcript upregulated shortly after TNFα treatment (136). Analysis of the sequence of A20 showed 7 zinc finger domains, although the function of these domains was not known at the time. Shortly after, Krikos *et al.* found that the induction of A20 by TNFα was mediated by NF-κB through binding of κB elements in the A20 promoter (137). The first report on the function of A20 showed that overexpression of A20 inhibits both TNFα and IL-1 signaling although a molecular mechanism was not identified (138). That same year, Song *et al.* published that A20 inhibits NF-κB signaling and was capable of binding TRAF1 and TRAF2, two proteins known to induce NF-κB (139). This interaction between A20 and TRAF proteins was extended when another group found that A20 could bind to TRAF6 and that the overexpression of A20 could inhibit TRAF6-induced NF-κB activation (140).

In 2004, a seminal paper was published in Nature outlining the molecular activity of A20. Wertz *et al.* showed that A20 has two major activities – de-ubiquinating activity through its amino-terminal OTU domain and ubiquitin E3 ligase activity through its carboxy-terminal zinc finger domains (141). First, they showed that the zinc finger domains from the carboxy-terminus of A20 can auto-ubiquitinate A20 and ubiquitinate TRAF6 and RIP1 *in vitro*. This activity was found to be

dependent on the fourth zinc finger domain as mutation of this domain abolished this activity. This A20-mediated ubiquitination was linked through the K^{48} residue of ubiquitin causing destabilization of the RIP1 protein. Next they showed that A20 removes K^{63}-linked ubiquitin from RIP1, a post-translational modification known to be important for RIP1 activity. Taken as a whole, this paper reported that A20 inhibits NF-κB by removing K^{63}-linked activating ubiquitin from RIP1 and TRAF6 replacing it with K^{48}-linked ubiquitin. This change in ubiquitination state destabilizes the proteins leading to their degradation and thus the downregulation of NF-κB activity. While minor modifications have been made to this mechanism, like the fact that A20 does not remove individual ubiquitin molecules but instead removes the entire ubiquitin chain at once, the overall mechanism of A20 activity has remained relatively unchanged since this paper was published (142).

Due to its inhibition of the pro-survival, cancer-associated transcription factor NF-κB, A20 is commonly targeted for inactivation in human cancers. A20 has been found to be mutated or deleted in marginal zone B cell, mucosa-associated lymphoid tissue (MALT), and non-Hodgkin's lymphomas (143-145). The promoter of A20 has also been found to be silenced by methylation in MALT lymphomas (144). A20 inactivation is required for maintenance of cell survival in certain tumor cell lines, as overexpression of A20 in L-1236 and KM-H2 cells inhibits cell metabolism and survival as seen by MTS assay (146). A20, through its regulation of NF-κB, also inhibits invasion. Novak *et al.* found that overexpression of A20 in ACC-2 cells, a salivary adenoid cystic carcinoma cell line, caused a NF-κB-dependent reduction in invasion of Matrigel-coated filters *in vitro* (143).

In 2001, while screening the human genome for genes with homology to A20, Evans *et al.* identified two A20-like proteins – TRABID and Cezanne/OTUD7B/Za20d1 (147). Both TRABID and Cezanne were found to bind to TRAF6 by co-immunoprecipitation, but only Cezanne was capable of inhibiting a NF-κB luciferase construct. The amino-terminus of Cezanne contains an OTU catalytic domain similar to A20 that is capable of de-ubiquitinating branched and linear ubiquitin chains (148). Activity of this domain is dependent on the C209 cysteine residue as mutation of this residue abolishes Cezanne de-ubiquitinating activity. Cezanne can also remove ubiquitin from ubiquitin-conjugated proteins as overexpression of Cezanne decreases global ubiquitin as seen by immunoblot. The first specific target of Cezanne was identified in 2008 by Enesa *et al.* They showed that Cezanne, like A20, is induced following NF-κB activation. Cezanne is then recruited to activated TNFα receptors where it removes K^{63}-linked activating ubiquitin from RIP1, suppressing its activity and thus inhibiting NF-κB (149). Finally, Cezanne is thought to be sensitive to oxidation as H_2O_2 treatment was shown to prolong NF-κB activation through the inhibition of Cezanne, although a mechanism for this inhibition was not identified (149).

The tie between Cezanne and cancer is not as well studied as the association between A20 and cancer. Only one report has addressed this possible connection. La Starza *et al.* found a 93-kb DNA sequence that is frequently duplicated in acute lymphoblastic leukemia and Burkitt lymphoma (150). This region at 1q21.2 encodes several genes including Cezanne. Unfortunately, the importance of Cezanne in this duplication was not addressed. While duplication of the gene in cancer would

suggest a putative oncogenic function of Cezanne, its relation to A20 and its inhibition of NF-κB would suggest it should function as tumor suppressor. More studies using multiple different cancer cell types will need to be completed to elucidate the tie between Cezanne and cancer as tumors that overexpress A20 are not unheard of (151).

While many similarities exist between Cezanne and A20, they are functionally distinct. Cezanne, similar to A20, binds RIP1 and TRAF6, but Cezanne only removes ubiquitin as it lacks ubiquitin E3 ligase activity. The research studying Cezanne has been guided by the A20 literature, but due to the known differences between the proteins, including Cezanne's wide expression profile, suggests Cezanne may have more distinct functions yet to be identified (Fig. 1.8).

1.11 Antagonistic crosstalk between the Nrf2 and NF-κB pathways

While Nrf2 and NF-κB control the antioxidant and inflammatory response respectively, these transcription factors, which are both positively regulated by DJ-1, have similarities rooted in their primary function in cell survival. Due to this connection, it is therefore not surprising that Nrf2 and NF-κB can be activated by similar stimuli. Both Nrf2 and NF-κB are induced by ROS, LPS, oxidized LDL, and cigarette smoke (152-156). They even cooperate to induce some common downstream targets including HO-1, GCLC, aldose reductase, and Gαi2 (157-163). Analysis of crosstalk between these two pathways tells a different story. While Nrf2 and NF-κB might cooperate together to promote cell survival in the face of shared

stimuli, they balance each other through antagonistic crosstalk. This work will identify a novel mechanism of antagonistic crosstalk between the Nrf2 and NF-κB pathways.

Nrf2 is not known to directly antagonize NF-κB, but it does inhibit NF-κB activity through its downstream targets and modulation of the oxidative environment of the cell. Nrf2 knockout mice have a pro-inflammatory phenotype. This has been seen repeatedly in mouse emphysema, brain trauma, cigarette smoking, diesel exhaust, and asthma models. Using an asthma model, Rangasamy *et al.* showed that p65 and p50 protein levels were increased in *Nrf2*$^{-/-}$ mice compared to wild type controls (164). This increase in NF-κB activity in the absence of Nrf2 is most likely mediated in two ways. First, the increase in ROS in the *Nrf2*$^{-/-}$ mice leads to the activation of NF-κB. As an antioxidant master regulator, Nrf2 is activated in the presence of ROS leading to the induction of a gambit of downstream effectors which detoxify the ROS. In the absence of Nrf2, ROS are not detoxified and build up unchecked. NF-κB activated by intracellular ROS as deletion of subunits of the ROS-producing NADPH oxidase complex inhibits NF-κB activity (165). Therefore, the ROS buildup caused by the absence of Nrf2 may lead to NF-κB activation. Second, loss of Nrf2 decreases the expression of known NF-κB inhibitors. Four targets of Nrf2, namely HO-1, NQO1, thioredoxin, and Keap1, are known to inhibit NF-κB under certain conditions (156, 166, 167). It is not clear if HO-1, NQO1, and thioredoxin inhibit NF-κB directly or through modulation of ROS levels. Keap1, on the other hand, is known to directly inhibit NF-κB by mediating the ubiquitination and

degradation of IKKβ (168). The loss of expression of these proteins in the absence of Nrf2 may release NF-κB inhibition leading to an increase in NF-κB activity.

NF-κB inhibits Nrf2 directly and through indirect inhibition via its downstream effectors. When in the nucleus, Nrf2 forms heterodimers with small MAF proteins and recruits co-activators, such as CBP, allowing it to bind to ARE sites on DNA and induce transcription. NF-κB inhibits this process through two mechanisms. First, NF-κB binds to CBP depriving Nrf2 of this co-activator. Lui *et al.* showed that overexpression of p65 decreased Nrf2 activity as seen by luciferase, but that this inhibition of Nrf2 could be rescued through the overexpression of CBP (169). Second, p65 overexpression increases the association of the transcriptional silencer, HDAC3, with both the Nrf2-binding MafK as well as ARE sites. Recruitment of HDAC3 to Nrf2 target gene promoters, such as was seen with HO-1, causes deacetylation, as thus silencing, of the target gene (169). In a similar fashion to Nrf2's inhibition of NF-κB, NF-κB also inhibits Nrf2 activity through downstream targets. During shear stress of chondrocytes, COX-2 is induced by NF-κB. Healy *et al.* showed that this increase in COX-2 is mirrored by a decrease in NQO1 levels and presumably Nrf2 activity (170). They showed that this decrease in NQO1 expression was dependent on COX-2 by rescuing NQO1 expression with CAY10404, a COX-2 specific inhibitor. Taken as a whole, the literature looking at the activity and crosstalk of Nrf2 and NF-κB shows two transcription factors with similar overall outcome that balance each other's activity through antagonistic crosstalk at multiple levels (Fig. 1.9). The antagonist nature of the relationship of Nrf2 and NF-κB will be highlighted in this thesis.

Chapter 2 will focus on a novel pathway in which DJ-1, a known positive regulator of Nrf2, enhances NF-κB activity through the inhibition of the de-ubiquitinating enzyme Cezanne, an inhibitor of NF-κB. DJ-1 and Cezanne will be shown to regulate the NF-κB targets *IL-8* and *ICAM-1* as well as cell survival. This adds DJ-1 to the list of proteins and stimuli that can induce both the Nrf2 and NF-κB pathways. In chapter 3, we will explore a novel mechanism of crosstalk between Nrf2 and NF-κB, namely the interaction of Keap1 and A20. This interaction of known inhibitors of Nrf2 and NF-κB respectively has implications for the activity of both transcription factors as well as the research focused on the crosstalk between these two critically important pathways.

Figure 1.1: DJ-1 RNA expression profile

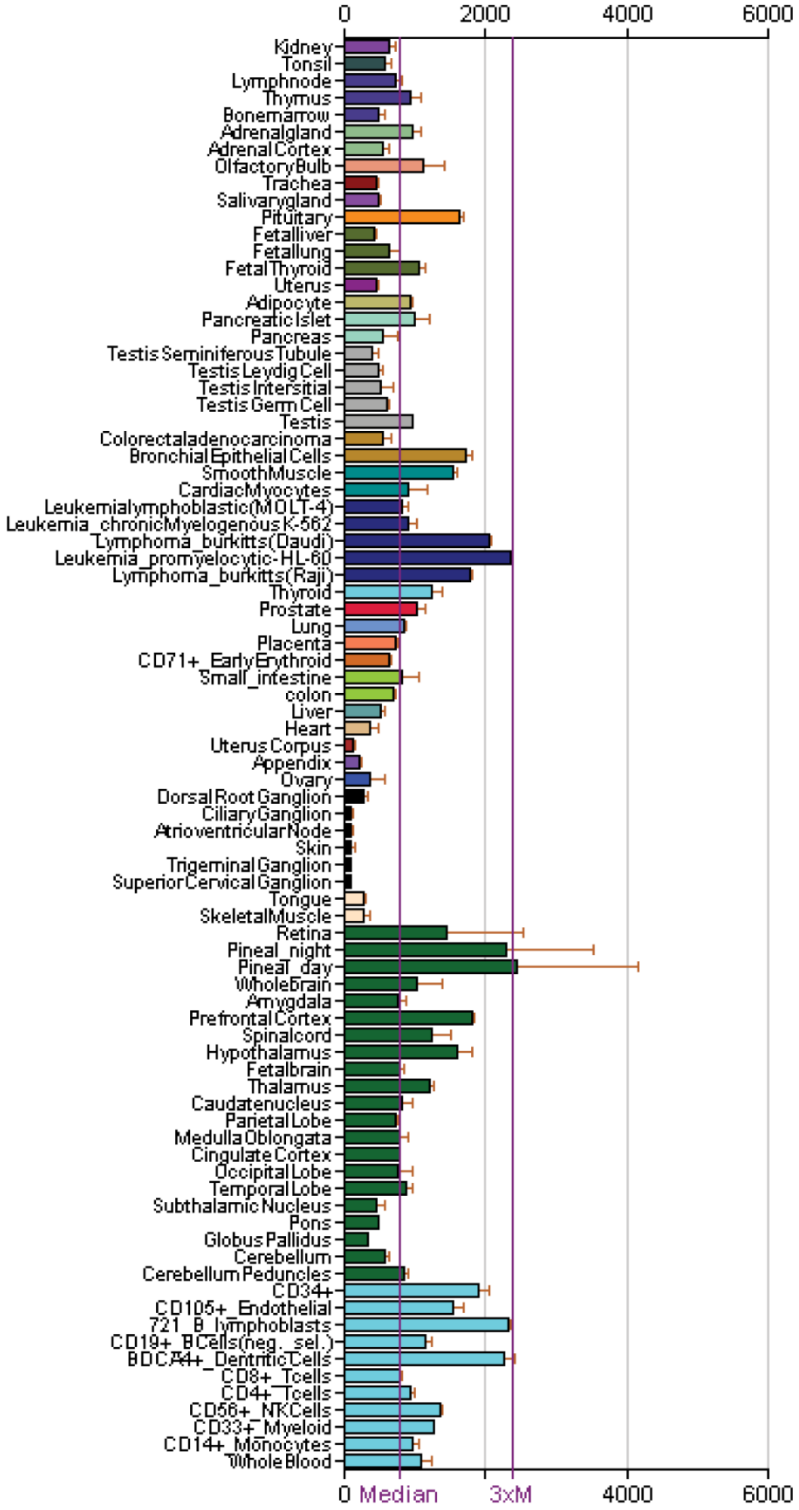

Figure 1.1 DJ-1 human RNA expression profile. Data mined from Novartis GeneAtlas show the wide range of human cell types that express DJ-1 (http://biogps.gnf.org/#goto=welcome).

Figure 1.2: Crystal Structure of DJ-1

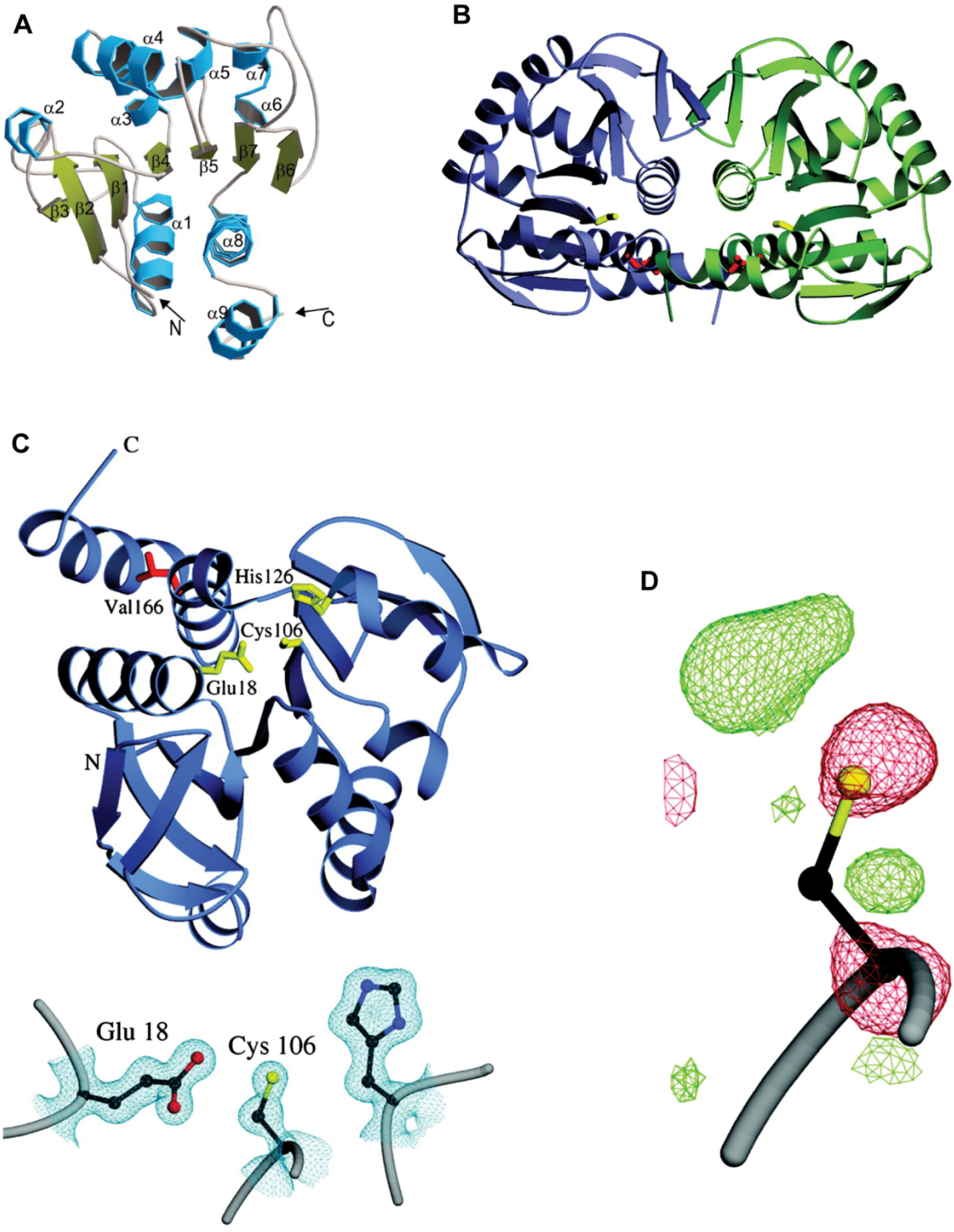

Figure 1.2 DJ-1 structure as determined by X-ray crystallography. (A) Structure of a DJ-1 monomer. Alpha-helices and beta-sheets as well as N-terminus and C-terminus of protein are denoted. (B) Structure of a DJ-1 dimer. DJ-1 monomers are colored blue and green. L166 and C106 residues marked in red and yellow respectively highlighting the proximity of the L166 residue to the interaction interface. (C) Three dimensional arrangement of the DJ-1 putative cysteine protease site. Top panel shows the proximity of the necessary Cys106, His126, and Glu18 residues by ribbon diagram. Bottom panel shows electron density of triad in a non-favorable conformation for proton transfer. (D) Electron density around C106 residue. Fourier difference (F_o - F_c) electron density shown contoured at +3.0 σ (green) and -3.0 σ (red). Variation in electron density suggests that C106 is prone to radiation-induced damage or oxidation. Figures reproduced from (51, 53) with permission.

Figure 1.3: DJ-1/ThiJ/PfpI Superfamily cladogram

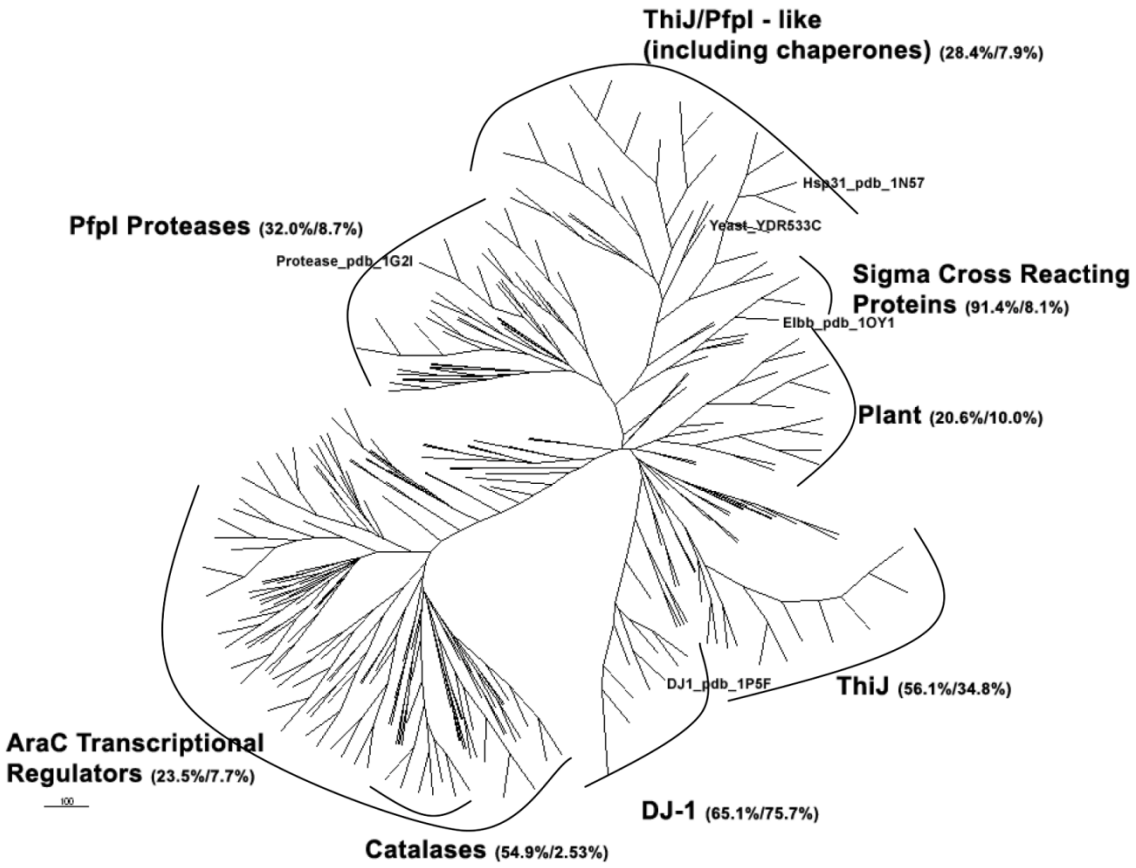

Figure 1.3 DJ-1/ThiJ/PfpI superfamily cladogram. Consensus maximum likelihood tree with branch length corresponding to level of bootstrap support. Groupings within superfamily show diverse function of superfamily members. Numbers in parentheses denote identity within group and with human DJ-1 respectively. Figure reproduced from (64) with permission.

Figure 1.4: Alignment of DJ-1 homologs

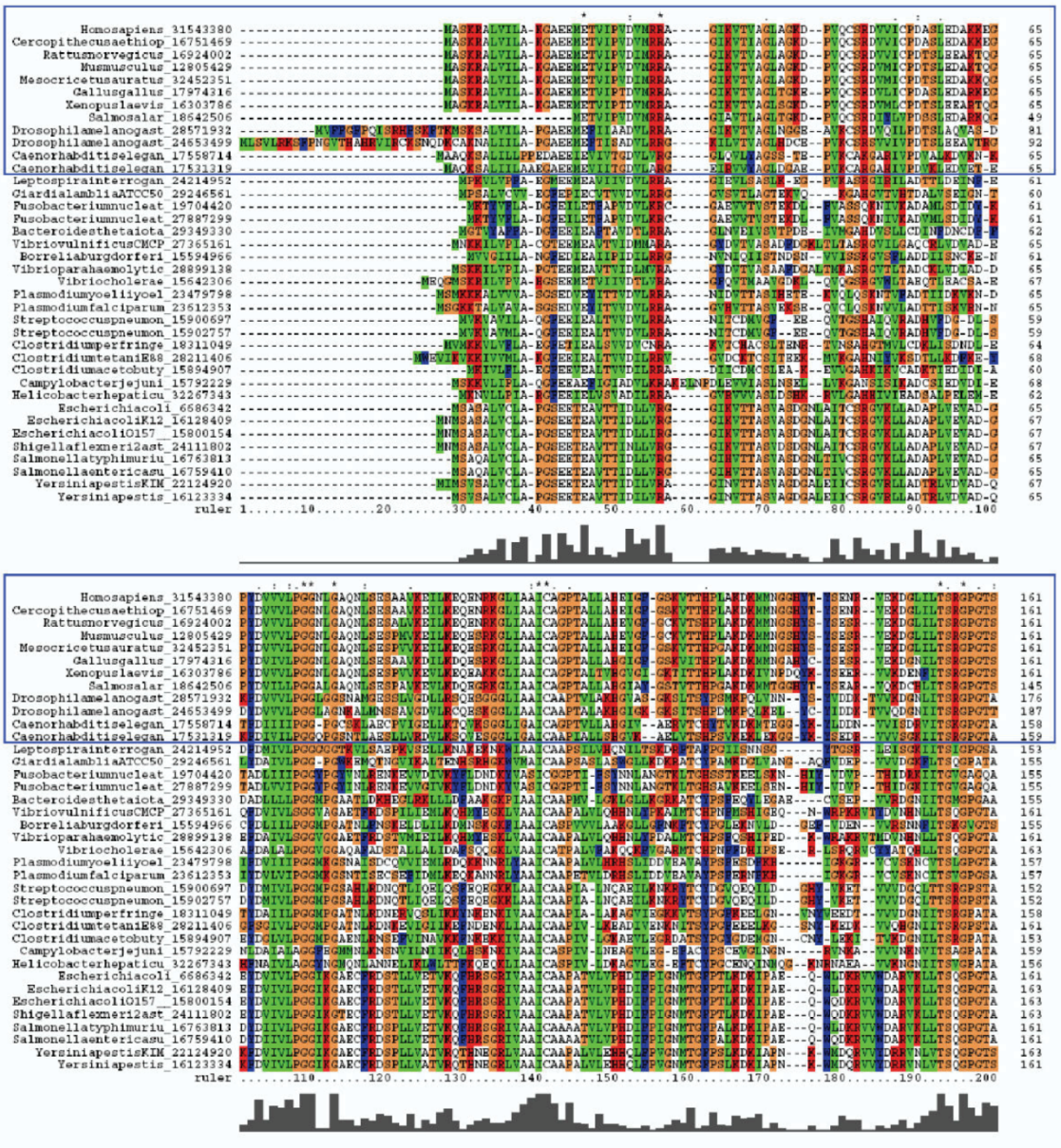

Figure 1.4 Amino acid alignment of DJ-1 and ThiJ subgroups. Sequences show high homology and the presence of residues which are perfectly conserved. C106 residue of DJ-1 is seen at ruler mark 144 as some prokaryotic sequences contain unaligned animo-terminal residues. Bar graph denotes increasing conservation of residue. Eukaryotic DJ-1 family is boxed in blue. Figure reproduced from (64) with permission.

Figure 1.5: Oxidative regulation of Nrf2

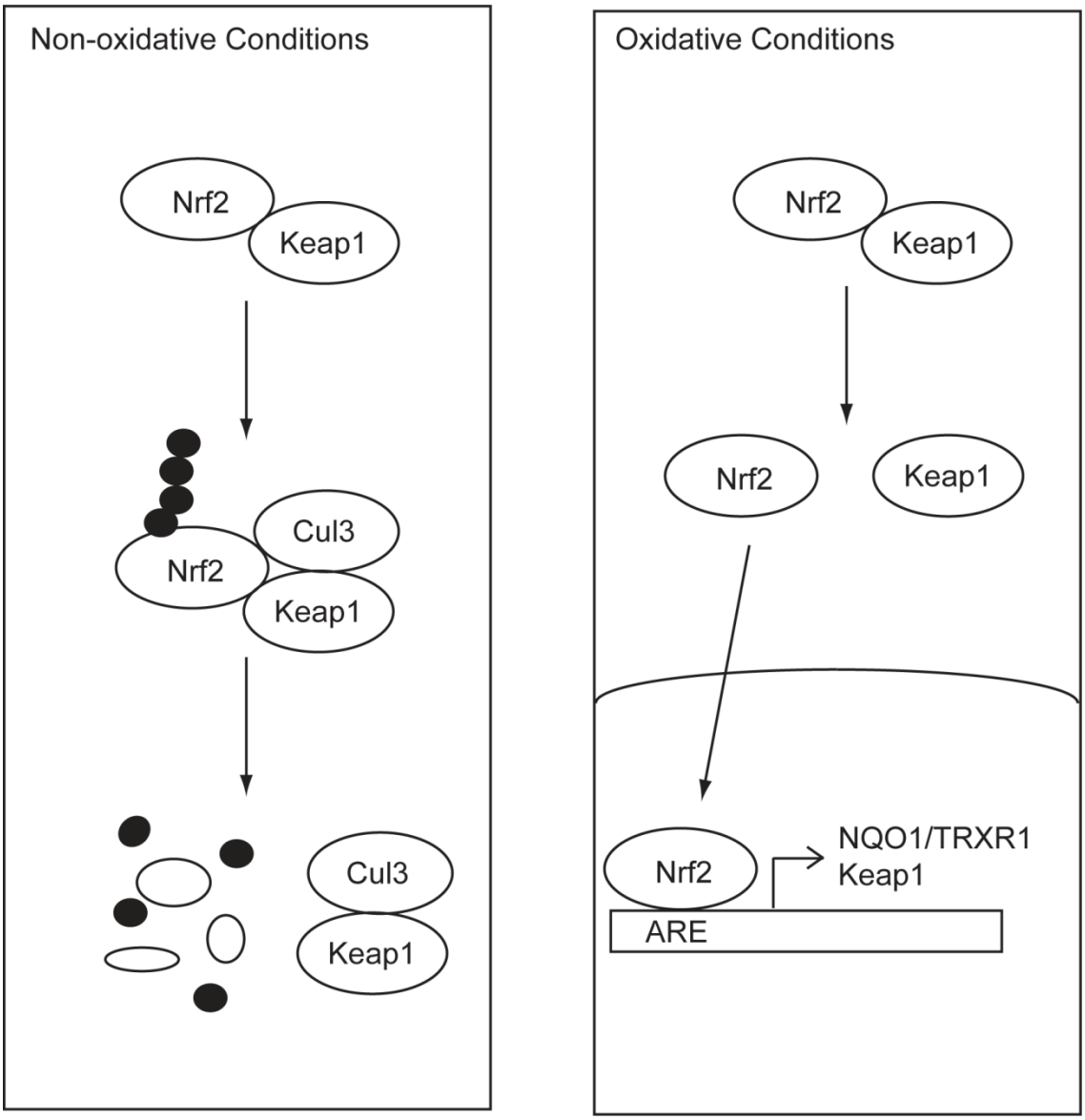

Figure 1.5 Schematic of the oxidative regulation of Nrf2. In non-oxidative conditions, Nrf2 is bound to its cytoplasmic inhibitor Keap1 which catalyzes the ubiquitination and degradation of Nrf2 in a cullin-3 and proteosome-dependent mechanism. In the presence of oxidative stress, Nrf2 is released from the Keap1-mediated inhibition allowing Nrf2 to translocate to the nucleus where it binds ARE sites and causes transcription of its downstream targets.

Figure 1.6: Overview of the effect of DJ-1 on signaling and transcription

Figure 1.6 Overview of the effect of DJ-1 on intracellular signaling and transcription. Figure split according to DJ-1's role in inhibiting apoptotic signals, inducing pro-survival signals, and stimulating oxidative response pathways.

Figure 1.7: Overview of NF-κB activation by TNFα

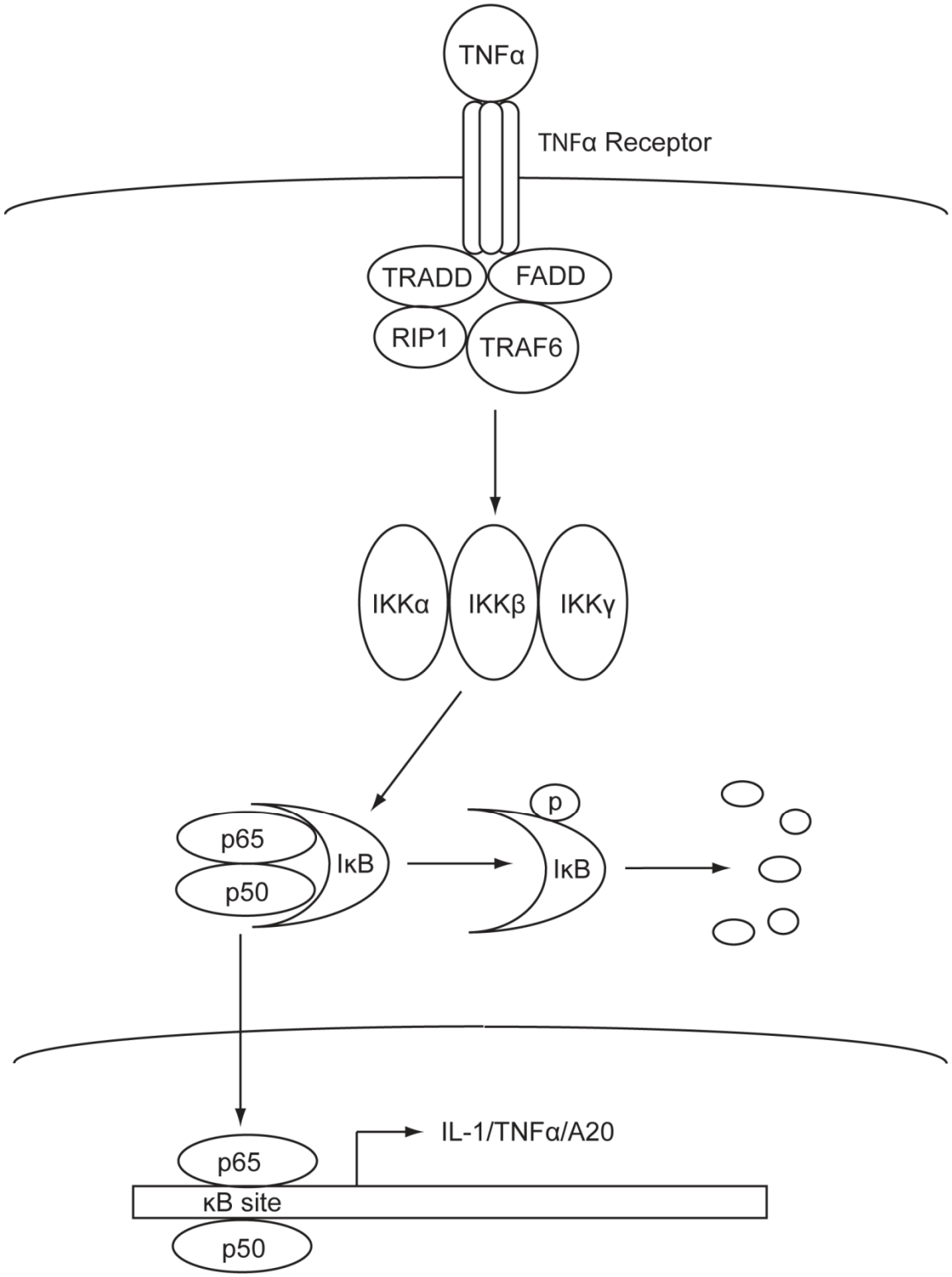

Figure 1.7 Overview of NF-κB activation by TNFα. Binding of TNFα to its receptor causes the recruitment of RIP1, TRAF6, TRADD, and FADD. These proteins activate the IKKα/β/γ complex which phosphorylates and causes the degradation of IκB. Release of IκB-mediated inhibition of p65/p50 allows these NF-κB subunits to translocate to the nucleus, bind κB sites, and induce transcription of their targets.

Figure 1.8: Comparison of Cezanne and A20 RNA Rxpression Profiles

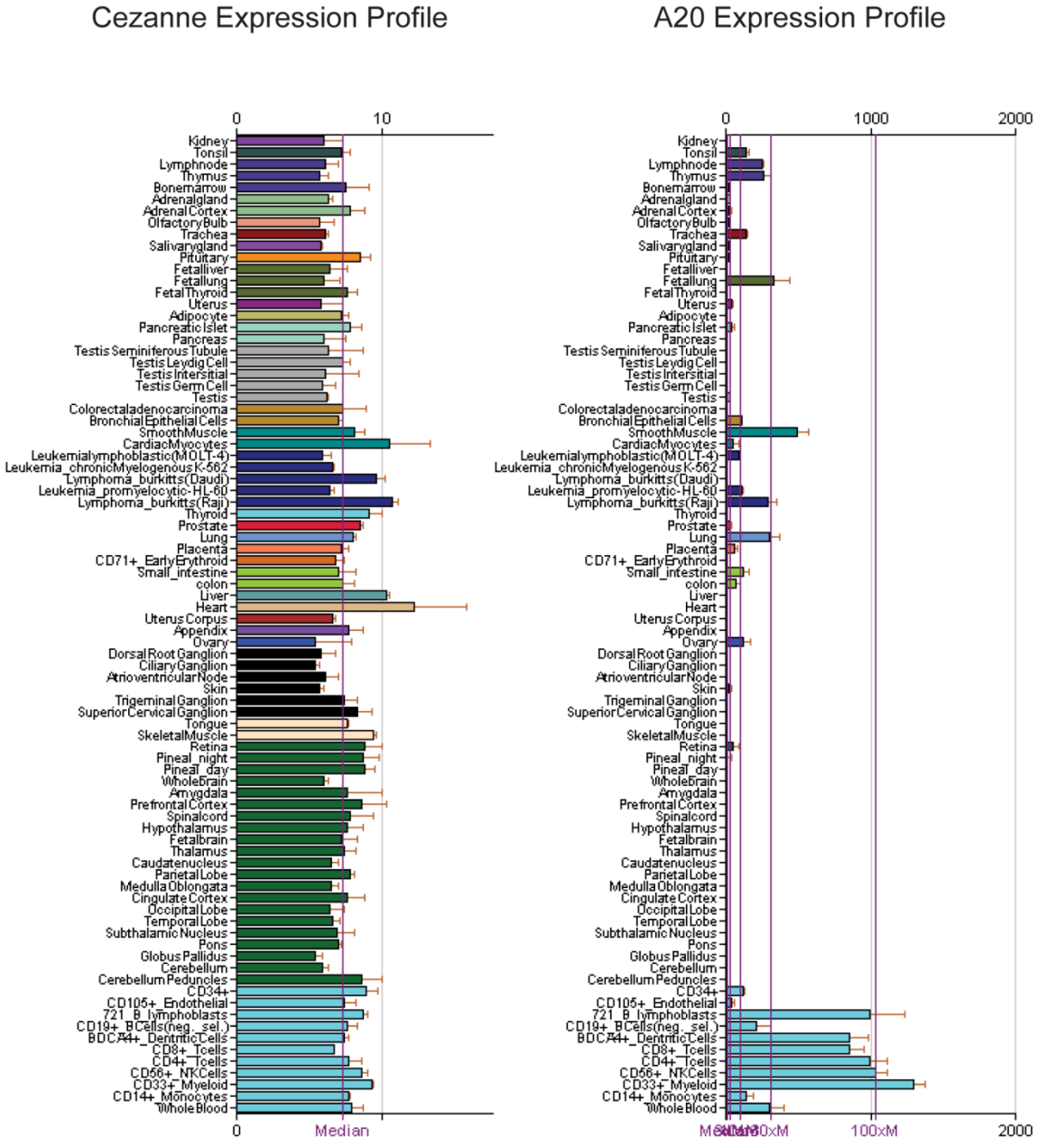

Figure 1.8 Comparison of the expression profiles of Cezanne and A20. Data mined from Novartis GeneAtlas shows the wide RNA expression profile of Cezanne versus A20, which is found primarily in immune cell types (http://biogps.gnf.org/#goto=welcome).

Figure 1.9: Nrf2 and NF-κB pathway crosstalk mechanisms

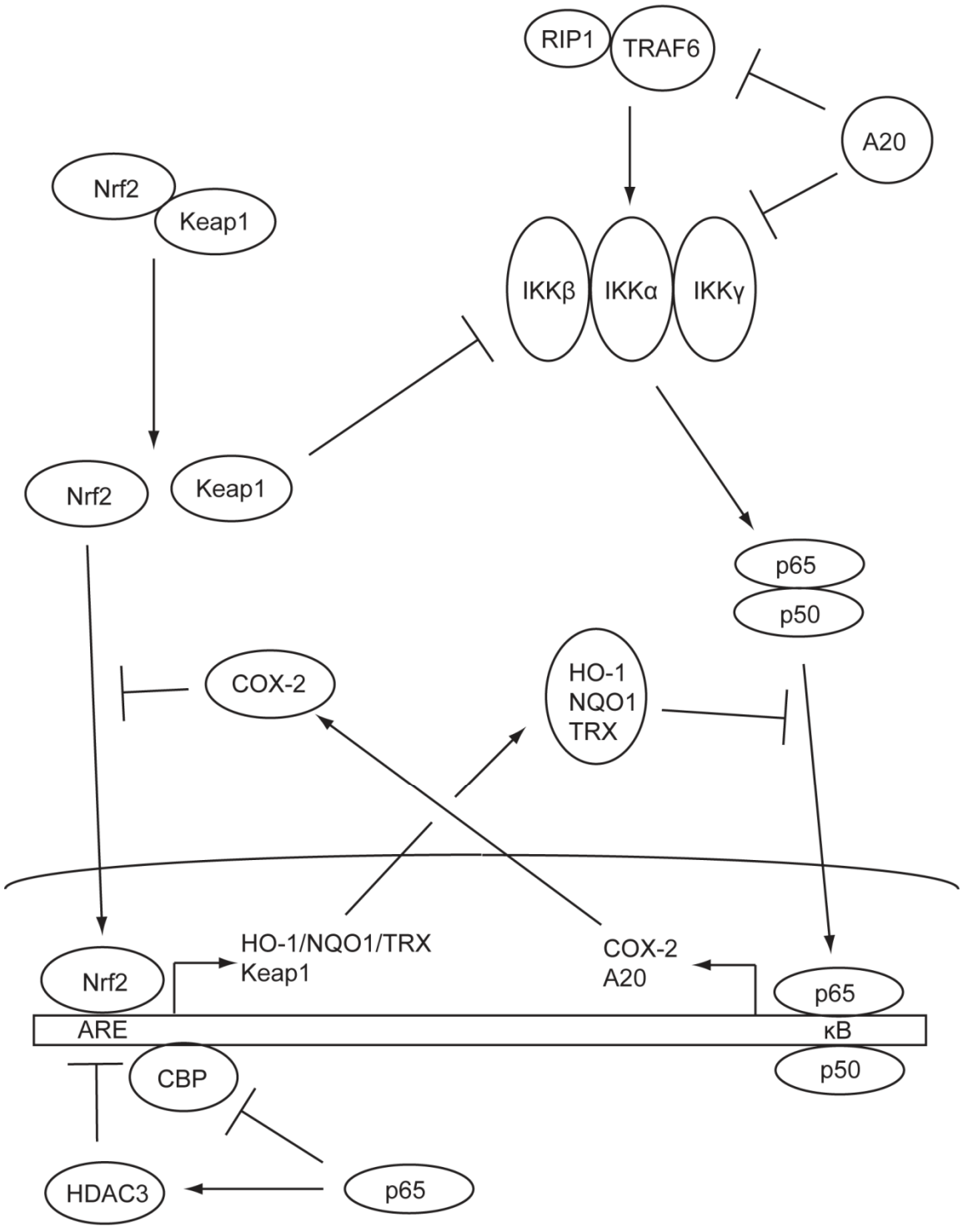

Figure 1.9 Overview of known Nrf2 and NF-κB crosstalk mechanisms. Nrf2 indirectly inhibits NF-κB through its downstream targets, namely Keap1, HO-1, TRX, and NQO1. While NF-κB indirectly inhibits Nrf2 through COX-2, it also directly inhibits Nrf2 through the binding of CBP and the recruitment of HDAC3 to ARE sites.

Chapter II

NOVEL REGULATORY ROLE OF DJ-1 IN CELL SURVIVAL THROUGH THE DIRECT BINDING OF CEZANNE, A NEGATIVE REGULATOR OF NF-KB

2.1 Abstract

Heightened DJ-1 expression is associated with a reduction in chemotherapeutic-induced cell death and poor prognosis in several cancers, while the loss of DJ-1 function is found in a subgroup of Parkinson's disease associated with neuronal death. This chapter describes a novel pathway by which DJ-1 modulates cell survival. Mass spectrometry detected that DJ-1 interacts with BBS1, CLCF1, MTREF, and Cezanne. Among these, Cezanne is a known de-ubiquitination enzyme that inhibits NF-κB activity. DJ-1/Cezanne interaction is confirmed by co-immunoprecipitation of overexpressed and endogenous proteins, maps to the N-terminal 70 residues of DJ-1, and leads to the inhibition of Cezanne's de-ubiquitinating activity. Microarray profiling of shRNA transduced cells shows that DJ-1 and Cezanne regulate *IL-8* and *ICAM-1* expression in opposing directions. Similarly, DJ-1 enhances NF-κB nuclear translocation and cell survival while Cezanne reduces these outcomes. Analysis of mouse *Park7*$^{-/-}$ primary cells confirms the regulation of ICAM-1 by DJ-1 and Cezanne. As NF-κB is important in cellular survival and transformation, IL-8 functions as an angiogenic factor and pro-survival signal, and ICAM-1 has been implicated in tumor progression, invasion, and metastasis; these data provide an additional modality by which DJ-1 controls cell survival and possibly tumor progression via interaction with Cezanne.

2.2 Introduction

Lung cancer is the leading cause of cancer-related mortality in the world. It is estimated that over 215,000 new cases were diagnosed in the United States in 2008 alone (9). Of the two major types of lung cancer, approximately 85% are non-small cell lung carcinomas (NSCLC) (10). With NSCLC, the best chance for a long-term cure is surgery. Unfortunately, 70% of NSCLC patients are contraindicated for surgery due to locally invasive or metastatic disease (11). For these patients, the current treatment options are combination chemotherapy and radiation. With treatment, NSCLC patients have a 5 year survival rate of 15%. It is therefore imperative to investigate new pathways to target in NSCLC therapies. Our work in the H157 NSCLC squamous cell line has focused on the role of DJ-1.

DJ-1 activity is associated with a spectrum of human disease. Loss of DJ-1 activity, due to inactivation by L166 residue mutation or genetic deletion, leads to early onset Parkinson's disease with high penetrance (30). Due to DJ-1's protective effects against toxic insults, this association is hypothesized to be due to a protective role of DJ-1 in dopaminergic neurons of the substantia nigra (37, 38, 44). As loss of DJ-1 activity leads to neuronal cell death, increased DJ-1 activity can promote cell survival leading to its association with human malignancies. The initial research on the role of DJ-1 in cancer showed that while DJ-1 can weakly transform cells alone, it can act synergistically in combination with Ras (1). DJ-1 is highly expressed in a number of cancer types including acute leukemia, breast, prostate, ovarian, thyroid, and NSCLC and is associated with tumor progression in esophageal and cervical cancer (4, 7, 8, 15, 171-173). Our lab and others have shown that increased DJ-1

expression confers protection against toxic insults including oxidative and ER stress, proteosome inhibition, and chemotherapeutic agents (3, 58, 174). This protection is partially mediated by DJ-1's ability to inhibit p53 and PTEN, an inhibitor of the PI3K cell survival pathway, and to positively regulate the Nrf2 detoxification pathway (15, 48, 50). Here we examine a novel pathway in which DJ-1 binds to and inhibits Cezanne, a negative regulator of the cell survival associated transcription factor NF-κB.

Cezanne is a member of the A20 family of de-ubiquitination enzymes (148). Similar to A20, Cezanne has been shown to inhibit NF-κB through modulation of the ubiquitination state of two of its positive regulators, RIP-1 and TRAF6 (148, 149). Cezanne is implicated in cancer biology, as a 93-kb sequence containing Cezanne was shown to be duplicated in acute lymphoblastic leukemia and Burkitt lymphoma (150). While the precise role of Cezanne in cancer is unknown, its inhibition of NF-κB would suggest Cezanne may act as a tumor suppressor.

While typically associated with regulating the inflammatory response to infection or injury, NF-κB subunits are constitutively activated in a number of human carcinomas (113, 175, 176). This family of transcription factors is important in cancer biology for cell survival, angiogenesis, invasion, progression, and metastasis. Two important targets of NF-κB-mediated transcription in relation to cancer are interleukin 8 (*IL-8*) and intercellular adhesion molecule 1 (*ICAM-1*). These two proteins are involved in the homing and extravasation of neutrophils from the blood into inflamed tissues but have additional functions in cancer biology. IL-8 expression has been associated with cancer progression, invasion, angiogenesis, and

metastasis (121-127). It is also secreted by certain NSCLC cell lines, including H157 cells, in response to Paclitaxel treatment activating a pro-survival positive feedback loop via signaling through the CXCR1 receptor (13, 129). Blockade of IL-8 binding to its receptor causes a decrease in tumor size, angiogenesis, tumor growth, and metastasis while promoting cancer cell apoptosis (130). ICAM-1 is overexpressed in multiple human cancers as well (131-133). While it has not been associated with effects on cancer cell survival, ICAM-1 has been linked to both tumor progression and metastasis through its ability to mediate cell adhesion and extravagation (127, 134, 135).

In this study, we identify Cezanne as a binding partner of DJ-1. This interaction can be mediated by the amino terminus of DJ-1 and leads to the inhibition of Cezanne's de-ubiquitinating activity *in vitro*. Microarray analysis on H157 cells shows that DJ-1 and Cezanne shRNA regulate IL-8 and ICAM-1 gene expression, albeit in opposing directions. DJ-1 and Cezanne shRNA also resulted in reciprocal phenotypes on chemotherapeutic-induced cell death and NF-κB nuclear localization *in vitro*. Finally we analyzed ICAM-1 expression in *Park7* $^{-/-}$ mouse embryonic fibroblasts (MEF) to verify that this pathway is intact in a primary cell line. These findings identify a novel pathway through which DJ-1 modulates a number of critical aspects of cancer cell biology. This work emphasizes the importance of future research on pharmacologic inhibitors of the DJ-1/Cezanne pathway and the role of DJ-1 in cancer biology *in vivo*.

2.3 Results

Q-TOF Mass Spectrometric Identification of DJ-1 Interacting Proteins

To help understand the mechanism of action of DJ-1, we used Q-TOF mass spectrometry to identify binding partners of DJ-1. Several controls were built into the experimental design to minimize artifacts. First, previous published data have highlighted the importance of oxidative state on DJ-1 function (177). Therefore, we designed our initial experiments to identify proteins that bound DJ-1 under oxidative and non-oxidative conditions (Fig. 2.1A). Second, we used *Park7* $^{-/-}$ MEFs to eliminate the ability of the abundantly-expressed endogenous DJ-1 to bind proteins of interest and decrease the assay sensitivity. To start, we transfected *Park7* $^{-/-}$ MEFs with either FLAG™-tagged DJ-1 or FLAG™-tagged C106A mutant DJ-1. Since the C106 residue is known to be oxidized and affect DJ-1 function, the C106A mutant was used to assess the oxidative dependence of binding as alanine is non-oxidizable (61). To mimic physiologic oxidative stress, the transfected samples were then treated with H_2O_2 or left untreated. After treatment, the FLAG™-tagged DJ-1 was immunoprecipitated and eluted with FLAG™ peptide. This eluate was trypsinized and run on a Q-TOF mass spectrometer. Using a mock transfected control to remove any proteins that bound non-specifically to the FLAG™ beads, we identified four proteins that bound specifically to DJ-1 (Table 2.1). We selected Cezanne for further study due to its known ability to regulate NF-κB and therefore

potential to affect cell survival, a topic relevant to cancer biology and Parkinson's disease (Fig. 2.1B).

DJ-1 Binds to Cezanne and Inhibits Its De-ubiquitinating Activity

To confirm the interaction between DJ-1 and Cezanne, we performed a series of co-immunoprecipitation experiments. The interaction was first confirmed using an overexpression system (Fig. 2.2A). FLAG™-DJ-1 was overexpressed in HEK293T cells in the presence or absence of V5-epitope tagged Cezanne. After immunoprecipitation of Cezanne, DJ-1 was co-immunoprecipitated in the presence of Cezanne but not in its absence as detected by immunoblot. To confirm an endogenous interaction between DJ-1 and Cezanne (Fig. 2.2B), we immunoprecipitated endogenous DJ-1 from cell lysates of HEK293T cells treated with H_2O_2 or left untreated. Western blot of the immunoprecipitation samples showed the presence of endogenous Cezanne only in the samples where DJ-1 was immunoprecipitated. Our previous Q-TOF MS data would predict an increase in DJ-1/Cezanne interaction with H_2O_2 treatment, but a modest increase with treatment was detected with only one anti-Cezanne antibody in HEK293T cells as compared to data obtained in MEFs. This suggests that there might be a form of Cezanne that is recognized by antibody 2 which more efficiently interacts with oxidized DJ-1.

To verify the effect of DJ-1 C106 residue oxidation, we tested the ability of overexpressed wild type DJ-1, non-oxidizable C106A mutant DJ-1, or the Parkinson's disease associated L166P mutant DJ-1 to bind endogenous Cezanne in

the presence of H_2O_2 (Fig. 2.2C). Each of the three constructs was overexpressed in HEK293T cells treated with H_2O_2. As expected, lower expression of L166P DJ-1 was seen due to its known decreased stability (178). After immunoprecipitation for the FLAG™-tagged DJ-1 proteins, immunoblot analysis was performed to detect endogenous Cezanne. Cezanne was co-immunoprecipitated with wild type DJ-1 and the L166P mutant. The C106A mutant DJ-1 co-precipitated Cezanne at a reduced level compared to wild type DJ-1 but more than the untransfected negative control. This datum shows that oxidation of the C106 residue of DJ-1 is not required but does enhance DJ-1/Cezanne interaction while mutation of the L166P residue has no effect.

To identify the structural element of DJ-1 that binds Cezanne, we produced a series of truncation mutant constructs by sequentially removing approximately 100 bp off of the 3' end of the 570 bp open reading frame of DJ-1 in a FLAG™-tagged construct (Fig. 2.2D). This method was used due to the lack of multiple domain structures in DJ-1. These constructs were transfected into HEK293T cells treated with H_2O_2 and the samples were immunoprecipitated with FLAG™ agarose. Expression of the smaller amino terminal fragments of DJ-1 showed a progressively reduced expression, which is consistent with the smaller sizes of the truncation constructs DJ-1 490T to 298T, except for DJ-1 211T which displayed a reduction in expression that cannot be accounted for by its reduced size, which may be due to reduced expression or decreased stability (73). All of the truncation constructs immunoprecipitated Cezanne as well as the WT control. The efficient interaction of 211T DJ-1 and endogenous Cezanne shows that the amino-terminal 70 residues of

DJ-1 are sufficient for interaction with Cezanne. Residues encoded by nucleotides 298 to 211 might be inhibitory of this binding as their removal results in more efficient binding, considering that the expression of DJ-1 211T is much less than DJ-1 298T (Fig. 2.2E).

Due to the known de-ubiquitinating activity of Cezanne *in vitro* and the interaction between DJ-1 and Cezanne, we produced recombinant DJ-1 and analyzed its effect on the de-ubiquitination activity of Cezanne in a cell-free system (Fig. 2.2F). To assess Cezanne's de-ubiquitinating activity, we incubated synthetic ubiquitin chains with recombinant Cezanne in the presence or absence of DJ-1 (148). After incubation, we analyzed the reduction in ubiquitin chain size by Western blot. While Cezanne caused a decrease in both long and medium length ubiquitin chains (Lanes 2 and 3), DJ-1 significantly inhibited Cezanne's activity in a dose-dependent manner (Lanes 4-6). The activity of DJ-1 was found to be specific for Cezanne as DJ-1 did not inhibit the de-ubiquinating activity of IsoT on long length ubiquitin chains (Lanes 7 and 8).

Identification of IL-8 and ICAM-1 as Downstream Targets by Affymetrix Microarray

Due to the known effects of DJ-1 and Cezanne on the transcriptome, we assessed the effect of their interaction on global transcription using microarray. To identify possible downstream transcripts of DJ-1 and Cezanne, we generated recombinant lentivirus encoding shRNA oligonucleotides specific for DJ-1 or

Cezanne and their respective mutant negative controls. After transduction of H157 cells with recombinant lentivirus, we extracted RNA from each sample and assessed targeted gene expression using semi-quantitative RT-PCR (Fig. 2.3A). These samples showed significant reduction of *Cezanne* and *DJ-1* gene expression compared to matched negative controls. The RNA was then validated for microarray, used to produce cRNA, and hybridized on a GeneChip human gene 1.0 ST array. The normalized intensities for the three negative controls were averaged. We then filtered out any readings below 20th percentile intensity and calculated fold changes comparing the DJ-1 and Cezanne knockdown samples against the control using a 1.7 fold change cutoff. Due to our interest in genes regulated by both DJ-1 and Cezanne, we cross-referenced the lists of genes regulated by DJ-1 or Cezanne (Fig. 2.3B and Table 2.2). This search showed that *IL-8* and *ICAM-1*, two genes regulated by NF-κB, were reciprocally controlled by DJ-1 and Cezanne (Fig. 2.3C), while no role for Cezanne was seen in Nrf2-mediated transcription (Fig. 2.4).

DJ-1 and Cezanne affect IL-8 and ICAM-1 mRNA and Protein Levels

To verify the microarray results, we used real time PCR to verify the regulation of IL-8 and ICAM-1 by DJ-1 and Cezanne. After transducing H157 cells with lentivirus carrying control, DJ-1, or Cezanne shRNA, real time PCR was performed for human *β-actin*, *IL-8*, and *ICAM-1* (Fig. 2.5A). Data analysis yielded C_t values that were used to calculate fold changes for IL-8 and ICAM-1 as compared to the matched β-*actin* control using the $\Delta\Delta C_t$ method. This analysis confirmed a

significant decrease in IL-8 and ICAM-1 expression with DJ-1 shRNA and an increased expression of these genes with Cezanne shRNA, consistent with the microarray results. To assess the effect of DJ-1 and Cezanne on IL-8 secretion, supernatants from lentiviral transduced H157 cell lines were analyzed using IL-8 ELISA. The datum showed DJ-1 shRNA decreased IL-8 production while Cezanne shRNA increased IL-8, matching the observations seen at the transcript level (Fig. 2.5B). Immunoblot analysis of transduced H157 cells treated with TNF-α showed a decrease in ICAM-1 protein levels with DJ-1 shRNA and an increase in ICAM-1 levels with Cezanne shRNA consistent with the IL-8 ELISA data (Fig. 2.5C).

As NF-κB is a known target of Cezanne as well as an inducer of IL-8 and ICAM-1 transcription, we evaluated the nuclear localization of NF-κB in DJ-1 and Cezanne shRNA treated H157 cells. After transduction with DJ-1 or Cezanne shRNA, nuclear and cytoplasmic fractions were collected and analyzed by immunoblot. Immunoblot for the p65 NF-κB subunit showed that DJ-1 shRNA caused a decrease in nuclear p65 compared to the shRNA control, while Cezanne shRNA treated samples caused increased nuclear p65 (Fig. 2.5D). Immunoblot for histone deacetylase 2 (HDAC2) and β-actin were used to show equal loading and nuclear fraction purity respectively.

Due to the known pro-survival effect of DJ-1 overexpression on cancer cells undergoing chemotherapeutic treatment (3), we assessed the effect of DJ-1 and Cezanne shRNA on chemotherapeutic-induced H157 cell death. We treated lentiviral transduced H157 cells with Paclitaxel and MEK inhibitor for 24 hours, a combination treatment shown to be effective in H157 cells (3). After treatment, cell

death was analyzed using a histone-based cell death ELISA (Roche). Untreated samples were used to account for homeostatic cell turnover and fold changes in cell death were calculated compared to the mutant shRNA control. A statistically significant increase in cell death was seen with DJ-1 shRNA, while a decrease was seen in the Cezanne shRNA samples (Fig. 2.5E). Similar results were obtained using the fluorescence-based Toxilight (Lonza) cell death assay (data not shown).

ICAM-1 is Regulated by DJ-1 and Cezanne in Primary MEFs

The above results were obtained with transformed cell line, thus it was important to analyze the expression of ICAM-1 in a primary cell line such as MEFs. Only ICAM-1 was assayed since mouse cells do not express IL-8. *Park7* $^{+/+}$ and *Park7* $^{-/-}$ MEFs were treated with increasing levels of TNFα to induce ICAM-1 expression. After 6 hours of TNFα treatment, the levels of *ICAM-1*, *DJ-1*, and *GAPDH* were assessed by semi-quantitative PCR (Fig. 2.6A). *DJ-1* was expressed in *Park7*$^{+/+}$ but not *Park7*$^{-/-}$ cells and the expression of *ICAM-1* was reduced in the *Park7*$^{-/-}$ cells relative to *GAPDH* control. This finding confirms the positive regulatory role of DJ-1 in *ICAM-1* transcript expression in primary MEFs. To assess the effect of Cezanne on ICAM-1 expression in this cell type, ICAM-1 expression was measured by real-time PCR in TNF-α treated or untreated *Park7* $^{+/+}$ MEFs transduced with Cezanne shRNA or a matched mutant control (Fig. 2.6B). Cezanne shRNA caused an increase in ICAM-1 expression in TNFα treated MEFs.

These data confirmed an activating role of DJ-1 and an inhibitory role of Cezanne on ICAM-1 expression in MEFs.

2.4 Discussion

Due to the prominent link between DJ-1 genetic inactivation and early onset Parkinson's disease in humans, a large portion of the DJ-1 literature has focused on the role of DJ-1 in neuronal cell death (31, 36). That work uncovered a broader role of DJ-1 in cell survival outside of the nervous system. DJ-1 has been shown to be a central molecule in cell survival by positively regulating Nrf2-dependent detoxification pathways (50), inhibiting p53-mediated cell cycle checkpoints (48), and inducing Akt activity through the inhibition of PTEN (15). Likely due to its effects on cell survival, DJ-1 has been found to be dysregulated in several human cancers (1, 3, 7, 172). Overexpression of DJ-1 has been shown in a number of human carcinomas and is associated with negative survival outcomes and resistance to chemotherapeutics.

In this chapter, we identify a novel pathway by which DJ-1 modulates IL-8 and ICAM-1 levels through the regulation of Cezanne and NF-κB activity. Using a proteomic approach, we identify four binding partners of DJ-1. One of these DJ-1 binding partners, Cezanne, is a member of the A20 family of immunoregulatory de-ubiquitinating enzymes. Similar to A20, Cezanne is known to inhibit NF-κB through modulation of the ubiquitination status of RIP-1 and TRAF6 (148, 149) . NF-κB, a cell survival-associated transcription factor, is known to be dysregulated in a variety of cancer types including NSCLC (113, 175, 176, 179). After confirming endogenous interaction of DJ-1 and Cezanne, we showed that the amino-terminus

of DJ-1 is capable of mediating this interaction. The interaction also leads to the inhibition of Cezanne's de-ubiquitinating activity *in vitro*. We used microarray analysis to identify the transcriptional targets and thus the pathways regulated by the DJ-1/Cezanne interaction. DJ-1 and Cezanne shRNA were found to reciprocally regulate ICAM-1 and IL-8. As targets of NF-κB, this datum suggests a role of DJ-1 and Cezanne in NF-κB-mediated transcription while no role of Cezanne was seen in Nrf2-mediated transcription as downstream targets of Nrf2 were unchanged in the presence of Cezanne shRNA. This link between DJ-1 and NF-κB was confirmed as nuclear p65 was found to be decreased in the presence of DJ-1 shRNA, making this work the first to identify DJ-1 as a positive regulator of NF-κB.

IL-8 is released by a subset of NSCLC cell lines in response to chemotherapy treatment (13). As a pro-survival signal, this IL-8 release can inhibit chemotherapeutic efficacy (126). Acting in an autocrine or paracrine fashion to activate NF-κB through stimulation of the CXCR1 receptor, IL-8 causes its continued release completing a pro-survival positive feedback loop (13, 129). Through inhibition of DJ-1 or activation of Cezanne, we can disrupt this IL-8 controlled pro-survival loop, thus increasing the sensitivity of IL-8 secreting tumors to chemotherapeutics (130). Aside from its effects on cell survival, IL-8 has been shown to promote angiogenesis, cancer progression, invasion, and metastasis (121, 123-127). Concordant with IL-8, ICAM-1 dysregulation has been associated with tumor progress, invasion, and metastasis (127, 134, 135). Through regulation of IL-8 and ICAM-1, DJ-1 and Cezanne may impact angiogenesis and tumor progression

leading to changes in tumor growth and survival in *in vivo* cancer models separate from their effects on cell survival and drug efficacy seen *in vitro*.

As a whole, we identified a pathway pertinent to cancer cell survival that is regulated by DJ-1. Future studies should confirm that this pathway is mediated through Cezanne's de-ubiquitination of RIP-1 and TRAF6 as well as identify other NF-κB targets regulated by DJ-1 under cell stimulation. Finally, mouse tumor models will be necessary to examine the effects of DJ-1 and Cezanne expression on tumor growth *in vivo*. Due to the central role of DJ-1 in transcriptional regulation, identification of DJ-1 inhibitors may lead to novel treatment regimens that modulate cancer hallmarks including cancer cell growth, survival, angiogenesis, progression, invasion, and metastasis as well as boosting current chemotherapeutic efficacy.

2.5 Materials and Methods

Cell culture, treatments, and plasmid constructs. H157 cells were grown in RPMI 1640 (Gibco) with 10% FCS (Hyclone). HEK293T cells and MEFs were grown in high glucose DMEM (Gibco) with 10% FCS. MEFs were isolated from 13.5 day embryos and used within 3 passages from initial isolation. All mammalian cell cultures were incubated at 37° C with 5% CO_2 in the presence of penicillin and streptomycin to prevent bacterial contamination. H_2O_2 (Sigma) was diluted in media prior to addition to cells at a final concentration of 100μM for 1 hour. TNF-α (eBioscience) was added to sample wells at a final concentration of 5-50 ng/mL for 6 hours before sample harvest. For cell death assays, Paclitaxel and U0126 (Sigma) reconstituted in DMSO were used at 500nM and 10μM respectively.

Human Cezanne ORF was subcloned into the V5/His-tagged pcDNA3.1D-Topo plasmid (Invitrogen) using the primers 5'-CACCATGACCCTGGACATGGATGCTG-3' and 5'-GAACCTGTGCACCAGGAGCT-3'. Directionality and expression were verified by sequencing and immunoblot analysis respectively. The FLAG™-DJ-1 construct was generously given to us by Hod, Y (172). The point and truncation mutants of FLAG™-DJ-1 were produced using Quik-change mutagenesis (Stratagene) and verified by sequencing. MEF cultures were transfected using Lipofectamine 2000 (Invitrogen) at a 4:1 reagent to DNA ratio and HEK293T cultures were transfected using Fugene 6 (Roche) at a 3:1 ratio as per the manufacturer's instructions.

Q-TOF Mass Spectrometry. *Park7* $^{-/-}$ MEFs were transfected with either FLAG™-DJ-1 or C016A- FLAG™ and incubated overnight. After H_2O_2 or vehicle control treatment, samples were lysed in 0.5% Tx-100 lysis buffer and immunoprecipitated with anti-FLAG™ M2 agarose (Sigma). After elution with FLAG™ peptide, samples were desalted using a C4 Reverse-phase media loaded micropipette tip (Millipore, Billerica MA). The desalted proteins were eluted from the tip using a solution of 80% methanol with 0.1% formic acid then lyophilized to dryness. After reconstitution in 25mM ammonium bicarbonate, the protein samples were enzymatically digested with sequencing-grade trypsin (Promega, Madison WI). The tryptic peptides were analyzed by nano LC-MS/MS using a Waters (Millford, MA) API-US Q-TOF, equipped with a Waters capLC system and a 75μ id x 15 cm PepMap C18 column (Dionex, Sunnyvale CA). The Q-TOF data was processed using Waters' MassLynx and ProteinLynx software, and searched against the NCBInr mouse database for possible protein matches using the Mascot™ (Boston, MA) database search engine. The search parameters include a peptide mass tolerance of +/- 200 ppm, fragment mass tolerance of +/- 0.2 Da, trypsin as the enzyme with 1 possible missed cleavage.

Lentiviral Vector Construction and Production. Oligonucleotides containing 19-mers targeting DJ-1 (5'-GACCCAGUACAGUGUAGCC-3'), human Cezanne (5'-GATCATGAATGGAGGAATA-3' and 5'- GCAGCAAGCTCAAGAAGAA-3'), mouse Cezanne (5'- GGCGGAAGGAGAAGTCAAA-3'), or non-silencing controls (5'-GACGCTGAAGACTCTTGGC-3', 5'- GATGAAGTAAGCACGTAAA -3', 5'-

GCACCTACCACTACATGTA-3') with appropriate start (5'- TCCGCTCGAGAAAAA-3'), loop (5'- TCTCTTGAA-3'), antisense, and termination (5'-GGTGTTTCGTCCTTTCCACAAGATATATAAAGCC-3') sequences were synthesized (IDT) and cloned into FG12 vectors (Qin PNAS 2003). Lentiviral particles were then produced by co-expressing the FG12 constructs with lentiviral VSVg, Rev, and GAGPOL vectors in HEK293T cells (180, 181). Lentiviral transduction and gene expression were assessed by GFP fluorescence and semi-quantitative RT-PCR for *DJ-1*, *Cezanne*, and *β-actin* respectively.

Affymetrix Analysis. RNA was harvested from H157 cells transduced with DJ-1, Cezanne, or mutant control shRNA lentivirus using the RNeasy RNA extraction kit (Qiagen). After RNA quality assessment using an Agilent Bioanalyzer (Agilent), a custom cDNA kit was used with a T7-(dT)24 primer to produce cDNA (Life Technologies). Biotinylated cRNA was then generated from the cDNA using the BioArray High Yield RNA Transcript Kit (Enzo Biotech). The cRNA was then fragmented in 40mM Tris-acetate, pH8.1, 100mM KOAc, 30mM MgOAc at 94oC for 35 minutes before the chip hybridization. The cRNA was added to a hybridization cocktail (50 pM control oligonucleotide B2, BioB, BioC, BioD, and cre hybridization controls, 0.1 mg/ml herring sperm DNA, 0.5 mg/ml acetylated BSA, 100mM MES, 1M Na+, 20mM EDTA, 0.01% Tween 20) and hybridized for 16 hours at 45°C on a GeneChip Human Gene 1.0 ST Array (Affymetrix). The arrays were washed and stained with R-phycoerythrin streptavidin in the GeneChip Fluidics Station 400 (Affymetrix). After this, the arrays were scanned with the Hewlett Packard

GeneArray Scanner (HP). Affymetrix GeneChip Microarray Suite 5.0 software was used for washing, scanning, and basic analysis. Sample quality was assessed by examination of 3' to 5' intensity ratios of certain genes. Final filtering and analysis of the raw data was performed using Genespring GX (Agilent). We eliminated dots with < 20 percentile intensity, averaged the dot intensities of the three mutant control samples, and calculated fold changes on hits shared between the shDJ-1 and shCezanne experimental groups. The fold change cut off was set at > 1.7.

***In vitro* De-ubiquitination Assay.** Vectors for production of recombinant DJ-1 and Cezanne were produced by cloning *DJ-1* and *Cezanne* ORFs into the 6x His-tagged pQE-82L (Qiagen) and pET101D (Invitrogen) vectors respectively. Following transformation into BL21 star (Invitrogen) *E.coli*, log phase bacterial cultures were stimulated with 1 mM Isopropyl β-D-1-thiogalactopyranoside (Sigma) for 5-6 hours. The bacteria were lysed by sonication in the presence of hen egg lysozyme (Sigma) and benzonase (Novagen) and the target recombinant proteins were purified using a Ni-NTA agarose (Invitrogen) column. Recombinant protein expression and purity were assessed by Coomassie staining and Western blot. The K48-linked ubiquitin chains (Ub2-16) and recombinant IsoT were purchased (Biomol). Each sample containing 1μg of ubiquitin chains and the appropriate proteins was incubated at 37°C for 6 hours in de-ubiquitination buffer (50 mM hepes pH 7.8, 0.5mM EDTA, 0.01% Brij 35, 3 mM DTT) and ubiquitin chain degradation was assessed by Western blot.

Western Blot Analysis and Immunoprecipitation. For Western blots, cells were lysed in RIPA buffer with protease inhibitors (Roche). Lysate protein concentrations were assessed by BCA (Pierce) and equilibrated through addition of RIPA buffer, NuPAGE LDS loading buffer (Invitrogen), and DTT. After brief sample boiling, proteins were separated by molecular weight on NuPAGE 4-12% gradient SDS-PAGE gels (Invitrogen) and transferred to a nitrocellulose membrane (Biorad) that was subsequently blocked using 5% non-fat dry milk in TBS with 0.1% Tween-20. Primary antibodies used for blotting were anti-FLAG™ M2-HRP (Sigma), anti-V5-HRP (Invitrogen), anti-β-actin-HRP C11 (Santa Cruz), Cezanne rabbit polyclonal, DJ-1 rabbit polyclonal, HDAC2 (Santa Cruz), anti-ubiquitin P4D1 (Santa Cruz), and anti-ICAM-1 EP1442Y (Abcam). Goat anti-mouse-HRP and goat anti-rabbit HRP antibodies were used as secondary antibodies (Santa Cruz).

Samples for immunoprecipitation were lysed in 0.5% Tx-100 lysis buffer (0.5% Tx-100, 150 mM, NaCl, 50mM Tris, 50mM NaF, 2mM EDTA), cleared by centrifugation, and precipitated overnight with appropriate beads at 4°C. V5-tagged and FLAG™-tagged proteins were precipitated using V5- (Invitrogen) or FLAG™-(Sigma) conjugated beads respectively while endogenous DJ-1 was precipitated using a custom DJ-1 4D1.3 mouse monoclonal antibody and protein A/G beads (Pierce). After overnight incubation, the samples were washed with 0.5% Tx-100 lysis buffer and eluted in 2x LDS loading buffer with DTT at 90°C. Input and eluate samples were then analyzed by Western blot for expression and protein association. Nuclear and cytoplasmic fractionation was performed using the NE-PER fractionation kit (Pierce) as per the manufacturer's instructions.

Real-Time and Reverse Transcriptase semi-quantitative PCR. Real-Time PCR was performed using an ABI 7900HT PCR system (Applied Biosystems) in a 384-well, 15μL sample format with Taqman Universal PCR master mix (Applied Biosystems). Pre-validated Taqman primer and probe sets against human/mouse *ICAM-1*, mouse *GAPDH*, human *IL-8*, and human β-*actin* were purchased from ABI. Real-time runs and data analysis were performed using the SDS software (Applied Biosystems). Total RNA was isolated from cells using RNeasy kits (Qiagen) and quantified using a Nanodrop ND-1000 (Nanodrop). CDNA reactions used 2μg of total RNA with MMLV (Invitrogen) primed with oligo dT (IDT) in the presence of RNasin (Promega). Semi-quantitative PCR was carried out using 2μL of the cDNA reaction with primers against human *DJ-1* (5'- ATGTCATGAGGCGAGCTG-3', 5'-ATTTTGTCTTTAGCAAGAGGG-3'), human *Cezanne* (5'-TGGCAGACACCATGCTGAGGG-3', 5'- CGCTTTGACTTCTCCTTCCGC-3'), human *β-actin* (5'- ATCTGGCACCACACCTTCTACAATGAGCTGCG-3', 5' CATACTCCTGCTTGCTGATCCACATC-3'), mouse *ICAM-1* (5'-CAGTCCGCTGTGCTTTGAGAACTGT-3', 5'-GGTATATCCGAGCTTCAGAGGCAGG-3'), mouse *DJ-1* (5'-GGAGCAGAGGAGATGGAGACAGTGA-3', 5'-CGCGGCTCTCTGAGTAGCTGTAGTGA-3'), and mouse *GAPDH* (5'-CCACTCACGGCAAATTCAACGGCACAG-3', 5'-GTGGCAGTGATGGCATGGACTGTGGTC-3'). The number of cycles run on the Mastercycler (Eppendorf) was dependent on the target (*GAPDH*/β-*actin*, 17; *DJ-1*, 21; *Cezanne*/*ICAM-1*, 25).

Figure 2.1: Overview of Q-TOF mass spectrometry results.

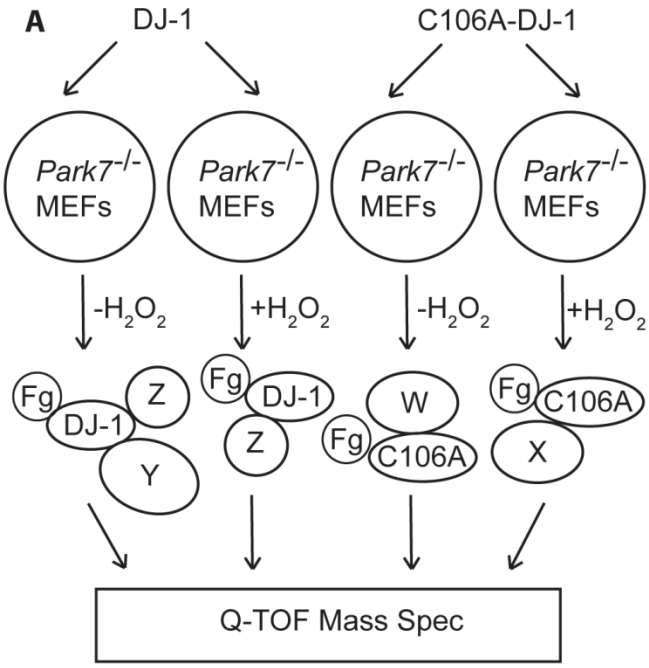

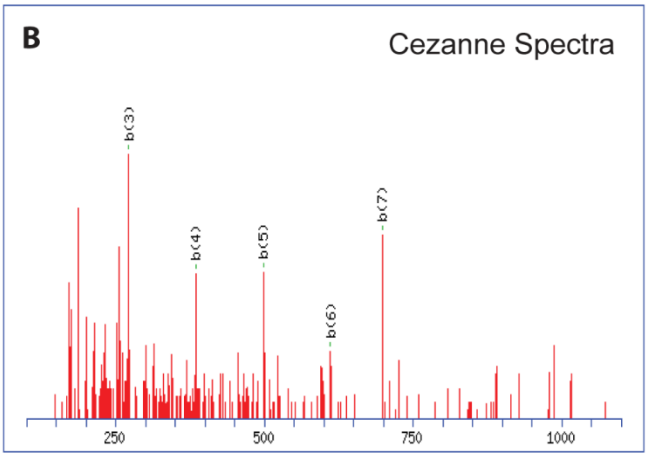

Figure 2.1 Overview of Q-TOF mass spectrometry results. (A) Schematic of Q-TOF MS experimental design. *Park7*$^{-/-}$ MEFs were transfected with FLAG™-tagged DJ-1 or C106A mutant DJ-1 and either left untreated or treated with 100μM H_2O_2 for 1 hour. After treatment, the samples were immunoprecipitated with FLAG™ agarose, eluted with FLAG™ peptide, and analyzed by mass spectrometry. (B) Peptide spectra for Cezanne, one of the four proteins found to interact with DJ-1 shown in Table 1.

Table 2.1 DJ-1-binding proteins identified by mass spectrometry.

Gene	Name	Known Functions
BBS1	Bardet-Biedl syndrome 1	Associated with syndrome characterized by retinitis pigmentosa, polydactyly, and obesity
CLCF1	Cardiotrophin-like cytokine factor 1	Cytokine in Interleukin 6 family
MTREF	MTREF domain containing 1	Mitochondrial transcription termination factor
OTUD7B	Cezanne/Za20d1	De-ubiquitination enzyme, inhibits NF-κB

Figure 2.2: DJ-1 binds to Cezanne and inhibits Cezanne's de-ubiquitinating activity.

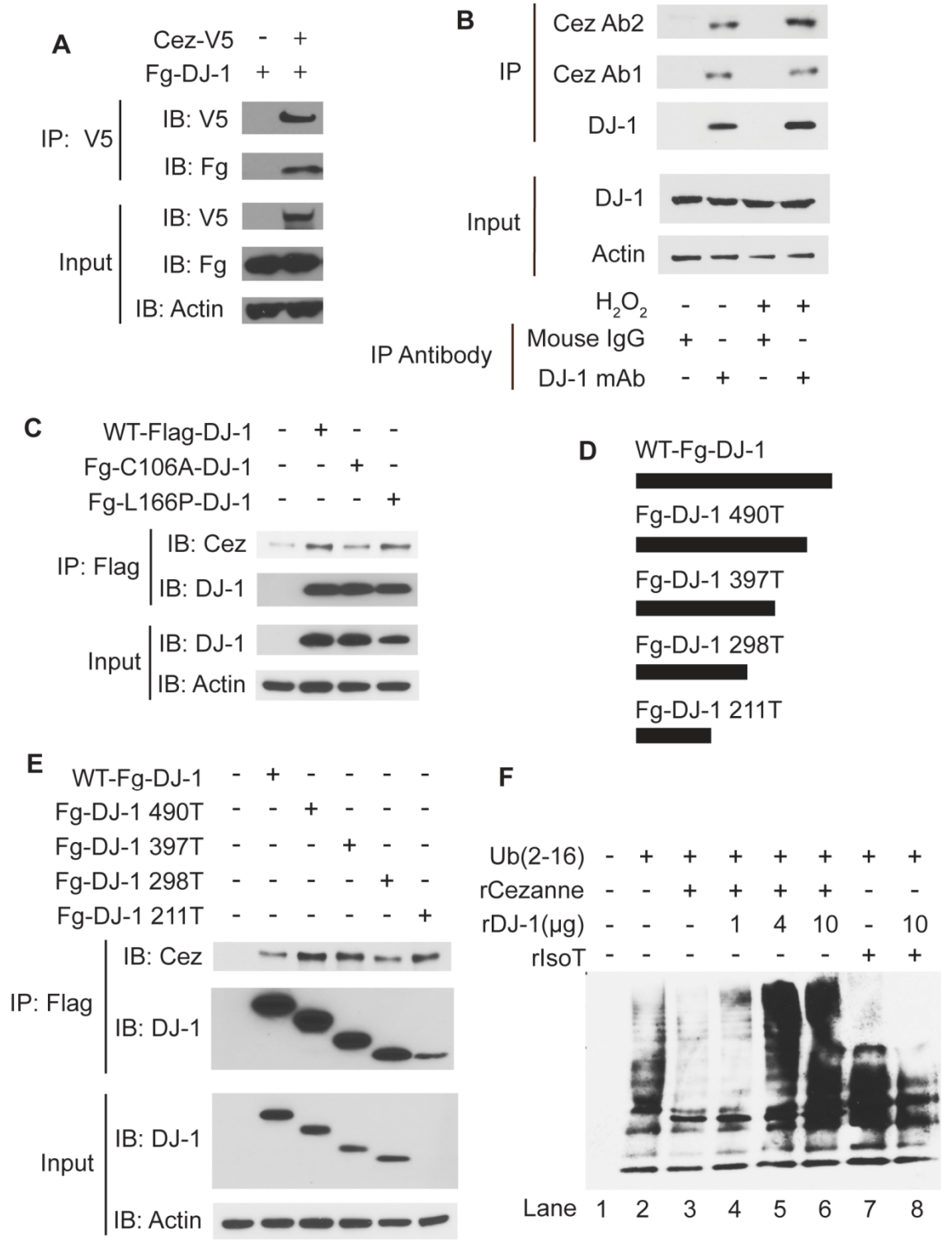

Figure 2.2 DJ-1 binds to Cezanne and inhibits Cezanne's de-ubiquitinating activity. (A) Co-immunoprecipitation to verify interaction between overexpressed DJ-1 and Cezanne. Cells were transfected with FLAG™-epitope tagged DJ-1 in the presence or absence of V5-tagged Cezanne. After immunoprecipitation with anti-V5 agarose, input controls and the IP samples were analyzed by immunoblot with the antibodies indicated. (B) Endogenous co-immunoprecipitation to verify an endogenous interaction of DJ-1 and Cezanne. Cells were either left untreated or treated with 100μM H_2O_2 for 1 hour and immunoprecipitated with either a mouse monoclonal antibody against DJ-1 or mouse control IgG in the presence of protein A/G beads. After immunoprecipitation, input controls and IP samples were analyzed by immunoblot with the indicated antibodies. (C) Hemi-endogenous co-immunoprecipitation to assess the effect of the C106 or L166 mutation on DJ-1's interaction with endogenous Cezanne. Wild type, C106A, and L166P DJ-1 were overexpressed in HEK293T cells. Following a 1 hour 100μM H_2O_2 treatment, the wild type and DJ-1 mutants were immunoprecipitated with FLAG™ agarose and input controls and IP samples were assessed by immunoblot. (D/E) Hemi-endogenous co-immunoprecipitation to identify which portion of DJ-1 binds endogenous Cezanne. DJ-1 truncation mutants shown in (D) were overexpressed in HEK293T cells. After a 1 hour treatment with 100μM H_2O_2, the samples were immunoprecipitated with Flag agarose and immunoblot was used to assess the input controls and IP samples. (F) *In vitro* de-ubiquitination assay. Synthetic ubiquitin chains were incubated with recombinant Cezanne or IsoT in the presence or

absence of DJ-1 at 37°C in assay buffer. After incubation, the samples were analyzed for ubiquitin chain degradation by immunoblot.

Figure 2.3: Microarray analysis of cells with DJ-1 or Cezanne shRNA.

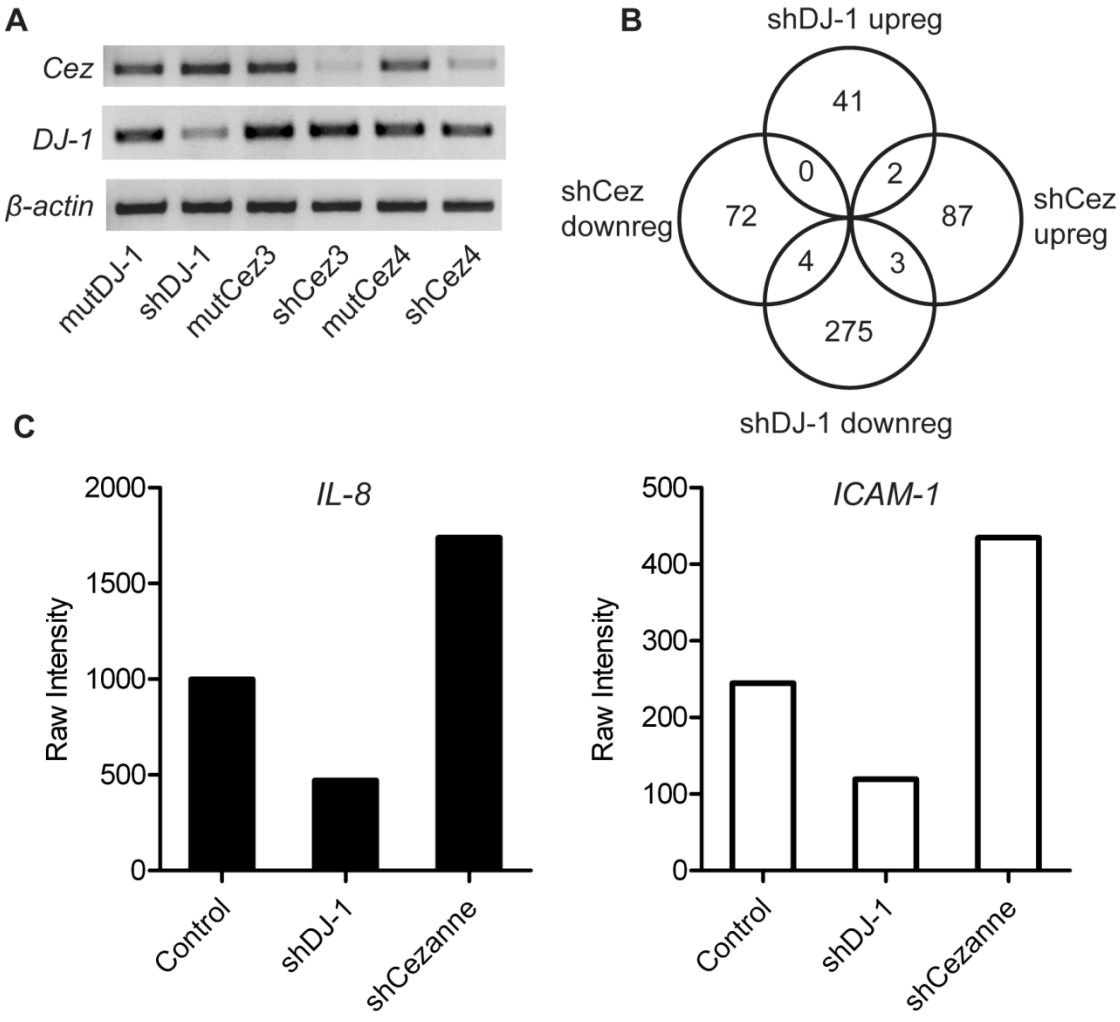

Figure 2.3 Affymetrix microarray analysis of cells with DJ-1 or Cezanne shRNA. (A) Semi-quantitative RT-PCR confirming reduced expression with DJ-1 or Cezanne shRNA in appropriate samples transduced with lentivirus. (B) Venn diagram showing the number of genes up or downregulated with DJ-1 or Cezanne shRNA. The raw intensities of replicate samples were averaged and filters were set for > 20 percentile intensity using a cutoff of > 1.7 fold as compared to the averaged negative control sample. (C) Graph showing the raw intensity results from the microarray after analysis for *IL-8* and *ICAM-1*, the only characterized targets differentially regulated by DJ-1 and Cezanne.

Table 2.2 Overview of genes regulated by DJ-1 and Cezanne.

Genes downregulated with DJ-1 and Cezanne shRNA

Probe	shDJ-1	shCez3	Gene Description
7969339	-1.91	-1.98	
8059186	-1.78	-2.56	Protein tyrosine phosphatase Receptor N
8076094	-1.84	-1.78	
8174985	-2.18	-1.85	SWI/SNF related, matrix assoc, actin-dep regulator of chromatin A1

Genes upregulated with DJ-1 and Cezanne shRNA

Probe	shDJ-1	shCez3	Gene Description
7964834	1.99	2.22	Carboxypeptidase M
8021635	2.70	2.49	Serpin peptidase inhibitor, clade B (ovalbumin), member 2

Genes downregulated with DJ-1 and upregulated with Cezanne shRNA

Probe	shDJ-1	shCez3	Gene Description
8025601	-1.92	1.72	Intercellular adhesion molecule 1 (CD54), human rhinovirus receptor
8091678	-2.04	2.03	Ventricular zone expressed PH domain homolog 1 (zebrafish)
8095680	-1.95	1.84	Interleukin 8

Figure 2.4: Effect of Cezanne shRNA on expression of Nrf2 targets

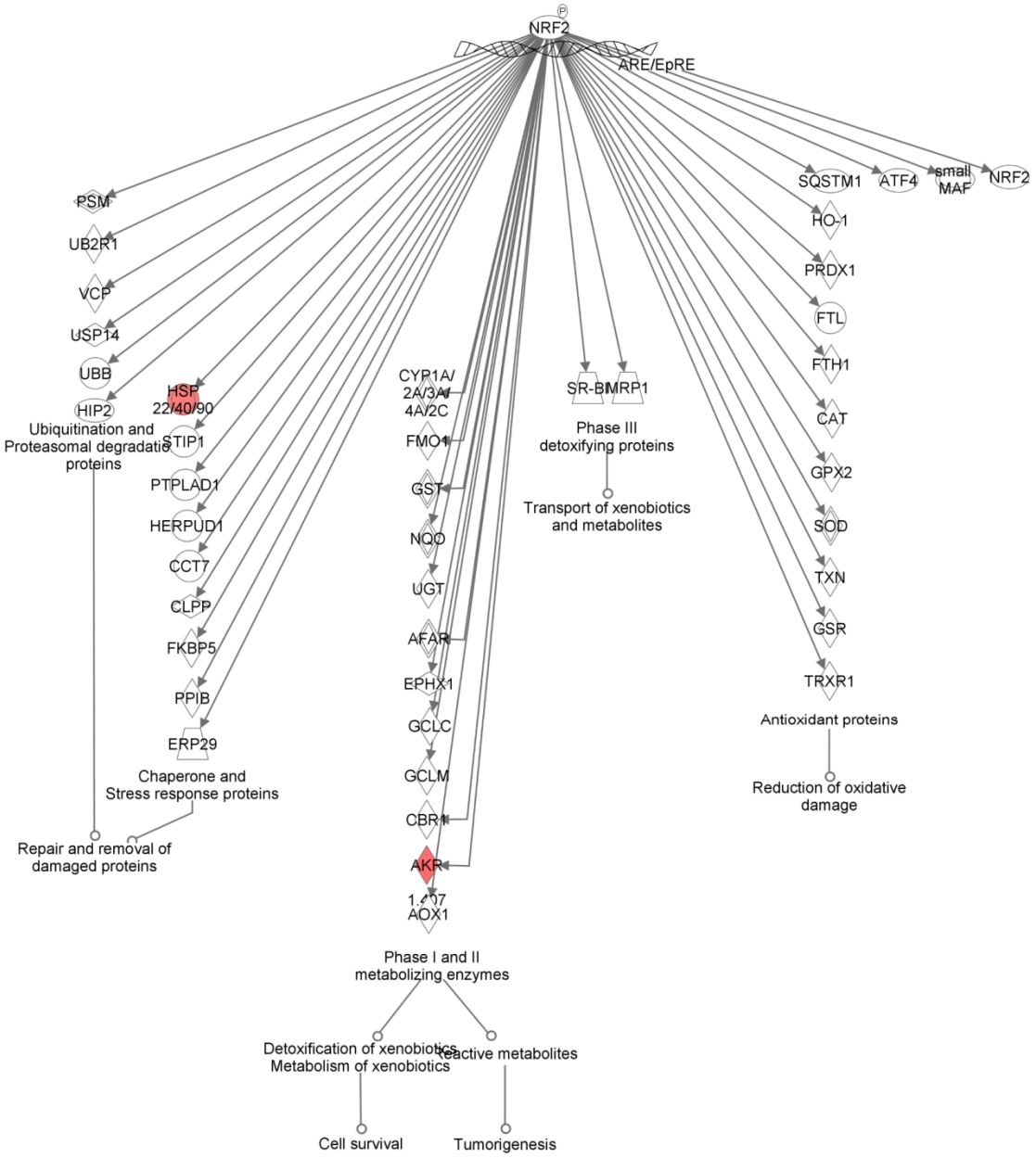

Figure 2.4 Effect of Cezanne shRNA on expression of Nrf2 targets. Microarray results from H157 cells treated with Cezanne shRNA as compared to control shRNA were evaluated using Ingenuity® pathway analysis (Ingenuity Systems). Genes found to be changed with Cezanne shRNA are overlaid on the Nrf2 pathway. Genes in red are increased in the presence of Cezanne shRNA while unmarked genes are unchanged. AKR and Hsp22/40/90 were increased 1.407 and 1.311 fold respectively but did not meet our 1.7 fold cut off.

Figure 2.5: DJ-1 and Cezanne regulate IL-8 and ICAM-1 at the transcript and protein levels.

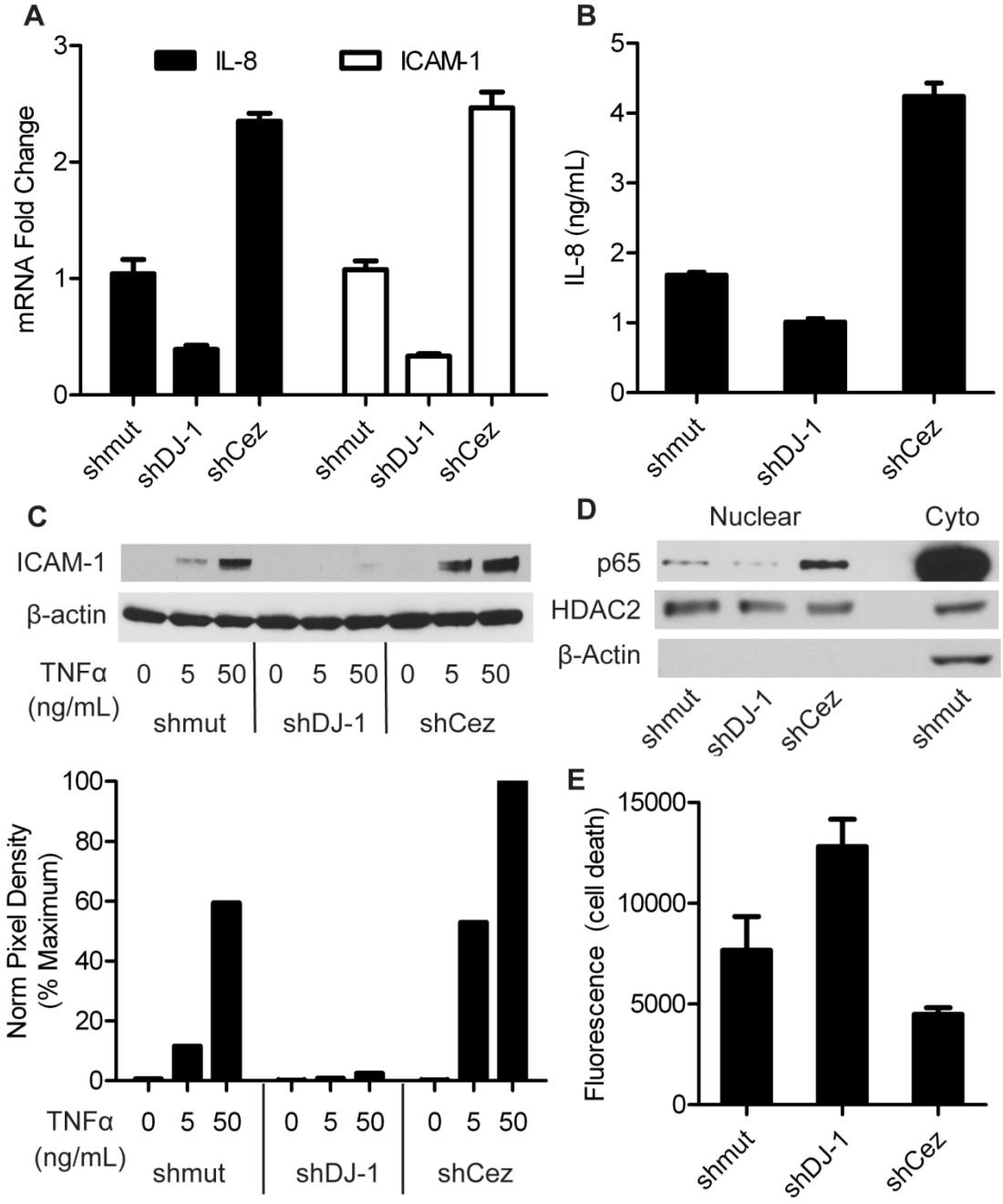

Figure 2.5 DJ-1 and Cezanne regulate IL-8 and ICAM-1 at the transcript and protein levels. (A) Real-time PCR for *IL-8* and *ICAM-1* in H157 cells with DJ-1 and Cezanne knockdown. RNA was harvested from DJ-1, Cezanne, and control shRNA treated samples and used to produce cDNA. The $\Delta\Delta C_t$ method was used to calculate fold changes based on differences in cycle number as compared to matched *β-actin* controls and mutant samples. (B) Transduced H157 cultures were incubated with fresh media for 6 hours, supernatants were collected, and secreted IL-8 levels were assessed by ELISA. (C) H157 cultures transduced with lentivirus were treated with increasing doses of TNFα for 6 hours and assessed for ICAM-1 protein levels by immunoblot. (D) Nuclear and cytoplasmic fractions collected from transduced H157 cultures were assessed for nuclear p65 by immunoblot. HDAC2 and β-actin were used as controls for loading and fractionation respectively. (E) Transduced H157 cultures were treated with 500nM Paclitaxel and 10μM U0126 for 24 hours. After treatment, the samples were collected and tested for cell death using a histone-based cell death ELISA. Untreated samples were used to control for cell turnover. Data expressed as fold change compared to mutant shRNA control samples.

Figure 2.6: ICAM-1 is regulated by DJ-1 and Cezanne in primary MEFs.

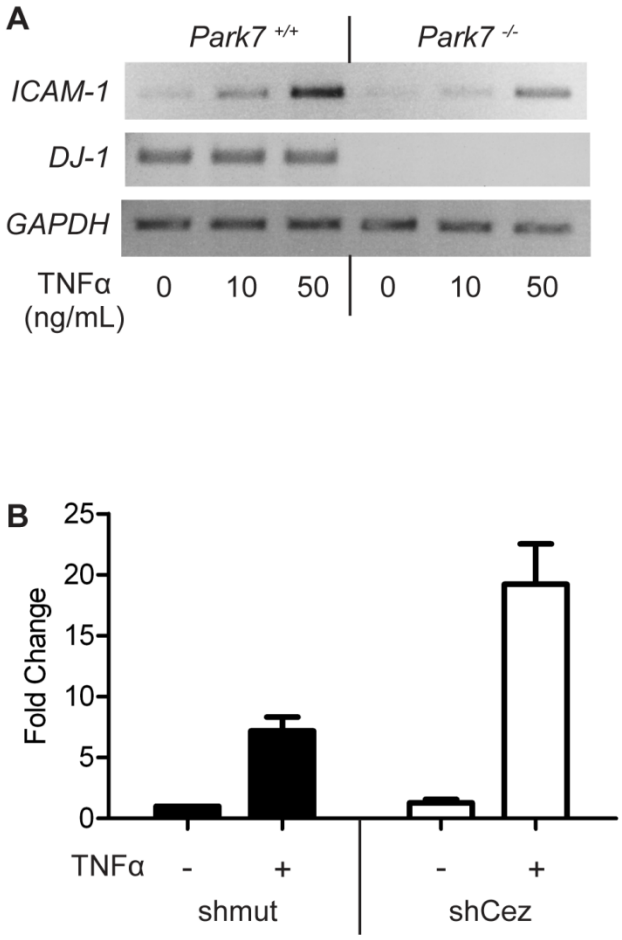

Figure 2.6 ICAM-1 is regulated by DJ-1 and Cezanne in primary MEFs. (A) RT-PCR was used to assess the effects of DJ-1 deletion on ICAM-1 expression. *Park7*$^{+/+}$ and *Park7*$^{-/-}$ MEFs were plated and treated with 0, 10, or 50ng/mL of TNFα for 6 hours. After treatment, RNA was harvested and *ICAM-1* levels were assessed by RT-PCR using DJ-1 to verify the genotype and *GAPDH* to show equal loading. (B) Real time PCR assessing the effects of Cezanne shRNA on *ICAM-1* expression in primary MEFs. *Park7*$^{+/+}$ MEFs were transduced with lentivirus carrying Cezanne or a mutant shRNA construct. The samples were treated with 50ng/mL of TNFα for 6 hours, RNA was harvested, and real time PCR was performed to assess *ICAM-1* expression and induction. Fold changes were calculated by the $\Delta\Delta C_t$ method using *GAPDH* as a reference control in matched samples.

Chapter III

KEAP1 AND A20 INTERACTION: IDENTIFICATION OF A PUTATIVE ANTAGONISTIC MECHANISM OF CROSSTALK BETWEEN THE NRF2 AND NF-KB PATHWAYS

3.1 Abstract

Cancer is the second leading cause of mortality in the United States. The ability of cancer cells to survive without growth factors or in the presence of pro-apoptotic factors is one of the hallmarks of cancer pathogenesis. This ability to survive is, in part due to the activation of pro-survival pathways. Due to their promotion of cell survival, both Nrf2 and NF-κB are aberrantly activated in human carcinomas. While they are activated by overlapping stimuli and lead to a similar cellular outcome, Nrf2 and NF-κB have been found to antagonize each other through direct and indirect mechanisms. In this chapter, we identify a new mechanism of crosstalk between these two pathways. We show that two inhibitors of Nrf2 and NF-κB, Keap1 and A20 respectively, interact leading to an increase in Keap1 ubiquitination. As expected, Keap1 protein levels and Nrf2 target transcription are increased in the absence of A20. Paradoxically, Nrf2 protein levels increase in *A20*$^{-/-}$ MEFs. The increase of NF-κB activity in the absence of A20 and the ability of NF-κB to inhibit Nrf2 in this cell type suggests that the effect of A20 on the Nrf2 pathway is obscured in this cell type due to this increase in NF-κB activity. While the consequences of the A20/Keap1 interaction are not elucidated due to the complex interplay between Nrf2 and NF-κB, this represents a novel mechanism by which Nrf2 and NF-κB may regulate one another. Future studies elucidating this crosstalk may identify novel targets for cancer therapy.

3.2 Introduction

Cancer pathogenesis is based on the unchecked growth of cells in the context of DNA damage. The current multi-hit hypothesis of cancer development is based on the accumulation of a series of mutations leading to the hallmarks of cancer including resistance to apoptosis, lack of requirement for growth factors, angiogenesis, and limitless replication potential. Unchecked oxidative stress is a well known cause of somatic mutations. Oxidative stress is caused by a variety of stimuli including UV radiation from the sun, oxygen, and chronic inflammation. The association between chronic inflammation, oxidative stress, DNA damage, and cancer pathogenesis has been well established in many human cancers including colon and lung cancer. While the inflammatory and antioxidant stress responses are regulated by a number of factors, two prominent transcription factors that control these responses are NF-κB and Nrf2 respectively. While both of these proteins promote cell survival, an antagonistic interplay has been uncovered between these two pathways. Elucidation of the mechanisms of this crosstalk is critical in understanding the modulation of inflammation and oxidative stress as they pertain to cancer pathogenesis.

The cap 'n' collar basic leucine zipper transcription factor Nrf2 is a master regulator of cellular anti-oxidant stress response (98, 182). In non-oxidative conditions, Nrf2 is found in the cytoplasm bound to its cytoplasmic inhibitor Keap1 (92). While Keap1 sequesters Nrf2 in the nucleus, it also aids in the ubiquitination of Nrf2 in a cullin3-dependent manner causing the degradation of Nrf2 by the proteosome (93, 94). In this manner, Nrf2 is regulated by both its cellular location

and constant baseline degradation. In oxidative conditions, Nrf2 is released from Keap1 and trans-locates to the nucleus. In the nucleus, Nrf2 binds small Maf proteins and recruits co-activators to anti-oxidant response elements (ARE) on DNA (95, 96). Through this binding, Nrf2 inducing target gene transcription. Nrf2 targets proteins of small molecule antioxidant pathways, antioxidant proteins, and detoxification enzymes (97, 98).

These downstream effectors, such as SOD3 and NQO1, detoxify the reactive oxygen species (ROS) thus promoting cell survival. This detoxification prevents ROS produced by inflammation or cellular metabolism from causing DNA damage through direct oxidation of nucleotides including formation of oxidized thymine and thymine dimers. Loss of Nrf2 activity has been shown in mouse models of skin and colorectal cancer to speed the onset and increase the incidence, multiplicity, and size of tumors (183, 184). Blocking DNA damage by activation of Nrf2 would therefore seem like an attractive option to prevent tumor formation. Unfortunately, modulation of Nrf2 to treat cancer is a double-edged sword. While activation of Nrf2 would theoretically inhibit the mutations that lead to cancer, many cancers actually have increased Nrf2 levels that are associated with enhanced cancer cell survival and resistance to chemotherapeutics.

Nrf2 is expressed at higher levels in both human head and neck squamous cell carcinomas and pancreatic cancer when compared to normal cells (185, 186). This increase in Nrf2 activity confers protection of the cancer cells from multiple chemotherapeutics including cisplatin, tamoxifen, etoposide, 5-fluorouracil (187-190). Nrf2 accomplishes this in two ways. First, Nrf2 causes the detoxification of

the chemotherapeutic compound. The downstream targets of Nrf2, including phase II detoxification enzymes, have evolved to render toxic substances like chemotherapeutics harmless. One target of Nrf2, HO-1, has specifically been shown to confer resistance to cisplatin. Inhibition of HO-1 by siRNA or the HO-1 specific inhibitor ZnPP augments cisplatin cytotoxicity in the A549 non-small cell lung carcinoma cell line (191). Second, Nrf2 induces the expression of transporters that export drugs out of the cancer cell. Multiple members of the ABC superfamily of drug transporters, such as MRP2-4 and ABCC2, are induced by Nrf2 (188, 192). Expression of these transporters leads to the export of chemotherapeutics, decreasing intracellular drug concentrations, and enhancing cancer cell survival.

While Nrf2 overexpression due to gene duplication occurs in certain cancers, mutations in either Nrf2 or Keap1 are more common. Mutations of Nrf2 or Keap1 have been found in lung, breast, and squamous cell carcinomas of the esophagus and skin (193-195). These mutations cluster in the domains of Nrf2 and Keap1 that mediate their interaction, namely the Neh2 domain of Nrf2 as well as the DGR and ETGE motifs of Keap1. Mutation of these interaction domains impairs Keap1's ability to inhibit Nrf2, thus increasing Nrf2 activity. Keap1 mutation is of particular interest as this may also lead to the downstream activation of the cancer-associated transcription factor NF-κB. A group recently reported that Keap1 downregulates NF-κB signaling by the ubiquitination and degradation of IKKβ, a known positive regulator of NF-κB (168). Mutations in the protein binding motifs of Keap1 may inhibit this activity causing the downstream activation of NF-κB in addition to Nrf2 activation in cancer cells.

NF-κB is one of the most studied transcription factors involved in the inflammatory response. Inactive NF-κB is found sequestered in the cytoplasm bound to IκB (102). Activation of multiple receptors can lead to the activation of NF-κB including growth factor receptors, Toll-like receptors, and pro-inflammatory cytokine receptors such as the TNFα receptor. Binding of TNFα to its receptor leads to the intracellular recruitment of positive regulators of NF-κB such as RIP1 and TRAF6 (103, 104). The downstream effect of these regulators is the activation of the IKK complex (105). Activation of this complex leads to the phosphorylation and degradation of IκB releasing NF-κB from its inhibition. NF-κB translocates to the nucleus where it induces the transcription of a myriad of genes involved in inflammation and cell survival. A subset of these genes inhibits and thus controls the NF-κB activation. One such gene is A20 (136, 137). A20, an ubiquitin-editing enzyme, removes activating ubiquitin from RIP1 and TRAF6 and replaces it with degradative ubiquitin (141). This decrease in RIP1 and TRAF6 protein levels by A20 constitutes a negative feedback loop to keep NF-κB activity in check.

Due to NF-κB's effect on cell survival, it is therefore not surprising that certain cancers have hijacked this pathway to promote their own survival. Although activation of NF-κB through direct mutation can be found in certain cancers, most aberrant activation of NF-κB in cancer is caused by changes in upstream signaling. One example is the mutation or deletion of A20 which has been seen in multiple human cancers (143-146). This increase in NF-κB activity promotes cell survival through the action of NF-κB targets. These targets include well known oncogenes including cyclin D, Bcl-2, and inhibitors of apoptosis (IAPs) which promote cell

division, stimulate cell survival, and inhibit apoptosis respectively (108-110). NF-κB also regulates other hallmarks of cancer including angiogenesis, through IL-8 secretion, and metastasis, through regulation of ICAM-1 levels (115-118, 121, 123, 133).

Although Nrf2 and NF-κB are both activated in cancers and lead to cell survival, a growing number of papers have found that these pathways antagonize each other at multiple levels. Nrf2 does not inhibit NF-κB directly but through its downstream targets. Four targets of Nrf2, HO-1, NQO1, thioredoxin, and Keap1, inhibit NF-κB (156, 166, 167). It is still not clear whether the inhibition of NF-κB by HO-1, NQO1, and thioredoxin is due to direct inhibition of NF-κB or through the inhibition of ROS levels. As ROS activates NF-κB, detoxification of ROS by the downstream targets of Nrf2 may indirectly inhibit NF-κB activity (165). Keap1, on the other hand, directly inhibits the NF-κB pathway by targeting IKKβ for degradation (168). NF-κB inhibits Nrf2 both directly and through its downstream targets. The p65 subunit of NF-κB inhibits Nrf2 activity in the nucleus in two ways. First, p65 binds to CBP depriving Nrf2 of this necessary co-activator (169). Second, p65 causes the recruitment of HDAC3 to ARE sites (169). This recruitment causes the de-acetylation and thus silencing of Nrf2 target genes. NF-κB also inhibits Nrf2 through target genes. COX-2, a target of NF-κB, has also been shown to inhibit Nrf2 although the mechanism of this inhibition is still poorly understood (170).

In this chapter, we will outline a novel pathway by which Nrf2 and NF-κB may interact. While screening for interacting proteins within these pathways, A20 and Keap1 were found to interact by co-immunoprecipitation of ectopically-expressed or

hemi-endogenous proteins. Binding by A20 was found to increase Keap1 ubiquitination and decrease Keap1 protein levels. As expected, this increase in Keap1 protein levels is associated with a decrease in the known Nrf2 targets TRXR1, NQO1, and GCLM. Paradoxically, an increase in total and nuclear Nrf2 levels was seen in the absence of A20. This suggests that Nrf2 pathway is being activated but there is an additional factor(s) that inhibits the nuclear Nrf2 in the *A20*$^{-/-}$ MEFs. We hypothesize that hyperactivity of NF-κB in the *A20*$^{-/-}$ cells is responsible for these findings as NF-κB is known to induce Nrf2-activating ROS and inhibit Nrf2 in the nucleus. As a whole, this work identifies a new pathway of crosstalk between Nrf2 and NF-κB, but the significance of this pathway is obscured in the cell type used due to NF-κB hyper-activation.

3.3 Results

A20 binds Keap1, the cytoplasmic inhibitor of Nrf2

Previous data in the lab showed an interaction between DJ-1 and Cezanne. Due to the sequence homology as well as the overlap in function between Cezanne and A20, we were interested if A20 bound DJ-1 or any other proteins in the DJ-1/Nrf2 pathway. While no interaction was seen between A20 and DJ-1 or Nrf2 (data not shown), overexpressed A20 was found to interact with the Nrf2 inhibitor Keap1 as detected by co-immunoprecipitation (Fig. 3.1A). HEK293T cells were transfected with FLAG-A20 with or without Keap1-V5. Keap1-V5 was immunoprecipitated using V5-agarose and the eluates were analyzed by immunoblot. Immunoblot for Fg-A20 in the eluate samples showed the immunoprecipitation of Fg-A20 in the presence of Keap1-V5 but not in its absence showing an interaction between overexpressed A20 and Keap1. We analyzed input samples with β-actin, V5-HRP, and FLAG-HRP antibody to ensure equal loading and appropriate overexpression of tagged constructs.

To confirm an A20/Keap1 interaction in a more physiologic system, we utilized a hemi-endogenous co-immunoprecipitation assay. HEK293T cells were transfected with Fg-A20 or an empty vector control. Following transfection, the samples were immunoprecipitated with FLAG-agarose and the eluates were evaluated by immunoblot. Immunoblot using endogenous Keap1 antibody showed immunoprecipitation of Keap1 in the presence of A20 overexpression but not in its

absence showing an interaction between endogenous Keap1 and overexpressed A20 (Fig. 3.1B). We used input controls to ensure equal loading and A20 overexpression in appropriate samples.

A20 ubiquitinates Keap1 and targets it for degradation

After confirmation of an interaction between A20 and Keap1, we began to study the consequences of this interaction. Both Keap1 and A20 regulate the ubiquitin status of their binding partners. The difference in their function is that Keap1 is an E3 ligase adaptor protein for the CUL3/RBX1 E3 ligase complex while A20 itself has E3 ligase activity. Keeping this in mind, we decided to start by examining the effects of A20 on Keap1 ubiquitination. HEK293T cells were transfected with overexpression vectors for Keap-V5, FLAG-A20, and HA-Ub. These samples were left untreated or treated with the Nrf2 activator tBHQ for 5 hours to induce Keap1 ubiquitination. We then lysed and boiled the samples in denaturing conditions to release all non-covalent interactions. After lysis buffer dilution to restore non-denaturing conditions, the samples were immunoprecipitated with V5-agarose and analyzed by V5 and HA immunoblot. V5 immunoblot showed relatively equal levels of Keap1 overexpression in Keap1-V5 transfected samples. The HA immunoblot showed 3 main findings. First, tBHQ treatment did increase Keap1 ubiquitination as expected. Second, lack of HA signal in the samples without Keap-V5 overexpression shows that the HA-Ub observed in samples containing transfected Keap1-V5 is specific for Keap1. Third, an increase in Keap1-V5

ubiquitination was seen in the samples in which FLAG-A20 was also overexpressed (Fig. 3.2A). Although this difference was more pronounced in the tBHQ treated samples, a modest increase in Keap1-V5 ubiquitination with A20 overexpression was seen in the vehicle control samples. This suggests that A20 ubiquitinates Keap1, either directly or indirectly. As the E3 ligase activity of A20 is thought to be restricted to K^{48}-linked degradative ubiquitin, we hypothesized that this activity of A20 would increase K^{48}-linked Keap1 ubiquitination, increasing Keap1 degradation and thus decreasing Keap1 levels.

As no overt changes in Keap1 expression were seen in the overexpression systems, we changed to a fully endogenous system to assess the effect of A20 expression on Keap1 protein levels. In this endogenous system, we expected to see an increase in Keap1 protein levels in the absence of A20-mediated ubiquitination and degradation. *A20*$^{+/+}$ and *A20*$^{-/-}$ MEF cultures were lysed and analyzed by immunoblot. After verifying equal loading using β-actin as a loading control, we saw an increase in Keap1 protein levels in *A20*$^{-/-}$ MEFs as compared to *A20*$^{+/+}$ MEFs as expected (Fig. 3.2B). This agrees with our hypothesis that A20 induces the degradation of Keap1. We also evaluated the levels of Keap1 in the presence of tBHQ treatment. *A20*$^{+/+}$ and *A20*$^{-/-}$ MEF cultures were either left untreated or treated with tBHQ for 6 hours. These cultures were lysed and analyzed for Keap1 expression by immunoblot using a non-specific band as a loading control. Although an increase in Keap1 levels was expected with tBHQ treatment, as Keap1 is transcribed by Nrf2, no change in Keap1 levels was seen with this treatment (Fig. 3.2C). This may be due to a balance between increased Keap1 degradation and

Nrf2-mediated induction of Keap1 transcription. This assay did confirm an increase in Keap1 levels in the absence of A20.

Expression of Nrf2 target genes is decreased in *A20*$^{-/-}$ MEFs

As Keap1 is the major inhibitor of Nrf2 activity, the increase in Keap1 protein levels in *A20*$^{-/-}$ MEFs should be accompanied by a decrease in Nrf2 activity and thus a decrease in the mRNA expression of Nrf2 targets. To test this, we extracted RNA from *A20*$^{+/+}$ and *A20*$^{-/-}$ MEFs during a time course with tBHQ. We produced cDNA from these RNA samples and assessed the mRNA levels of 3 genes transcriptionally regulated by Nrf2 by RT-PCR. Induction of TRXR1, NQO1, and GCLM by tBHQ was seen in the *A20*$^{+/+}$ MEFs showing their dependence on Nrf2 (Fig. 3.3A). A significant decrease in the mRNA levels of TRXR1, NQO1, and GCLM was seen in the *A20*$^{-/-}$ MEFs as compared to the *A20*$^{+/+}$ MEFs suggesting a decrease in Nrf2 activity as expected from the previous Keap1 expression data.

Paradoxically, nuclear Nrf2 protein levels are increased in *A20*$^{-/-}$ MEFs

With the decrease in Nrf2 activity seen in *A20*$^{-/-}$ MEFs, we expected to see an associated decrease in Nrf2 protein levels. We treated *A20*$^{+/+}$ and *A20*$^{-/-}$ MEFs with tBHQ and TNFα as indicted for 6 hours. After treatment, the samples were lysed and analyzed by immunoblot. Surprisingly, Nrf2 protein levels were actually increased in the *A20*$^{-/-}$ MEFs as compared to *A20*$^{+/+}$ MEFs in the tBHQ treated

samples (Fig. 3.4A). This increase in Nrf2 levels was further highlighted in the tBHQ/TNFα treated samples. Immunoblot for β-actin shows even loading across all the samples. One possible explanation for this paradox is that the increased Nrf2 might not be located in the nucleus where transcriptional activation takes place, we performed further experimentation which showed that this Nrf2 was exclusively nuclear (Fig. 3.4B).

These data lead to two conclusions. First, there must be a signal in the *A20*$^{-/-}$ MEFs that leads to the translocation of Nrf2 to the nucleus where is it is protected from Keap1-mediated degradation. We hypothesized that increased ROS may be activating the Nrf2 pathway in this cell type as activation of NF-κB, in this case by TNFα and the absence of A20-mediated inhibition, can lead to increased intracellular ROS levels. To test this hypothesis, we examined ROS levels using DHR123 in *A20*$^{+/+}$ and *A20*$^{-/-}$ MEFs that had been treated with H_2O_2 or left untreated. We saw no difference in ROS levels in the untreated MEFs (Fig. 3.5 top panel), but a modest increase in ROS levels was seen in *A20*$^{+/+}$ MEFs as compared to *A20*$^{-/-}$ MEFs with H_2O_2 treatment (Fig. 3.5 bottom panel). This data suggests that while an increase in nuclear Nrf2 is seen in *A20*$^{-/-}$ MEFs it is not due to an increase in ROS levels. While further experiments using TNFα and tBHQ would be needed to completely rule this out, the current data shows that the nuclear translocation of Nrf2 is caused by a non-oxidative process. This is not entirely surprising as Nrf2 can be activated by non-oxidative stimuli such as tBHQ.

The second conclusion drawn from this data is that the Nrf2 seen in the nucleus of *A20*$^{-/-}$ MEFs is inactive as it does not induce the transcription of its

downstream targets (see Fig. 3.3). This suggests that Nrf2 is either intrinsically inactive in this cell type or a protein is inhibiting Nrf2's activity in the nucleus. As there is nothing in the literature to suggest that the absence of A20 would cause an intrinsic defect in Nrf2 activity, we focused on nuclear proteins that may be causing the inactivation of Nrf2. The tie between A20 and NF-κB lead us to further investigate the relationship between nuclear Nrf2 and NF-κB.

Increased NF-κB activity inhibits nuclear Nrf2 in *A20*$^{-/-}$ MEFs

In the absence of A20-mediated inhibition, NF-κB's activity is increased. Based on the literature, we therefore hypothesized that increased NF-κB activity was responsible for the inhibition of nuclear Nrf2 in *A20*$^{-/-}$ MEFs. We first confirmed that NF-κB activity was indeed increased with A20 knockout in MEFs. RNA was extracted from *A20*$^{+/+}$ and *A20*$^{-/-}$ MEFs that were treated with a time course of TNFα. CDNA produced from that RNA was used to assess the expression of two targets of NF-κB, namely *ICAM-1* and *VCAM-1*, by RT-PCR. Equal loading between samples was verified using *GAPDH* as a control. We saw an increase in *ICAM-1* and *VCAM-1* expression in the *A20*$^{-/-}$ MEFs as compared to *A20*$^{+/+}$ MEFs at all TNFα-treated time points suggesting an increase in NF-κB activity in the absence of A20 as expected (Fig. 3.6A).

When these experiments were completed, only one publication had showed that NF-κB could inhibit Nrf2 in the nucleus. As this work was done in a different cell type, we set out to confirm inhibition of Nrf2 by NF-κB in MEFs. We obtained *p65*$^{+/+}$

and *p65*$^{-/-}$ MEFs and assessed their Nrf2 activity by luciferase. After transfecting the MEFs with Nrf2 reporter and p65 overexpression vector as indicated, we left the cultures untreated or treated them with tBHQ overnight. We found that Nrf2 activity was significantly increased in the *p65*$^{-/-}$ MEFs as compared to *p65*$^{+/+}$ control MEFs and that this activation of Nrf2 could be abrogated with overexpression of p65 (Fig. 3.6B). This confirmed that NF-κB inhibits Nrf2 activity in MEFs and may be the cause of the inhibition of nuclear Nrf2 seen in the *A20*$^{-/-}$ MEFs.

3.4 Discussion

Both Nrf2 and NF-κB are known to be aberrantly activated in human carcinomas (113, 183, 184). Typically activated in response to oxidative stress, Nrf2 induces a host of detoxification enzymes in cancer cells. These enzymes can detoxify chemotherapeutics rendering them harmless and preventing cancer cell death. NF-κB stimulates cancer cell proliferation and survival through the expression of numerous gene targets including cyclin D, Bcl-2, and IAPs (108-110). Other targets of NF-κB, such as IL-8 and ICAM-1, play a role in angiogenesis and cancer progression (121, 124, 135). The Nrf2 and NF-κB pathways have many things in common. They can both be activated by similar stimuli, they both promote cell survival, and they share some downstream transcriptional targets. Even with all these similarities, Nrf2 and NF-κB antagonize each other through multiple mechanisms.

Although Nrf2 does not directly inhibit NF-κB, it does indirectly inhibit NF-κB in two ways. First, Nrf2 activity decreases intracellular levels of ROS, a known positive regulator of NF-κB activity. Second, Nrf2 induces the transcription of Keap1, HO-1, NQO1, and TRX which have been shown to inhibit NF-κB under certain conditions (156, 166, 167). NF-κB indirectly inhibits Nrf2 through a downstream target as COX-2, a gene induced by NF-κB, has been shown to inhibit Nrf2 activity (170). NF-κB also inhibits Nrf2 directly through 2 ways. First, NF-κB binds to CBP preventing it from acting as a co-activator for Nrf2 (169). Second, NF-κB recruits HDAC3 to ARE sites (169). By recruiting this deacetylase, NF-κB can epigenetically silence Nrf2 targets.

In this chapter, we identified another mechanism by which Nrf2 and NF-κB may regulate one another. When activated, Nrf2 and NF-κB induce Keap1 and A20 expression respectively. Keap1 and A20 inhibit their respective transcription factor completing separate negative feedback loops. Using co-immunoprecipitation, we found that A20 binds overexpressed and endogenous Keap1. The consequence of this interaction is an increase in Keap1 ubiquitination. This ubiquitination is presumably K^{48}-linked degradative ubiquitin as Keap1 levels were seen to be increased in *A20*$^{-/-}$ MEFs as compared to wild type MEFs in the presence or absence of stimulation. As expected, this increase in Keap1 protein levels correlated with a decrease in Nrf2 activity as assessed by RT-PCR analysis of multiple Nrf2 targets.

Surprisingly, we found an increase in total and nuclear Nrf2 levels in the *A20*$^{-/-}$ MEFs treated with tBHQ with or without TNFα as compared to *A20*$^{+/+}$ MEFs. This result suggests that while the Nrf2 pathway is activated in *A20*$^{-/-}$ MEFs, a nuclear protein is inhibiting Nrf2's activity. While no mechanism for the aberrant activation of Nrf2 was identified, increased intracellular ROS in *A20*$^{-/-}$ MEFs was ruled out as ROS was not increased in this cell type. To identify the cause of the nuclear Nrf2 inhibition, we first confirmed that NF-κB activity was increased in the absence of A20 by examining *ICAM-1* and *VCAM-1* expression using RT-PCR. We then verified the ability of the p65 NF-κB subunit to inhibit Nrf2 in a similar cell type. Taken together, this data suggest that the increase in NF-κB activity in *A20*$^{-/-}$ MEFs may be the cause of the nuclear Nrf2 inhibition seen in the *A20*$^{-/-}$ cells.

The complex interplay between the Nrf2 and NF-κB pathways makes analysis of data obtained from the *A20*$^{+/+}$ and *A20*$^{-/-}$ MEFs very difficult to interpret. While A20 may be playing a role in the regulation of Keap1 and Nrf2, the increased activity of NF-κB in the *A20*$^{-/-}$ MEFs seems to be obscuring the effect of A20 on these proteins. Although this effects the endogenous data, our HEK293T data should not be similarly affected as the interaction and ubiquitination data is not dependent on the activity of Nrf2 or NF-κB. Using overexpression systems, we showed that overexpressed A20 can bind to exogenous and endogenous Keap1. Verification of a fully endogenous interaction would further confirm the physiological relevance of this interaction, but this experiment would require a more sensitive endogenous A20 antibody then is currently available. We also showed that Keap1 ubiquitination was increased with A20 overexpression. While the literature would suggest that this Keap1 ubiquitination should be K^{48}-linked, experiments using ubiquitin mutant vectors would be necessary to confirm this hypothesis. The type of ubiquitin ligated to Keap1 by A20 would help identify the possible consequences of this modification.

Identification of an interaction between two major inhibitors of the Nrf2 and NF-κB pathway is a significant addition to the literature elucidating the antagonistic nature of these two pathways. The paradoxical results found in *A20*$^{+/+}$ and *A20*$^{-/-}$ MEFs due to the complex interplay of these pathways make it too soon to identify the downstream consequences of this interaction. Three hypotheses do seem the most plausible based on our data and the corresponding literature. First, activation of A20 by NF-κB leads to the ubiquitination and degradation of Keap1. Decreased Keap1 levels would then cause an increase in Nrf2 activity. By inhibiting NF-κB and

activating Nrf2 through this Keap1-dependent mechanism, A20 would maintain a balance between these two pathways. Second, Keap1, similar to its role in cullin3-dependent ubiquitination, may act as an adaptor for A20-mediated ubiquitination. This activity would enhance A20-mediated ubiquitination and the downstream inhibition of NF-κB. A20-dependent inhibition of NF-κB by Keap1 would also fit with Keap1's known inhibition of NF-κB via targeting of the IKK complex. Third, Keap1 may target A20 for cullin3-mediated ubiquitination and degradation. This would release the A20-mediated inhibition of NF-κB causing an increase in NF-κB activity. While this hypothesis fits with the known activity of Keap1, it would be one of the very few examples of Nrf2 targets leading to the activation of NF-κB. While the downstream consequences of the A20/Keap1 interaction were not elucidated in this work, further investigation is warranted as the crosstalk between the Nrf2 and NF-κB has implications in antioxidant response and inflammation which may yield novel targets for therapies in asthma, sepsis, and cancer.

3.5 Materials and Methods

Cell culture, transfection, treatments, and plasmid constructs. HEK293T cells and mouse embryonic fibroblasts were grown in high glucose DMEM (Gibco) with 10% FBS (Hyclone). Cultures were grown at 37°C with 5% CO_2 in the presence of penicillin and streptomycin to prevent bacterial contamination. MEFs were isolated from 13.5 day embryos and used within 3 passages. HEK293T cells were transfected with Fugene 6 at a reagent to DNA ratio of 3:1 as according to the manufacturer's instructions (Roche). MEFs were transfected with Lipofectamine 2000 at a reagent to DNA ratio of 4:1 also according to the manufacturer's instructions. H_2O_2 was used at a concentration of 250μM for 1 hour prior to flow cytometric analysis of ROS levels (Sigma). TBHQ (Fluka) and TNFα (eBioscience) were used at 100μM and 50ng/mL respectively unless otherwise stated.

The Keap1 ORF was amplified with Pfx platinum polymerase (Invitrogen) using 5'-CACCATGCAGCCAGATCCCAGGCCTAGC-3' and 5'-ACAGGTACAGTTCTGCTGGTCAATCT-3' as primers. This ORF fragment was directionally cloned into the V5/His-tagged pcDNA3.1-D TOPO construct (Invitrogen). Expression and amplication fidelity were assessed by immunoblot and sequencing respectively. The Flag-A20, HA-Ub, p65 and NF-κB-pGL2-Luc, and NQO1-pGL2-Luc vectors were generously given to us by the Averil Ma (UCSF), Yue Xiong (UNC), Albert Baldwin (UNC), and Jaiswal labs (Baylor).

Co-immunoprecipitation and Immunoblot Analysis. HEK293T cells were transfected with appropriate constructs and incubated for 18 hours. After incubation, the cells were collected, washed with PBS, and lysed in 0.5% Tx-100 lysis buffer. After lysis, the samples were cleared of insoluble cellular material and nuclei by centrifugation. The cleared lysates were immunoprecipitated with V5 or FLAG-agarose for immunoprecipitation of V5-tagged Keap1 or FLAG-tagged A20 respectively. After incubation overnight at 4°C, the samples were washed 4 times with lysis buffer and eluted with a combination of 2x LDS loading buffer (Invitrogen), 100μM DTT (Sigma), and brief boiling. Samples for immunoblot analysis not subjected to previous immunoprecipitation were lysed in RIPA buffer. These lysates were run through a 27.5 gauge needle and cleared by centrifugation. Protein concentrations were analyzed by BCA, and the concentrations were equalized by dilution with lysis buffer, 2x LDS loading buffer, and 100μM DTT. Proteins were separated by molecular weight by SDS-PAGE gel electrophoresis and transferred to a nitrocellulose membrane subsequently blocked with 5% non-fat dry milk. Tagged proteins were blotted for using V5-HRP (Invitrogen), HA-HRP (Roche), or FLAG-HRP (Sigma) depending on the tag. Anti-Keap1 H-190 (Santa Cruz), anti-Nrf2 ab53019 (Abcam), and β-actin-HRP C-11 (Santa Cruz) antibody were used to assess the appropriate endogenous protein.

***In vitro* Ubiquitination Assay.** HEK293T cells were transfected with HA-Ub, Fg-A20, and V5-Keap1 as appropriate. After an overnight incubation, the samples were treated with tBHQ for 2 hours. The samples were harvested, washed with PBS, and

lysed in denaturing SDS lysis buffer. We then boiled the samples to ensure the removal of all non-covalent bonds. The samples were cleared by centrifugation and diluted with 0.5% Tx-100 lysis buffer to restore non-denaturing conditions. V5-tagged Keap1 was immunoprecipitated overnight with V5-agarose. After immunoprecipitation, samples were washed with lysis buffer, eluted, and analyzed by immunoblot. Immunoblot with V5-HRP was used to assess the Keap1 protein levels while HA-HRP antibody was used to analyze Keap1 ubiquitination.

Semi-quantitative Reverse Transcription PCR. Prior to RT-PCR analysis, MEF cultures were treated with tBHQ or TNFα as indicated. After treatment, the cultures were washed with PBS and RNA was extracted using the RNeasy Plus RNA extraction kit (Qiagen). CDNA was produced by oligodT-primed MMLV reverse transcriptase (Invitrogen) from 2μg of RNA per sample in the presence of the RNase inhibitor RNasin (Promega). PCR was performed on the sample cDNA using *Taq* polymerase with primers for mouse *TRXR1* (5'-CTT TGC TCG GAC AAG CTC TGA AAG A-3', 5'-CTG CAC ATT CCA AGG CGA CAT AGG A-3'), *NQO1* (5'-CAG ATA TTG TGG CCG AAC AC-3', 5'-CAG ACG GTT TCC AGA CGT TTC-3'), *GCLM* (5'-GCA CCA TGT CCC ATG CAG TGG AGA AG-3', 5'-GAG CTT CCT GGA AAC TTG CCT CAG AGA GC-3'), *GAPDH* (5'- CCA CTC ACG GCA AAT TCA ACG GCA CAG-3', 5'- GTG GCA GTG ATG GCA TGG ACT GTG GTC-3'), *ICAM-1* (5'-CAG TCC GCT GTG CTT TGA GAA CTG TGG C-3', 5' GGT ATA TCC GAG CTT CAG AGG CAG GAA AC-3'), and *VCAM-1* (5' GGC TCT GGG AAG CTG GAA CGA AGT ATC-3', 5'-CTC GCT GGA ACA GGT CAT TGT CAC AGC AC-3'). The number of

cycles run on the PCR Mastercycler (Eppendorf) was dependent on the target (GAPDH 17, TRXR1/GCLM/VCAM-1 20, NQO1/ICAM-1 23).

Assessment of Intracellular ROS Levels. MEFs were harvested, washed with PBS, and counted. Then $1x10^5$ cells per sample were resuspended in 100μL of PBS with 10% FBS. Samples were each left untreated or were treated with 250μM H_2O_2. During this 1 hour treatment period samples were stained with DHR123 (Anaspec). After treatment and staining, the samples were washed then run on a CyAn flow cytometry machine (Dako). Data acquisition and analysis was done using FlowJo software (FlowJo). Gates were set by forward and side scatter to include only live cells and unstained samples were used as a negative control for DHR123 on the FITC channel.

Luciferase Assay. MEF or HEK293T cells, as indicated, were plated in 6 well dishes at $2x10^5$ or $1x10^6$ cell per well respectively. After overnight incubation, the wells were transfected with 500 or 100ng of appropriate reporter and overexpression plasmids respectively. Empty vector was used to even the total vector amount for samples within a given experiment. After transfection, the samples were treated for 16 hours with tBHQ, TNFα, or vehicle control as indicated. The samples were washed with 1x PBS, 200μL of reporter lysis buffer (Promega) was added to each well, and the plates were freeze thawed at -20°C to ensure complete lysis. We then cleared the lysates by centrifugation and ran 50μL per sample in triplicate on a 96-

well plate. Luminescence was measured by 15 second integration on an Lmax 96-well luminometer (Molecular Devices) after injection of 50µL of luciferase assay buffer (25mM gly-gly, 15mM KH_2PO_4, 15mM $MgSO_4$, 4mM EGTA, 2mM APT, 1mM DTT) and luciferin substrate (200µM luciferin, 25mM gly-gly, 1mM DTT) per well. Relative light units (RLU) are reported normalized to protein concentration as assessed by BCA (Pierce).

Figure 3.1: A20 binds overexpressed and endogenous Keap1

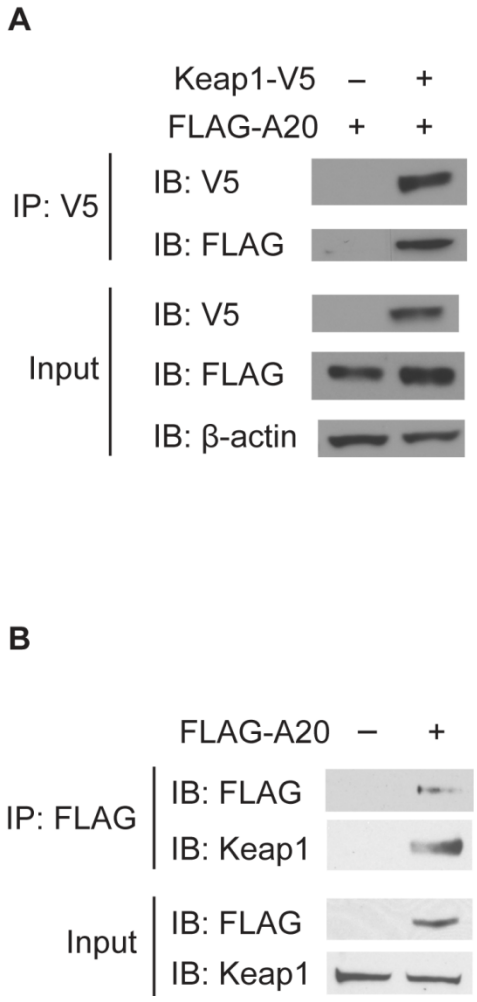

Figure 3.1 A20 binds overexpressed and endogenous Keap1. (A) A20 interacts with overexpressed Keap1. HEK293T cells were transfected with FLAG-A20 and Keap1-V5 as indicted. After overnight incubation, cultures were harvested, lysed, and immunoprecipitated with V5-agarose. Input and immunoprecipitation eluates were analyzed by immunoblot using the antibodies shown. (B) A20 interacts with endogenous Keap1. We transfected HEK293T cells with FLAG-A20 or empty vector control. After overnight incubation, the cultures were harvested, lysed, and immunoprecipitated with FLAG-agarose. Protein expression and binding was assessed by immunoblot on input and immunoprecipitation samples with the antibodies indicated.

Figure 3.2: A20 causes the ubiquitination and degradation of Keap1

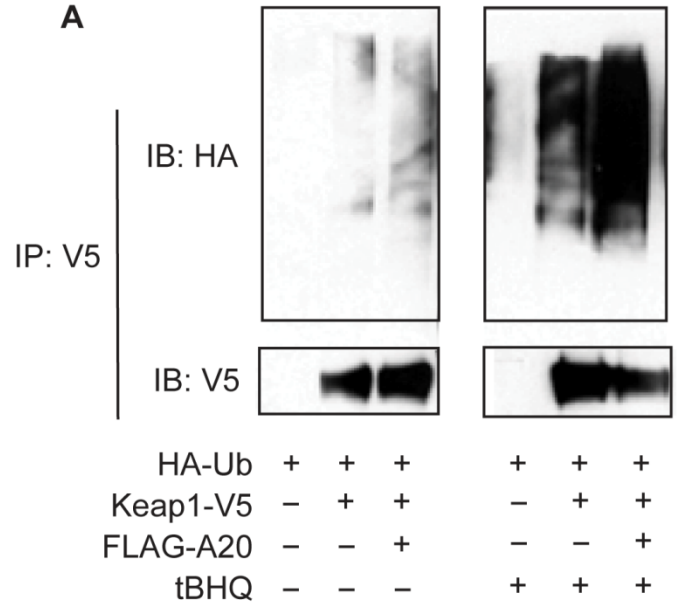

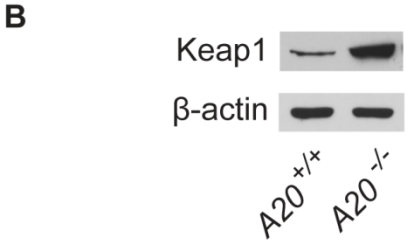

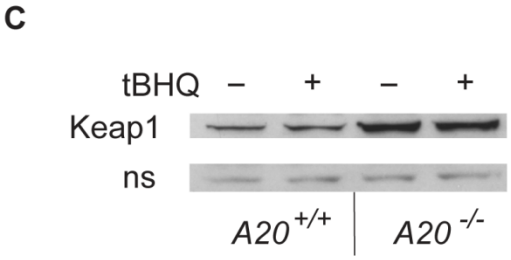

Figure 3.2 A20 causes the ubiquitination and degradation of Keap1. (A) A20 increases Keap1 ubiquitination. HEK293T cells were transfected with HA-Ub, Keap1-V5, and FLAG-A20 as indicated. We treated these cultures with tBHQ or left them untreated. The cultures were lysed, immunoprecipitated with V5-agarose, and the samples were analyzed by immunoblot with HA-HRP or V5-HRP antibody. (B/C) Keap1 protein levels are increased in the absence of A20. *A20*$^{+/+}$ and *A20*$^{-/-}$ MEFs were left untreated or treated with tBHQ. After treatment, whole cell lysates were produced and endogenous Keap1 levels were assessed by immunoblot using β-actin or a non-specific band as a loading control.

Figure 3.3: Nrf2 targets are decreased in *A20*$^{-/-}$ MEFs

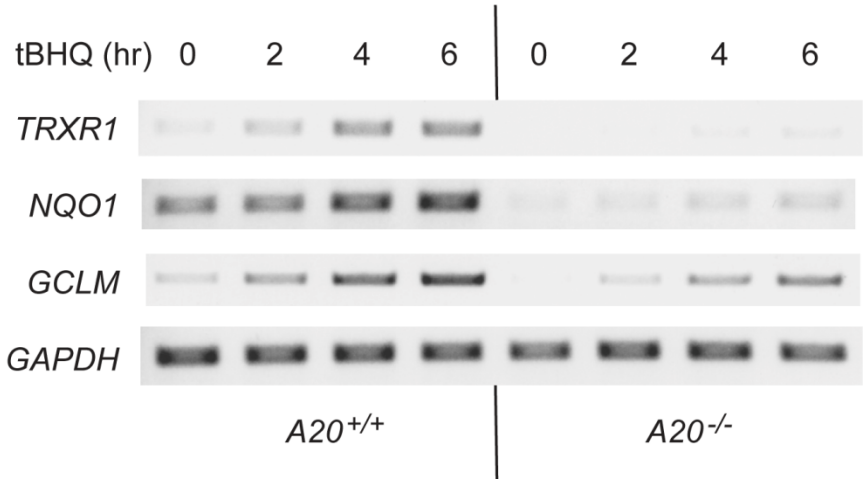

Figure 3.3 Nrf2 targets are decreased in *A20*$^{-/-}$ MEFs. (A) We treated *A20*$^{+/+}$ and *A20*$^{-/-}$ MEFs with tBHQ over a 6 hour time course. RNA was extracted and used to produce cDNA. Semi-quantitative RT-PCR was used to assess *TRXR1*, *NQO1*, *GCLM,* and *GAPDH* expression.

Figure 3.4: Nuclear Nrf2 levels are increased in *A20*$^{-/-}$ MEFs

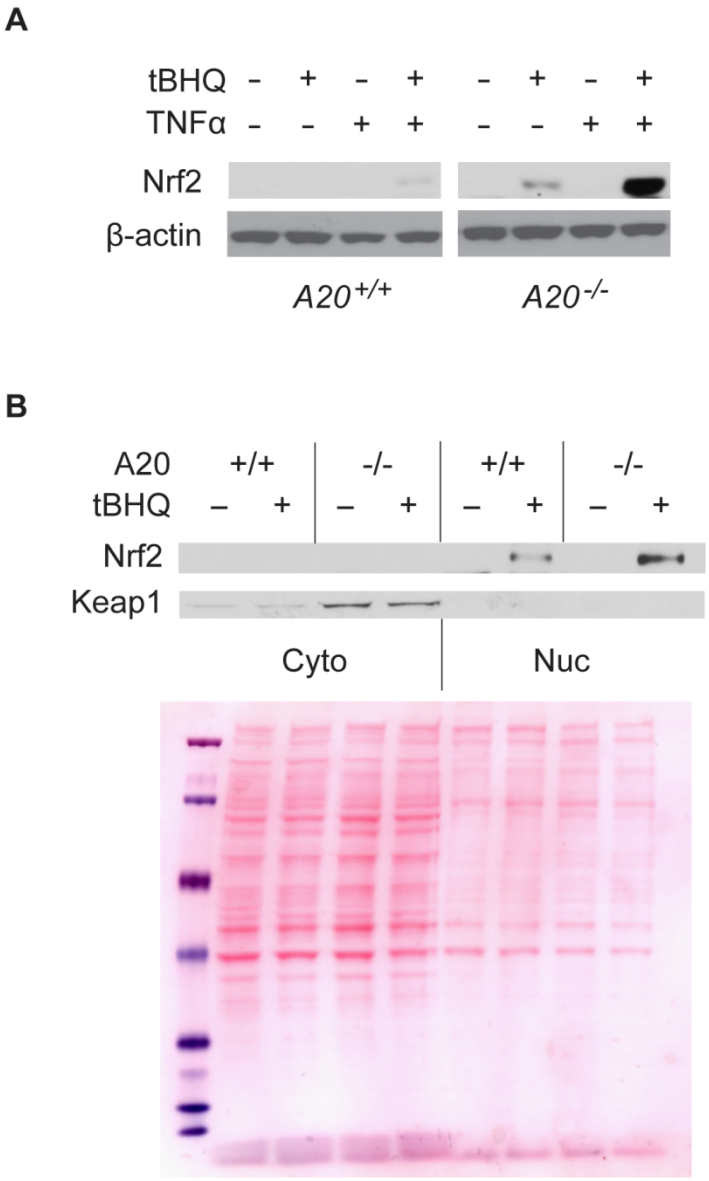

Figure 3.4 Nuclear Nrf2 levels are increased in *A20*$^{-/-}$ MEFs. (A) Total Nrf2 protein levels are increased in *A20*$^{-/-}$ MEFs. *A20*$^{+/+}$ and *A20*$^{-/-}$ MEF cultures were treated with tBHQ and TNFα as indicated. After treatment, lysates were analyzed by immunoblot for Nrf2 and β-actin. (B) *A20*$^{-/-}$ MEFs have increased nuclear Nrf2 levels. *A20*$^{+/+}$ and *A20*$^{-/-}$ MEF cultures were treated with tBHQ as indicated. Cultures were fractionated into cytoplasmic and nuclear fractions. These fractions were analyzed by immunoblot for Nrf2 and Keap1. Even loading was visualized using Coomassie stain.

Figure 3.5: ROS are not increased in *A20*$^{-/-}$ MEFs

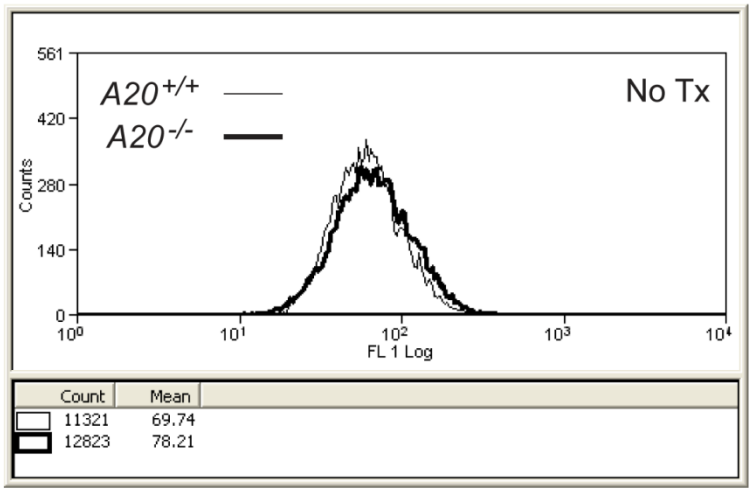

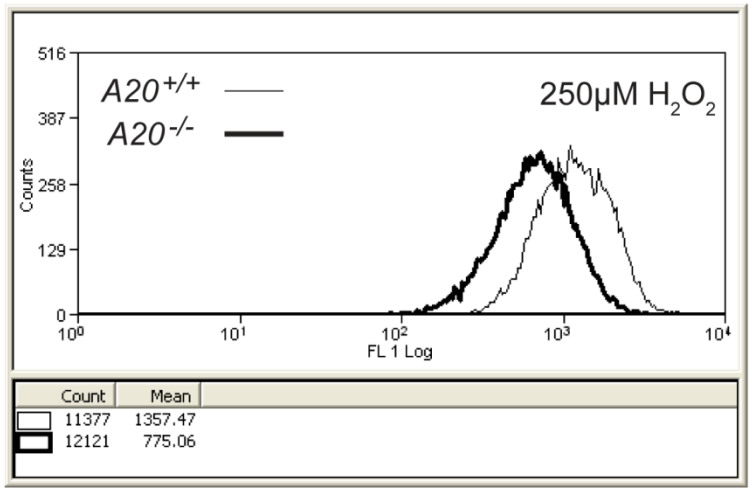

Figure 3.5 ROS are not increased in *A20*$^{-/-}$ MEFs. Suspensions of *A20*$^{+/+}$ (thin line) and *A20*$^{-/-}$ (thick line) MEFs were either left untreated (top panel) or treated with H_2O_2 (bottom panel) for 1 hour. During this time, the cells were stained with DHR123. After staining, ROS levels were assessed by DHR123 fluorescence on the FITC channel. Cell counts and MFI are shown below each graph.

Figure 3.6: Increased NF-κB activity in *A20*$^{-/-}$ MEFs inhibits Nrf2 activity.

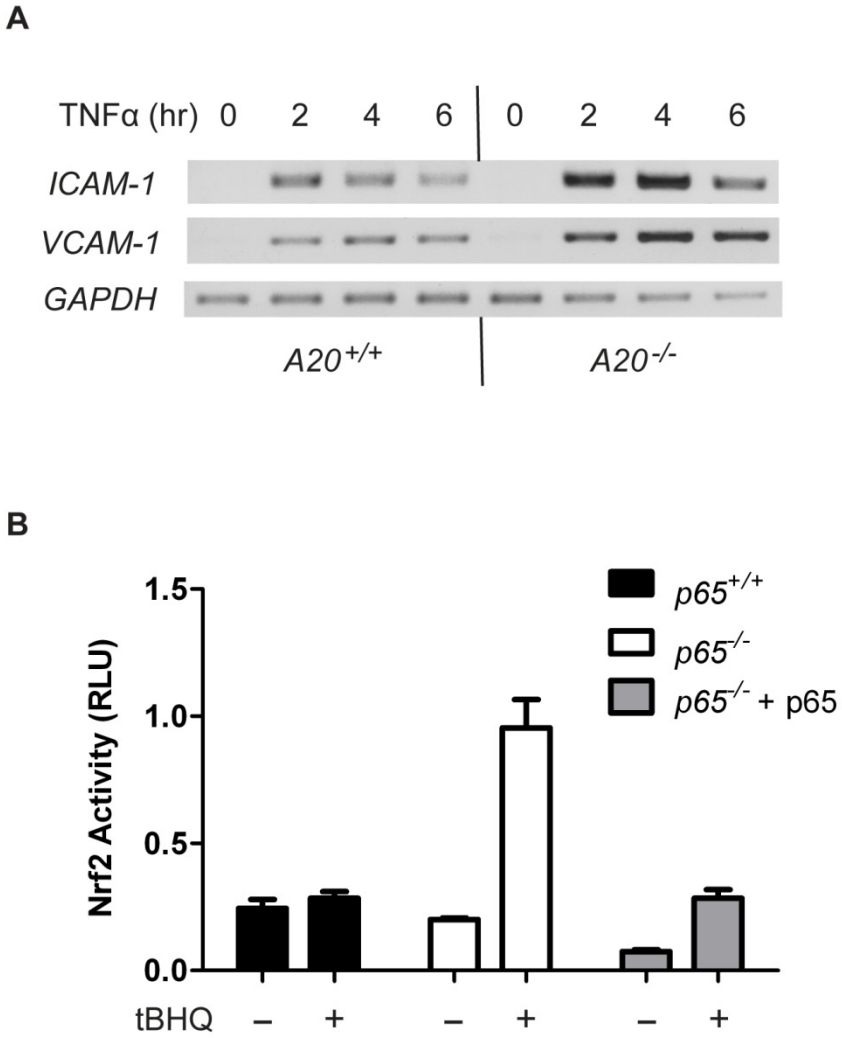

Figure 3.6 Increased NF-κB activity in *A20*$^{-/-}$ MEFs inhibits Nrf2 activity. (A) Expression of NF-κB targets is increased in *A20*$^{-/-}$ MEFs. *A20*$^{+/+}$ and *A20*$^{-/-}$ MEFs were treated with TNFα over a 6 hour time course. We extracted sample RNA, produced cDNA, and used semi-quantitative RT-PCR to analyze *ICAM-1*, *VCAM-1*, and *GAPDH* expression. (B) P65 inhibits Nrf2 activity in MEFs. *P65*$^{+/+}$ and *p65*$^{-/-}$ MEFs were transfected with p65 overexpression vector or empty vector and treated with tBHQ overnight as indicated. Cultures were lysed with reporter lysis buffer, subjected to one round of freeze thaw, cleared by centrifugation, and assessed for luminescence on a 96-well luminometer. RLUs are reported as RLU normalized to total protein in each sample.

Chapter IV

CONCLUSIONS

CONCLUSIONS

The work that initiated our study of DJ-1 started well over a decade ago. It began with the seemingly unrelated discovery that a subset of NSCLC cell lines, including H157 cells, produces IL-8 in response to Paclitaxel (13). This IL-8 secretion is dependent on both AP-1 and NF-κB as it can be inhibited using the MEK inhibitor U0126 or by overexpression of the IκB super-repressor respectively. Our group's hypothesis at the time was that the released IL-8 was serving a protective function. By combining Paclitaxel with U0126 to block the IL-8 secretion, our lab found a significant increase in cytotoxicity compared to either treatment alone (14). To better understand the mechanism of this combination therapy, 2D gels were run on H157 cells treated with U0126, Paclitaxel, or the U0126/Paclitaxel combination. The goal was to identify proteins specifically downregulated in the combination therapy sample. The two proteins pulled out of this screen were RhoGDI and DJ-1 (3). Overexpression of DJ-1 in H157 cells conferred protection from Paclitaxel and U0126-induced cell death and was present in 6 out of 7 human NSCLC tumor samples as compared to healthy tissue margins.

Very little was known about DJ-1 at that point in time, but its association with human diseases made its importance undeniable. The *Park7* gene, which encodes for DJ-1, is named due to DJ-1's association with PD (28). Mutation or deletion of the *Park7* gene was been found in multiple families with hereditary early-onset PD (28, 30). While direct genetic causes of PD constitute a minority of PD cases, they

offer a unique opportunity to study the development of PD. The hypothesis at the time was if loss of DJ-1 activity leads to the death of dopaminergic neurons in the substantia nigra, the hallmark of PD, then DJ-1 must protect these neurons from cellular insults or stress implicating DJ-1 in cell survival.

As loss of DJ-1 activity leads to cell death, an increase in DJ-1 activity enhances cell survival leading to its association with cancer. Early work on DJ-1 reported that DJ-1 transformed cells weakly by itself, but did so strongly in combination with H-Ras (1). Our lab was first to show that DJ-1 is overexpressed in NSCLC patient tumors and that DJ-1 overexpression protects cancer cells from chemotherapeutics (3). Since then, numerous types of cancer have been shown to have increased DJ-1 levels including ovarian, clear cell renal cell, pancreatic, and hepatocellular carcinoma. While DJ-1's effects on cell survival have been well documented since that time, no unified mechanism of action for DJ-1 has been identified that fully explains its association with both PD and cancer.

To elucidate the mechanism of action of DJ-1, our lab began studies on DJ-1 using two unbiased approaches. We used microarray and mass spectrometry to identify downstream targets and direct binders of DJ-1 respectively. Our plan was to use this information to formulate a better picture of how DJ-1 functions. The findings from our microarray studies were published in 2006. Microarray analysis of H157 cells treated with DJ-1 siRNA showed a decrease in the expression of NQO1, a downstream target of the transcription factor Nrf2 (50). We found that DJ-1 positively regulates Nrf2 by promoting the disassociation of Nrf2 from its cytoplasmic inhibitor Keap1. This disassociation increases Nrf2 protein half-life, protein

expression, and activity. Nrf2 targets include proteins in the small molecule antioxidant pathways, antioxidant proteins, and detoxification enzymes. These proteins are designed to detoxify ROS but they can also theoretically detoxify chemotherapeutics. Nrf2 can also decrease chemotherapeutic efficacy by inducing the expression of drug transporters. While this work identified a mechanism by which DJ-1 can affect cell survival in the face of toxic stimuli, we could not identify a direct mechanism of DJ-1 as DJ-1 does not bind to Nrf2, Keap1, or ARE binding sites. To analyze the direct effects of DJ-1 binding, we turned to mass spectrometry.

As outlined in chapter 2, our mass spectrometry experiment was designed with the characteristics of DJ-1 in mind. By using *Park7*$^{-/-}$ MEFs transfected with wild type or C106A DJ-1 and treated with H_2O_2, we identified proteins that bound to oxidized or non-oxidized DJ-1 with the highest sensitivity possible while minimizing background. This experiment found DJ-1 bound to 4 proteins – Cezanne, BBS1, CLCF1, and MTREF1. While novel at the time, an interaction between DJ-1 and BBS1 has been reported further validating our experimental design (196). We focused our attention on Cezanne for two reasons. First, Cezanne is a de-ubiquitinating enzyme and ubiquitin plays a critical role in Nrf2 regulation (148). Second, Cezanne already had known downstream effects through its inhibition of NF-κB (147). Using overexpression, hemi-endogenous, and fully endogenous co-immunoprecipitations, we confirmed an interaction between Cezanne and DJ-1, showed that this binding is enhanced by oxidation at the C106 residue of DJ-1, and found that the amino-terminus of DJ-1 is sufficient to mediate this interaction. We

also showed that this interaction leads to the inhibition of Cezanne's de-ubiquitination activity.

The big question at this time was which pathway this interaction affected as Cezanne could be the missing link between DJ-1 and Nrf2 regulation or DJ-1 could be regulating NF-κB through Cezanne. To answer this question, we again turned to microarray analysis. We compared untreated H157 cells that had been transduced with DJ-1 or Cezanne shRNA and cross-referenced the genes that were changed. As no Nrf2 targets were found to be changed in the Cezanne shRNA sample, a functional link between Cezanne and Nrf2 was rejected. Two NF-κB targets, IL-8 and ICAM-1, were found to be decreased in the absence of DJ-1 and increased in the absence of Cezanne. The microarray results were confirmed at the message and protein level by real-time PCR, immunoblot, and ELISA. This suggested a role of DJ-1 in NF-κB regulation which was confirmed as nuclear p65 was found to be decreased in the absence of DJ-1. We confirmed that DJ-1 protects cells from Paclitaxel/U0126 treatment while finding that Cezanne enhances cell death as H157 cells transduced with Cezanne shRNA were found to be resistant to Paclitaxel/U0126 treatment. Finally, this pathway was confirmed in primary MEFs to ensure that this was not an aberrant pathway found in only H157 cells.

This work is the first to identify a link between DJ-1 and the pro-survival transcription factor NF-κB. This pathway represents a novel mechanism by which DJ-1 can enhance cell survival. NF-κB is constitutively activated in numerous human cancers. This activation is not typically due to direct NF-κB activation but through the activation of upstream signaling molecules. Our findings suggest that

the NF-κB activation seen in cancer cells may partially be due to overexpression of DJ-1. The identification of IL-8 and ICAM-1 as affected NF-κB targets not only brings our project full circle, by tying in our original IL-8/Paclitaxel findings, but also implicates DJ-1 in cancer angiogenesis, invasion, progression, and metastasis. While cell survival is a hallmark of cancer, it is these hallmarks that define the most malignant, deadly, and aggressive tumors. Of course, further *in vivo* studies will be required to confirm a role of DJ-1 in these malignant tumor hallmarks.

In chapter 3, we uncovered a novel mechanism of crosstalk between the Nrf2 and NF-κB pathways. Due to the sequence homology between Cezanne and A20 (147), we tested the ability of A20 to bind DJ-1 and other proteins in the DJ-1/Nrf2 axis including Nrf2 and Keap1. Surprisingly, A20 did not bind DJ-1 but instead was found to bind Keap1 by overexpression co-immunoprecipitation. This interaction was confirmed by hemi-endogenous co-immunoprecipitation. During our search for the functional consequences of this interaction, our preliminary data showed that A20 positively regulates Nrf2 by the ubiquitination and degradation of Keap1. Unfortunately, inconsistencies in the data, including an unusual increase in inactive, nuclear Nrf2 in *A20*$^{-/-}$ cells, led us to hypothesize that the hyperactivation of NF-κB in the absence of A20 may be obscuring the role of A20 and Keap1 interaction in this cell type. This hypothesis was bolstered by data showing increased activity of NF-κB in *A20*$^{-/-}$ MEFs as well as the inhibition of Nrf2 activity by p65 in MEFs. Due to the importance of Keap1 and A20 as negative regulators of Nrf2 and NF-κB activity, this interaction represents a potentially key crosstalk mechanism between these two pathways. To further study the effect of the A20/Keap1 interaction on Nrf2 and NF-

κB, it may be necessary to knockout p65 or Nrf2 to eliminate crosstalk. This of course may then require the overexpression of A20 or Keap1 as these proteins are transcribed by the transcription factors they inhibit.

This dissertation identifies DJ-1 as one of the few stimuli known to positively regulate both Nrf2 and NF-κB while also identifying a putative crosstalk mechanism between these two downstream pathways. In our current model, DJ-1 binds to Cezanne blocking its de-ubiquitinating activity (Fig. 4.1). We hypothesize that this inhibition of Cezanne leads to an increase in activating ubiquitin on RIP1 and TRAF6, although further experiments will be required to confirm this. The downstream effect of the DJ-1/Cezanne interaction is enhanced NF-κB activity and increased transcription and protein expression of both IL-8 and ICAM-1. This increase in NF-κB activity is paired with the concurrent activation of Nrf2 by DJ-1 although the molecular mechanism of this Nrf2 activation remains elusive. While the paired activation of Nrf2 and NF-κB is modulated by inhibitory crosstalk between these two pathways, the final outcome is an increase in cell survival due to Nrf2-mediated protection of the cells from oxidative and toxic stress, including chemotherapeutics, and NF-κB-mediated cell cycle progression and cell survival through the induction of cyclin D, Bcl-2, and IAPs. Adding these pathways to the other signaling pathways shown to be regulated by DJ-1 in the last 4 years, we start to see a clearer picture of how vital a role DJ-1 plays in cell survival (Fig. 4.2).

Targeting DJ-1 in novel therapies is attractive for three main reasons. First, DJ-1's activity is associated with a spectrum of human disease suggesting that manipulation of DJ-1 activity may represent a way to treat disease. Second, DJ-1

has multiple downstream targets that play redundant roles. Using the example of DJ-1 inhibiting drugs in cancer treatment, this redundancy would allow DJ-1 inhibiting drugs to promote cancer cell death even in cancer cells with pro-survival mutations in multiple pathways. Third, DJ-1 can easily be measured in the serum using ELISA. In cancer patients, tumor overexpression of DJ-1 increases DJ-1 levels in the serum. Efficacy of DJ-1 inhibiting drugs can therefore be correlated with DJ-1 levels allowing tailoring of DJ-1 inhibiting therapies to the patients most likely to respond to treatment.

As of the writing of this dissertation, no specific small molecule inhibitors of DJ-1 exist for treatment of cells or patients. While we found a decrease in DJ-1 expression with Paclitaxel/U0126 combination treatment, this regimen is neither specific for DJ-1 nor approved for use in cancer patients. There are many potential hurdles in the development of drugs that manipulate DJ-1 activity. The first and foremost hurdle is the druggability. Only a subset of protein types is capable of being targeted with small molecule inhibitors. The major problem lies in the fact that while many molecular activities for DJ-1 have been proposed, no one activity has been shown to mediate all of its downstream activities. Continued research into the activity of DJ-1 will therefore be necessary to address the druggability of DJ-1. Even if it is determined that the primary activity of DJ-1 is not druggable, specific interactions, such as the DJ-1/Cezanne interaction, or known downstream effectors of DJ-1 can be targeted.

Drug targeting of DJ-1 is currently most pertinent as a treatment in cancer therapy. Inhibition of DJ-1 has the potential to sensitize cancer cells to

chemotherapeutics, increase cancer cell death, and decrease cancer angiogenesis, invasion, progression, and metastasis through DJ-1's multiple downstream targets. While this is an attractive hypothesis, the effect of any DJ-1 inhibiting drug must be ascertained in non-cancerous cells as inhibition of DJ-1 in dopaminergic neurons during treatment may have grave unintended side effects. These side effects may be minimized or completely avoided through the use of new cancer targeting modalities such as light activated liposomes, which only release drugs in areas bombarded with light.

Targeting DJ-1 in Parkinson's disease poses its own set of challenges. First, a drug must be developed to enhance DJ-1 activity which is no small feat in light of the fact that so little is known about the regulation of DJ-1 expression and activity. Second, the drug must be able to cross the blood-brain barrier if it is affect the target dopaminergic neurons. Third, specificity for dopaminergic neurons may be required to avoid unintended activation of DJ-1 in pre-cancerous cells. Finally, DJ-1 activating drugs may only be able to halt the progression of PD not completely reverse it. PD symptoms only appear after a majority of dopaminergic neurons have already been lost. Administration of DJ-1 activating drugs may protect the remaining neurons, but due to the lack of neuronal division in the central nervous system the number of dopaminergic neurons may not return to normal.

The work summarized here identifies a novel pathway by which DJ-1 promotes cell survival. We are the first to discover an association between DJ-1 and NF-κB as well as an effect of DJ-1 on a de-ubiquitinating enzyme. Although DJ-1 is already known to inhibit pro-apoptotic signals, induce pro-survival signals, and

control cellular oxidative responses, the role of NF-κB in cell survival, cancer development, and malignant cancer hallmarks reinforces the importance of DJ-1 research as well as development of DJ-1 small molecule inhibitors. Despite the barriers to development of drugs targeting DJ-1, the central role of DJ-1 in cell survival warrants further investigation as manipulation of DJ-1 activity may yield novel modalities to control the balance between cell survival and cell death with implications in Parkinson's disease and cancer.

Figure 4.1: Model of NF-κB activation by DJ-1

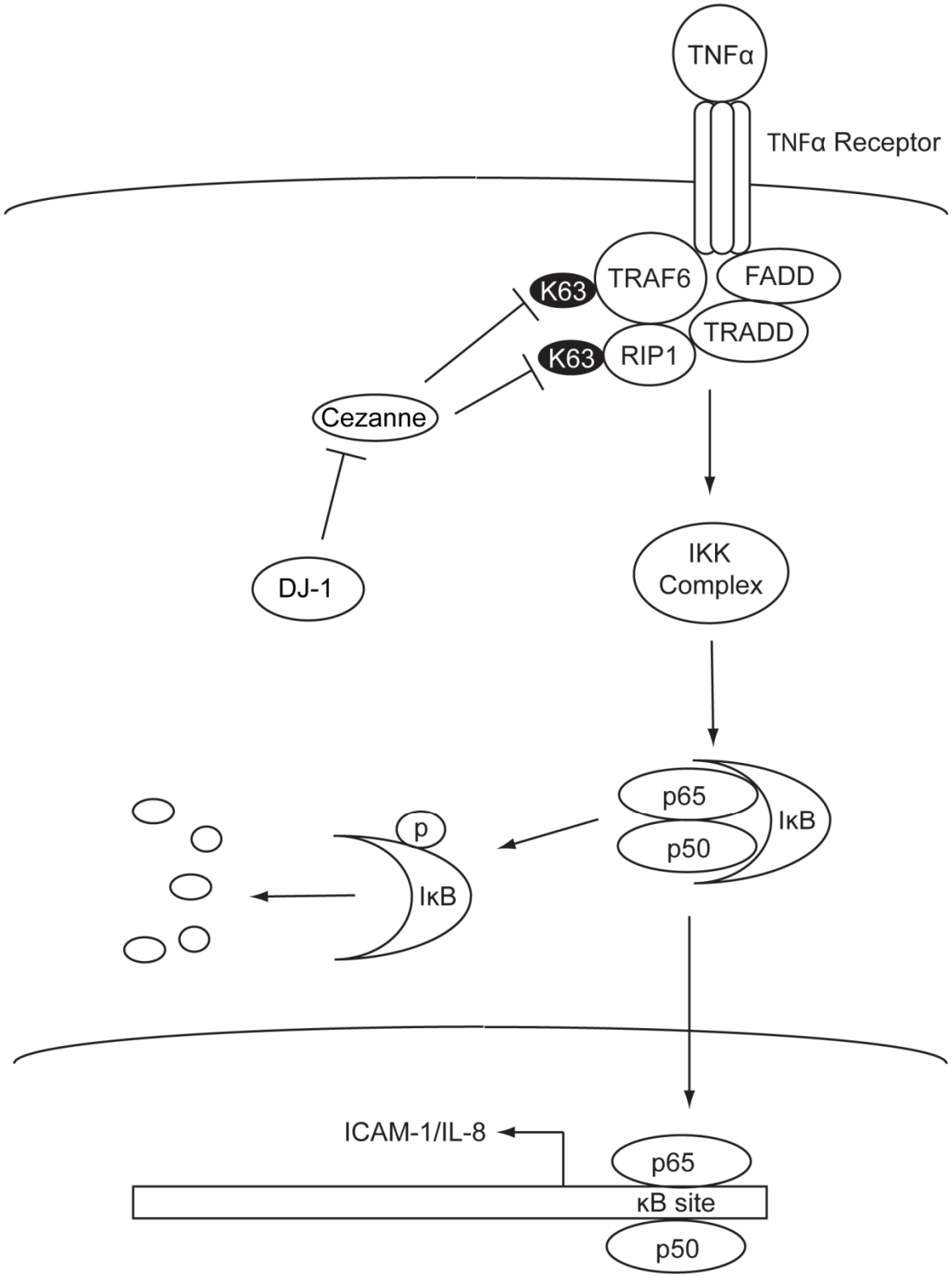

Figure 4.1 Model of NF-κB activation by DJ-1. DJ-1 inhibits the removal of activating ubiquitin from RIP-1 and TRAF6 by Cezanne. This leads to increased RIP-1 and TRAF6 activation as well as increased phosphorylation and degradation of IκB by the IKK complex. This results in NF-κB translocation, κB site binding, and activation of IL-8 and ICAM-1 transcription.

Figure 4.2: Overview of the effect of DJ-1 on signaling and transcription

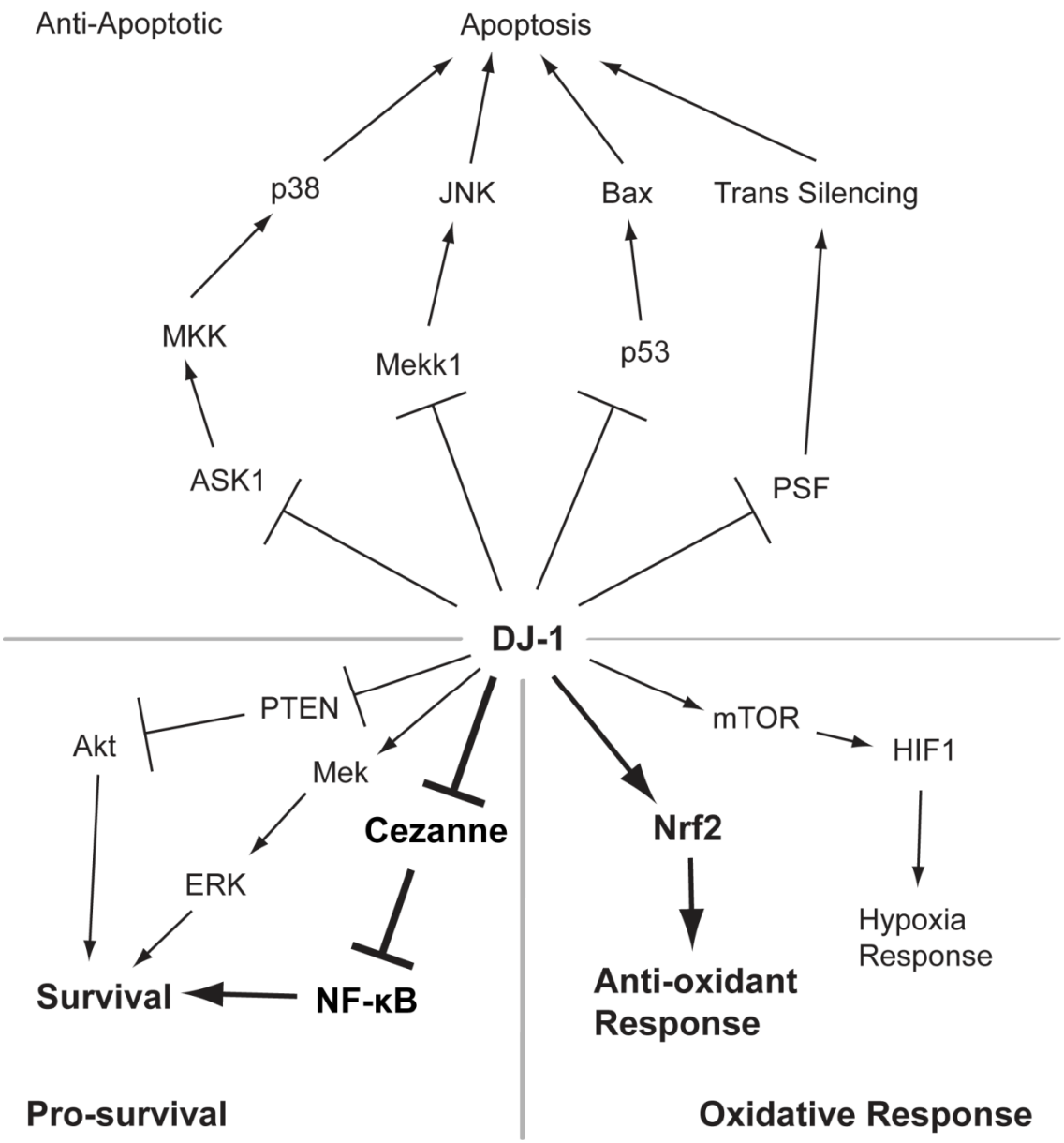

Figure 4.2 Overview of the effect of DJ-1 on signaling and transcription. Pathways are split in 3 major groups – anti-apoptotic, pro-survival, and oxidative response. Contributions from our lab are indicated in bold.

Appendix

DJ-1, A CANCER- AND PARKINSON'S DISEASE-ASSOCIATED PROTEIN, STABILIZES THE ANTIOXIDANT TRANSCRIPTIONAL MASTER REGULATOR NRF2

Clements CM, McNally RS, Conti BJ, Mak TW,Ting JP (2006) DJ-1, a cancer- and Parkinson's disease-associated protein, stabilizes the antioxidant transcriptional master regulator Nrf2. *Proc Natl Acad Sci U S A* 103: 15091-15096.

Abstract

DJ-1/PARK7, a cancer- and Parkinson's disease (PD)-associated protein, protects cells from toxic stresses. However, the functional basis of this protection has remained elusive. We found that loss of DJ-1 leads to deficits in NQO1 [NAD(P)H quinone oxidoreductase 1], a detoxification enzyme. This deficit is attributed to a loss of Nrf2 (nuclear factor erythroid 2-related factor), a master regulator of antioxidant transcriptional responses. DJ-1 stabilizes Nrf2 by preventing association with its inhibitor protein, Keap1, and Nrf2's subsequent ubiquitination. Without intact DJ-1, Nrf2 protein is unstable, and transcriptional responses are thereby decreased both basally and after induction. This effect of DJ-1 on Nrf2 is present in both transformed lines and primary cells across human and mouse species. DJ-1's effect on Nrf2 and subsequent effects on antioxidant responses may explain how DJ-1 affects the etiology of both cancer and PD, which are seemingly disparate disorders. Furthermore, this DJ-1/Nrf2 functional axis presents a therapeutic target in cancer treatment and justifies DJ-1 as a tumor biomarker.

Introduction

Oxidative stress has been implicated as a major contributing factor in a wide variety of ailments. Cancer, cardiovascular disease, neurodegenerative disorders, and aging all are associated with increased oxidative stress in tissues. Such stress results from the accumulation of oxidative species due to their metabolic generation and environmental exposures. These oxidative species are detoxified by a gambit of antioxidant enzymes and molecules. The balance between oxidative species generation and removal determines the oxidative stress on a given tissue. Not surprisingly, therefore, cellular responses to oxidative stress are major determinants of disease susceptibility, particularly in tissues that are sensitive to oxidative stress, such as in the central nervous system. Genetic defects in oxidative responses lead to neurodegenerative diseases. Examples include mutations in SOD1 (superoxide dismutase 1) that lead to ALS (197) and loss of DJ-1, which leads to early onset Parkinson's disease (PD) with high penetrance (198).

DJ-1 was initially described as a putative oncogene that is able to transform cells weakly on its own and more strongly in combination with Ras (1). DJ-1 is expressed at high levels in primary lung and prostate cancer biopsies (3, 172), and its expression correlates negatively with clinical outcomes in non-small cell lung carcinoma patients (36). The DJ-1 protein affects cell survival, in part, by modulating cellular signaling cascades such as PTEN/phosphatidylinositol 3-kinase/Akt (15) and altering p53 activity (199). Additionally, we and others have previously shown that DJ-1 expression in cancer cell lines conveys protection against stresses, including chemotherapy, oxidative stress, endoplasmic reticulum stress, and proteosome

inhibition (3, 58, 174). The mechanism by which DJ-1 imparts this protection remains unknown. We report here that DJ-1 is required for the activity of Nrf2 (nuclear factor erythroid 2-related factor), a master regulator of response to oxidative stress.

Nrf2 is a member of the cap 'n' collar family of basic leucine zipper transcription factors that regulate the expression of many antioxidant pathway genes (200). Nrf2 is maintained at basal levels in cells by binding to its inhibitor protein, Keap1 (92, 201). Keap1 is a BTB (Broad complex, Tramtrack, Bric-a-Brac) domain-containing protein that targets Nrf2 for ubiquitination by Cul3/Roc-1, leading to its constitutive degradation (94, 202-204). Upon exposure to oxidative stress, xenobiotics, or electrophilic compounds, Nrf2 protein is stabilized and translocates to the nucleus (34). There, it forms heterodimers with other transcription regulators, such as small Maf proteins, and induces the expression of antioxidant genes (97, 205). Nrf2 drives the expression of detoxification enzymes, such as NQO1 [NAD(P)H quinone oxidoreductase 1] and Hmox-1, and enzymes that generate antioxidant molecules, such as glutathione (98, 157). Nrf2 function and the expression of its regulated genes, including NQO1, have been implicated in the risk and/or prevention of both cancer and PD (206-211).

In this study, we find that DJ-1 is required for the expression of several genes, including the prototypic Nrf2-regulated antioxidant enzyme NQO1. We report here that DJ-1 is indispensable for Nrf2 stabilization by affecting Nrf2 association with Keap1, an inhibitor protein that promotes the ubiquitination and degradation of Nrf2. These findings implicate DJ-1's effects on Nrf2 in the development of Parkinson's disease and cancer and present potential therapeutic targets.

Results

siRNA-Mediated Knockdown of DJ-1 and Affymetrix GeneChip Analysis.

To explore DJ-1's function, we examined its effect on global gene expression. DJ-1 expression was reduced by siRNA in H157 non-small-cell lung carcinoma cells (Fig. 1). The characterization of the antibody used to verify DJ-1 expression is shown in Fig. 6, which is published as supporting information on the PNAS web site. The first DJ-1 siRNA (referred to as siDJ-1#1) caused a modest decrease in DJ-1, whereas siDJ-1#2 caused a profound decrease. RNA samples from cells with siDJ-1#1, two control scrambled oligomers (siCTL), and one mock-transfected sample were subjected to GeneChip profiling (Affymetrix, Santa Clara, CA). To ensure that changes warranted further study, we stringently filtered expression to exclude differences <3-fold and any genes having spots with a raw signal intensity of <500 units in the samples where a gene was determined to be present. This stringent filtering produced a list of 3 genes that were increased and 14 genes that were decreased in cells with siDJ-1 (Fig. 2). As expected, siDJ-1 reduced *DJ-1* expression.

Among the genes whose expression decreased in the absence of DJ-1, one of particular interest was *NQO1*. NQO1 is a well described detoxification enzyme (212) that has been implicated in the risk and prevention of cancer and neurodegenerative diseases (213-216). NQO1 is regulated to a large degree by gene transcription by means of an antioxidant response element (ARE) in its

promoter (217), which is a prototypic target of the antioxidant transcription factor Nrf2 (98). With this fact in mind, we used the tfsearch algorithm (218) to search for putative AREs within 1,000 bp upstream of the transcriptional start site of the genes identified in Fig. 2. Seven of 17 genes that were changed by >3-fold by siDJ-1 contained an ARE-like sequence (TMAnnRTGAYnnnGCRwwww) in their promoters (Fig. 2, rightmost column). We then reanalyzed our microarray data with respect to Nrf2 and found that several Nrf2-regulated genes were altered in the absence of DJ-1 (Fig. 7). All array data have been deposited in the Gene Expression Omnibus online repository.

DJ-1 Is Required for Nrf2-Mediated Transcription.

To verify the microarray data, we used *NQO1* as a prototypic target gene of DJ-1. Real-time PCR analysis shows that siDJ-1#2 reduced DJ-1 and NQO1 by >80%. However, Nrf2 mRNA expression was not changed (Fig. 3*A*), indicating that NQO1 expression differences are not due to a reduction of Nrf2 mRNA. To determine whether DJ-1 affects *NQO1* gene transcription by means of Nrf2 function, we used a reporter construct, pGL2-ARE, which contains the firefly luciferase gene under the control of an ARE from the human *NQO1* promoter (Fig. 3*B*). This construct was tested in the absence or presence of DJ-1. The liver cell line Huh7 was used because Nrf2 activity can be induced in these cells by the nontoxic food preservative *tert*-butylhydroquinone (tBHQ) (219). Cells were treated with either 50 μM tBHQ or DMSO vehicle control, and luciferase activity was measured (Fig. 3*B*).

Flag-Nrf2 was transfected into cells as a positive control. Overexpressed Nrf2 robustly activated ARE-regulated luciferase (Fig. 3*B*, lanes 1 vs. lane 2). Cells with siCTL produced a basal level of luciferase, whereas tBHQ induced luciferase expression as expected (220) (Fig. 3*B*, lanes 3 and 4). In the presence of siDJ-1#1 or siDJ-1#2, luciferase activity was reduced (Fig. 3*B*, lanes 5 and 7), and it was no longer stimulated by tBHQ treatment (lanes 6 and 8). This effect is specific for the ARE element, as evidenced by the fact that siDJ-1 did not affect other promoter elements (Fig. 3 *C* and *D*).

DJ-1 Is Required for Nrf2 Protein Stability.

Given that DJ-1 was required for both basal and induced ARE-driven transcription, we explored some possible mechanisms. DJ-1 was not associated with the*NQO1*promoter as assessed by chromatin immunoprecipitation assay, suggesting that DJ-1 is not likely tethered on the *NQO1* promoter with Nrf2 (Fig. 8). Furthermore, RNA expression of Nrf2 (see Fig. 2*A*) or its inhibitor, Keap1, was not changed by siDJ-1 (Fig. 9). However, Western blot analysis revealed that Nrf2 protein expression was drastically reduced in the absence of DJ-1, with siDJ-1#1 causing a more modest decrease and siDJ-1#2 causing a dramatic decrease (Fig. 4*A*), consistent with the level of DJ-1 reduction achieved with these two siRNA (see Fig. 1*A*).

To determine whether DJ-1 reduced Nrf2 stability, DJ-1 was decreased by siDJ-1 in Huh7 cells, and the cells were treated with the translation inhibitor

cyclohexamide to prevent new protein synthesis. Cells were lysed at various time points, and the degradation kinetics of Nrf2 and actin (as a control) was analyzed by Western blot. Nrf2 protein was decreased by siDJ-1 compared with siCTL or transfection reagents alone, and, by 90 min, Nrf2 disappeared in cells with siDJ-1 (Fig. 4*B*), indicating that DJ-1 stabilizes Nrf2 protein.

Nrf2 protein stability is an important regulatory event that is tightly controlled by its association with a cytosolic inhibitor protein, Keap1 (92, 201). Under unstimulated conditions, Nrf2 associates with Keap1, which targets Nrf2 for ubiquitination by a Cullin-3-dependent mechanism (94, 202-204), leading to proteosome-dependent degradation (221). Given our data implicating DJ-1 in Nrf2 stability, we tested DJ-1's effect on Nrf2 ubiquitination (Fig. 4*C*). Huh7 cells expressing HA-tagged ubiquitin and Nrf2 were transfected with DJ-1 or pcDNA. Nrf2 was immunoprecipitated from denatured lysates, isolating only molecules covalently linked to Nrf2. Ubiquitin-Nrf2 conjugates were visualized by immunoblotting for the ubiquitin epitopeHA.Nrf2 was ubiquitinated to a much lesser degree when DJ-1 was overexpressed (Fig. 4*C*, upper blot, lanes 1 and 2), correlating with an increase of Nrf-2 protein in the presence of DJ-1 (lower blot). The addition of the proteosome inhibitor MG132 prevented degradation of ubiquitinated Nrf2 (Fig. 4*C*, lanes 5 and 6).

Given that the association of Keap1 with Nrf2 is known to trigger Nrf2 ubiquitination and degradation (93) and that DJ-1 reduces Nrf2 ubiquitination, we determined whether DJ-1 affects the association of Nrf2 and Keap1. Huh7 cells were transfected with V5-tagged Keap1 (the tagged epitope is required because of the

lack of a sufficient and commercially available Keap1 antibody). The anti-V5 antibody recognized V5-Keap1 and co-immunoprecipitated Nrf2 (Fig. 4*D*, lane 1); the inclusion of Flag-DJ-1 eliminated this co-immunoprecipitation (Fig. 4*D*, lane 2). Reverse immunoprecipitation shows that antibody to endogenous Nrf2 co-precipitated V5-Keap1 (Fig. 4*D*, lane 4), which was also decreased by Flag-DJ-1 (lane 5). These data suggest that DJ-1 stabilizes Nrf2 by preventing its association with Keap1.

Although the above experiments demonstrate a strong functional link between DJ-1 and Nrf2, we have so far been unable to determine where DJ-1 physically exerts this effect. Co-immunoprecipitation experiments have failed to find DJ-1 in physical association with Nrf2, Keap1, or Cullin-3 (Fig. 10). Therefore, it remains to be determined whether DJ-1's profound effect on Nrf2 is the result of direct or indirect molecular mechanisms.

DJ-1 Is Required for Nrf2 Function in Primary Mouse Embryonic Fibroblasts (MEFs).

To determine whether DJ-1 is required for Nrf2 expression in primary untransformed cells, we isolated day-13.5 MEFs from *DJ-1*$^{-/-}$ mice (36) and induced Nrf2 protein expression by using tBHQ treatment. tBHQ induced murine Nrf2 (mNrf2) protein expression in WT littermates (n = 4; two are shown in Fig. 5*A*), whereas *DJ-1*$^{-/-}$ mice failed to show induced mNrf2 expression (n = 4; two are shown in Fig. 5*A*). Restoration of DJ-1 with a Flag-DJ-1 expression plasmid also restored

Nrf2 protein expression with tBHQ treatment (Fig. 5*B*), which indicates that the loss of Nrf2 protein in *DJ-1*$^{-/-}$ fibroblasts is a specific consequence of the loss of DJ-1.

To examine the necessity of DJ-1 for Nrf2 function, we resorted to the Nrf2-activated reporter plasmid pGL2-ARE. *DJ-1*$^{+/+}$ and *DJ-1*$^{-/-}$ MEFs from four mice (two representatives are shown in Fig. 5*C*) were separately transfected with pGL2-ARE and then induced with 50 μM tBHQ. WT *DJ-1*$^{+/+}$ cells showed increased luciferase expression upon tBHQ treatment, whereas *DJ-1*$^{-/-}$ cells did not (Fig. 5*C Left*). SV40 promoter activity was independent of DJ-1 (Fig. 5*C Right*).

To use a more physiologic measurement, we tested the effect of DJ-1 on the expression of Nrf2-regulated detoxification enzymes: NQO1 and GCLM (glutathione cysteine ligase modifier subunit) (Fig. 5*D*). Based on the microarray analysis (Fig. 7), siDJ-1 reduced GCLM expression by 1.478-fold; hence, we selected it in addition to NQO1 for further analysis. Induction of MEF cultures with 25 μM tBHQ led to a substantial increase of mNQO1 in *DJ-1*$^{+/+}$ MEFs, but this increase was drastically reduced in *DJ-1*$^{-/-}$ cells. This pattern is also found for murine GCLM. However, at higher (100 μM) dosage, even though differences in mNrf2 protein expression persisted (Fig. 5*A*), induction of detoxification enzymes was only slightly reduced in *DJ-1*$^{-/-}$ compared with *DJ-1*$^{+/+}$ MEFs (Fig. 11), indicating that a high concentration of tBHQ can activate a DJ-1-independent pathway to cause NQO1 and GCLM expression.

Discussion

In summary, this work describes functional effects of the DJ-1 protein by means of Nrf2, a master regulator of antioxidant gene responses. Cancer and PD lie at opposite ends of a spectrum defined by dysfunctions in cell death. Our finding may explain how DJ-1 plays an important role in both diseases. One of the hallmarks of PD is the loss of substantia nigra dopaminergic neurons, leading to motor deficits (222). *DJ-1*$^{-/-}$ mice did not exhibit widespread neuronal loss in a PD disease model (32, 36), but these neurons were more susceptible to death after toxic insults (36). Likewise, human neuronal cell lines with DJ-1 knockdown are more sensitive to toxic compounds (58, 174). The loss of antioxidant gene transcription could account for these phenotypes that are only evident after environmental harm.

It is noteworthy that we initially identified DJ-1's effect on Nrf2 in lung tumor cells. Studies of Nrf2 knockout mice show that Nrf2 plays a significant role in lung biology (200). In our studies, we found that the H157 lung tumor cells did not consistently induce Nrf2 activity after tBHQ treatment; instead, they had a very high basal level of activity that was not inducible by treatment (data not shown). High basal NQO1 expression allowed us to confidently quantify changes in NQO1 expression and implicated the broader effect of DJ-1 on Nrf2. To study gene induction, we then used liver cell line models, which are highly inducible. These

models allowed us to identify the effects of DJ-1 on Nrf2, which heretofore remained unrecognized.

Enhanced expression of DJ-1 in cancer cells, leading to increased detoxification enzymes, is likely to provide a survival advantage. These enzymes may be exploited as treatment targets in tumors. For example, NQO1, an obligate two-electron reductase, can reduce antitumor quinones, leading to their bioactivation. Mitomycin C (MMC) and the antitumor compound 2,5-diaziridinyl-3-(hydroxymethyl)-6-methyl-1,4-benzoquinone are activated by NQO1 activity, and NQO1 is shown to increase the efficacy of MMC *in vivo* (223). It is possible that tumors with high DJ-1 levels might be more susceptible to therapies that rely on enzymes such as NQO1, underscoring the potential of DJ-1 as a biomarker to define specific antitumor therapies.

Materials and Methods

Cell Cultures, Treatments, and Plasmid Constructs. Huh7 cells were grown in DMEM (Sigma, St. Louis, MO) with 7% FCS. H157 cells were grown in RPMI medium 1640 (Gibco, Carlsbad, CA) plus 10% FCS. All mammalian cell cultures were grown in the presence of penicillin and streptomycin to minimize contamination effects.

tBHQ (Fluka, St. Louis, MO) was dissolved in DMSO (final concentration on cells was 0.0001%), and cells were treated for 18–24 h. Dexamethasone and forskolin (MP Biochemicals, Irvine, CA) were dissolved in DMSO and ethanol, respectively. Dexamethasone was used at a final concentration of 100 μM, and forskolin was used at 10 μM. In experiments determining Nrf2 protein stability, cells were treated with cyclohexamide (Sigma) in DMSO at a concentration of 75 μg/ml for up to 2 h. The peptide proteosome inhibitor MG132 (Calbiochem, San Diego, CA) was used at 25 μM for 4–6 h for ubiquitination studies.

Other investigators generously provided Flag-DJ-1 (172), Flag-Nrf2 (204), and hNQO1-ARE-pGL2 (224) plasmids. SV40-luciferase (pGL3-control), GRE-luciferase (pGRE-Luc, Clontech, Mountain View, CA), and CRE-luciferase (pCRE-Luc; Clontech) were all purchased from commercial sources. We directionally cloned human Keap1 into the V5/His-containing pcDNA3.1D-Topo plasmid (Invitrogen, Carlsbad, CA) by amplifying the Keap1 ORF with the primers 5'- ACC ATG CAG CCA GAT CCC AGG CCT AGC-3' and 5'-ACA GGT ACA GTT CTG CTG GTC AAT

CT-3' by using platinum-*pfx* polymerase (Invitrogen). Clone directionality and expression was verified by sequencing and Western blot analysis. Human cell lines were transfected with DNA by using FuGENE 6 (Roche, Basel, Switzerland), and MEF cultures were transfected with Lipofectamine 2000 (Invitrogen) per the manufacturer's instructions.

siRNA Knockdown of DJ-1. Cell lines were transfected with siDJ-1-1 5'-NNG ACC CAG UAC AGU GUA GCC-3', siDJ-1-2 5'-NNU GGA GAC GGU CAU CCC UGU-3', scrambled control oligomer (Xeragon, Huntsville, AL), siCONTROL (siCTL) nontargeting siRNA no. 1 (Dharmacon, Lafayette, CO), or transfection reagent alone by using Oligofectamine (Invitrogen) for H157 cells and Lipofectamine 2000 (Invitrogen) for Huh7 cells per the manufacturer's protocols. Cells were transfected on consecutive days for 2–3 days in a row, and lysates were taken for RNA and protein analysis 96 h after the first transfection.

Generation of Anti-DJ-1 Antibody. DJ-1 was cloned into 6X histidine- tagged *Escherichia coli* overexpression vector QE82L (Qiagen, Valencia, CA) by standard methodology. Expression of DJ-1 was induced with 1 mM isopropyl-β-D-thiogalactopyranoside in the *E. coli* strain BL21 (DE3). Cells were lysed in PBS plus EDTA-free protease inhibitor mixture (Roche), and DJ-1 was purified to >95% homogeneity with Ni-nitrilotriacetic acid (Qiagen) according to the manufacturer's

instructions. Recombinant DJ-1 was sent to Proteintech Group (Chicago, IL) for the production of the anti-DJ-1 rabbit polyclonal serum.

Affymetrix GeneChip Analysis. Total RNA isolated from H157 cells was DNase I-treated and column-purified (Promega, Madison, WI). The quality of the RNA was determined by formamide agarose electrophoresis and comparison of expression of housekeeping genes. Seven micrograms of total RNA was used to synthesize cDNA. A custom cDNA kit from Life Technologies (Carlsbad, CA) was used with a T7-(dT)24 primer for this reaction. Biotinylated cRNA was then generated from the cDNA reaction by using the BioArray High Yield RNA transcript kit (Ento Life Sciences, Farmingdale, NY). The cRNA was fragmented in fragmentation buffer (5X fragmentation buffer: 200 mM Tris-acetate, pH 8.1/500 mM KOAc/150 mM MgOAc) at 94°C for 35 min before the chip hybridization. Fragmented cRNA (15 μg) was then added to the hybridization mixture (0.05 μg/μl fragmented cRNA/50 pM control oligonucleotide B2, *BioB*, *BioC*, *BioD*, and *cre* hybridization controls/0.1 mg/ml herring sperm DNA/0.5 mg/ml acetylated BSA/100 mM Mes/1 M [Na+]/20 mM EDTA/0.01% Tween 20). Ten micrograms of cRNA was used for hybridization. Arrays were hybridized for 16 h at 45°C in the GeneChip Hybridization Oven 640. The arrays were washed and stained with R-phycoerythrin streptavidin in the GeneChip Fluidics Station 400. After this, the arrays were scanned with a GeneArray scanner (Hewlett–Packard, Palo Alto, CA). Affymetrix GeneChip Microarray Suite 5.0 software was used for washing, scanning, and basic analysis.

Sample quality was assessed by examination of 3’ to 5’ intensity ratios of certain genes.

These data were then further analyzed, filtered, and compared by using GeneSpring software (Silicon Genetics, Redwood City, CA). Genes defined as ‘‘changed’’ were filtered to include those differing >3-fold between both siCTL chips and siDJ-1 chips, with a raw fluorescence intensity of at least 500 in both of the highly expressed (present) arrays. Both siDJ-1 arrays were transfected with siDJ-1#1 and then verified by real-time PCR using both siDJ-1#1 and siDJ-1#2.

Real-Time Quantitative PCR. Reactions were carried out in an ABI 7900HT PCR system (Applied Biosystems, Foster City, CA) using a 15-μl, 384-well format and master mixes from ABGene (Rochester, NY). TaqMan PCR primer/probe sets were designed for human DJ-1: primer 1, 5’-CCA TAT GAT GTG GTG GTT CTA C-3’; primer 2, 5’-ACT TCC ACA ACC TAT TTC ATG AG-3’; probe, 5’-[6-FAM]ACC TGC ACA GAT GGC GGC TAT CA[Tamra-Q]-3’. Primer/probe sets for human NQO1 were as follows: primer 1, 5’-CCG TGG ATC CCT TGC AGA GA-3’; primer 2, 5’-AGG ACC CTT CCG GAG TAA GA-3’; probe, 5’-[6-FAM]ACA TGG AGC CAC TGC CAC CA[Tamra-Q]-3’. SYBR green real-time PCR primers were designed for human Nrf2: primer 1, 5’-AGT GGA TCT GCC AAC TAC TC- 3’; primer 2, 5’-CAT CTA CAA ACG GGA ATG TCT G-3’. We used previously published mouse G3PDH primers that were designed to be used with SYBR green quantitation (225).

Predesigned TaqMan PCR primer and probe sets were purchased from Applied Biosystems for mouse NQO1 and GCLM.

Luciferase Reporter Gene Assays. Cells were grown and transfected as described above in six-well plates (Falcon, San Jose, CA). Cultures were lysed in reporter lysis buffer (Promega) by using a single round of freeze–thaw at -80°C. Luciferase assays were then performed as described in ref. (226).

Western Blot Analysis and Immunoprecipitation. For all Western blot analyses, cells were lysed in RIPA buffer (10 mM NaPO4, pH 7.4/300 mM NaCl/0.1% SDS/1% Nonidet P-40/1% deoxycholic acid/2 mM EDTA) with protease inhibitors (Roche), diluted with SDS loading buffer, and boiled in the presence of the reducing agent DTT. Proteins were then separated by molecular weight by SDS/PAGE through polyacrylamide gels ranging from 6% to 12%. Proteins were electrophoretically transferred to nitrocellulose membranes and blocked by using 5% nonfat dry milk in TBS with 0.1% Tween 20. Antibodies used for blotting were anti-Nrf2 H-300 (Santa Cruz Biotechnology, Santa Cruz, CA), rabbit polyclonal anti-DJ-1, anti-actin-HRP (Santa Cruz Biotechnology), anti-G3PDH, anti-HA-HRP (Roche), and anti-Flag (M2)-HRP (Sigma).

Protein complexes were isolated from cell lysates by immunoprecipitation using antibodies specific for Nrf2 (H-300, Santa Cruz Biotechnology) and anti-V5 (Invitrogen), followed by incubation with protein A/G agarose (Pierce

Biotechnologies, Rockford, IL). Protein A/G antibody–protein complexes were washed extensively and eluted by boiling in loading buffer with reducing equivalents. Eluates and input lysate controls were then Western blotted to assay for protein expression and isolation.

Ubiquitination assays were performed in Huh7 cells transfected with epitope-tagged Nrf2 and ubiquitin grown in 100-mm2 plates. The cells were lysed in 200 μl of SDS lysis buffer (50 mM Tris HCl, pH 7.5/0.5 mM EDTA/1% SDS/1 mM DTT) and boiled for 10 min. Cellular debris was pelleted, and SDS concentrations were diluted by the addition of 1,200 μl of 0.5% Nonidet P-40 lysis buffer with added protease inhibitors. Anti-Flag (M2) agarose was then added and incubated for 14–16 h. The agarose matrix was washed extensively with 0.5% Nonidet P-40 lysis buffer, and the proteins were eluted by boiling in 2X loading buffer with DTT. The eluates were then analyzed by Western blot analysis for the expression of the epitope tags.

DJ-1 Knockout Mice and Embryonic Fibroblast Culture. DJ-1 knockout mice and WT littermates (36), backcrossed six generations onto the C57BL6 strain, were housed according to the guidelines of the National Institutes of Health under an approved Institutional Animal Care and Use Committee protocol at the University of North Carolina. Primary MEFs were isolated from day-13.5 embryos and grown in DMEM supplemented with 10% FCS. All MEF experiments were performed on cells within two cell passages of isolation from the mice.

Figure 1: siRNA-mediated knockdown of DJ-1 and GeneChip analysis

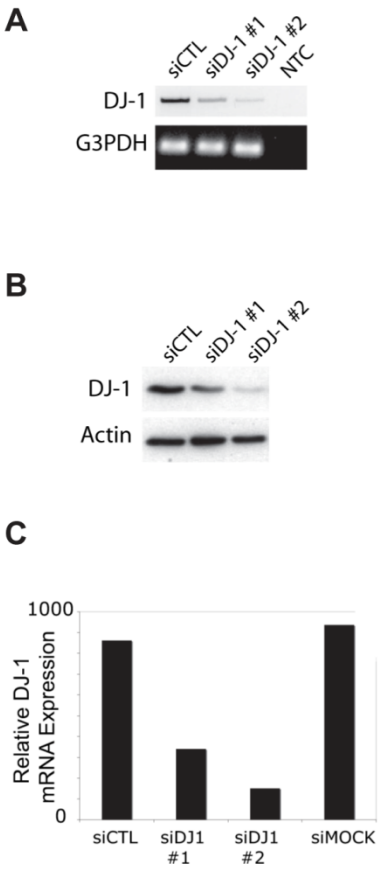

Figure 1. siRNA-mediated knockdown of DJ-1 and GeneChip analysis. (*A*) End-point RT-PCR of H157 cells transfected with control siRNA (siCTL) or two different siRNA targeting DJ-1 (siDJ-1#1 and siDJ-1#2). The DJ-1 RT-PCR gel is presented as a negative image so bands can be more easily visualized. NTC is a nontemplate control. (*B*) Western blot analysis of siRNA-transfected H157 cells demonstrating DJ-1 knockdown at the protein level. (*C*) Quantitative real-time PCR of DJ-1 mRNA after siRNA transfection. Relative mRNA quantitation is normalized to 18S rRNA expression. siDJ-1#2 reduced DJ-1 expression to a greater degree than siDJ-1#1, whereas transfection with either a scrambled nonspecific oligomer siRNA or transfection reagent alone (siMOCK) did not affect DJ-1 expression.

Figure 2: Summary of Affymetrix GeneChip analysis

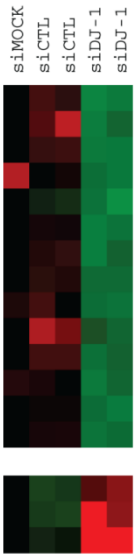

		Fold Change	Upstream ARE-like sequence
TOMM20	TRANSLOCASE OF OUTER MITOCHONDRIAL MEMBRANE 20	-5.02	
RRN3	RNA POLYMERASE I TRANSCRIPTION FACTOR	-4.81	GGAGGCTGAGGCACGAGAAT
P24A/TMED2	TRANSMEMBRANE EMP24 TRANSPORT DOMAIN-CONTAINING PROT.	-4.34	CGAGGCTGAGGCACGAGAAT
LAMP1	LYSOSOME-ASSOCIATED MEMBRANE PROTEIN 1	-4.33	
ABCC3	ATP-BINDING CASSETTE, SUBFAMILY C, MEMBER 3	-3.88	ACTCAATGACTCATCGGCCC
CLNS1A	CHLORIDE CHANNEL, NUCLEOTIDE SENSITIVE, 1A	-3.79	TTGCGCTGAGTCAGTTCCTG
DJ-1	ONCOGENE DJ-1/PARK7	-3.69	CGGACGTGACGCAGCGTGAG
PSIP1	PC4- AND SFRS1-INTERACTING PROTEIN 1	-3.57	
OB-RG/LEPR	LEPTIN-RELATED GENE/LEPTIN RECEPTOR	-3.49	
RAB14	RAS-ASSOCIATED PROTEIN	-3.38	
PIGB	PHOSPHATIDYLINOSITOL GLYCAN, CLASS B	-3.35	
NQO1	NAD(P)H DEHYDROGENASE, QUINONE 1	-3.32	TCACAGTGACTCAGCAGAAT
HRASLS3	HRAS-LIKE SUPPRESSOR 3	-3.31	
NOG1	NOGGIN HOMOLOG	-3.02	
GREM1	GREMLIN 1 HOMOLOG, CYSTEINE KNOT SUPERFAMILY	+4.00	
CALR	CALRETICULIN	+3.27	
CTGF	CONNECTIVE TISSUE GROWTH FACTOR	+3.10	GCATCCTGAGTCACACGCGT

Figure 2. Summary of Affymetrix GeneChip analysis. Genes shown represent changes of >3-fold between siCTL- and siDJ-1-transfected samples; fluorescence in the present (P) state is >500 in all samples. Green indicates decreased expression in normalized fluorescence; red indicates higher expression. Putative Nrf2-binding sequences within 1,000 bp upstream of the transcription start site are included to the right where present and were identified by using tfsearch and a score of >85.0.

Figure 3: DJ-1 is required for Nrf2-mediated transcription

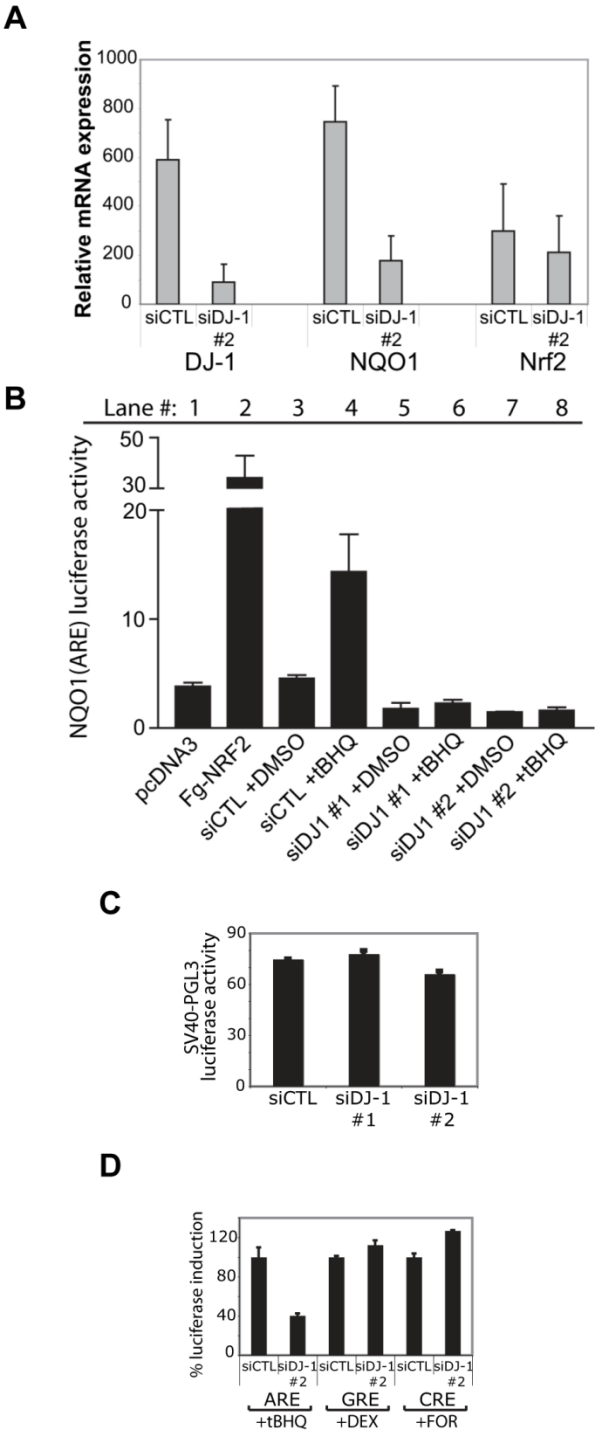

Figure 3. DJ-1 is required for Nrf2-mediated transcription. (*A*) Real-time quantitative PCR analysis of mRNA expression verifies that siDJ-1#2 reduced DJ-1 mRNA expression, as well as NQO1 mRNA expression. However, the mRNA of Nrf2, a master regulator of NQO1 expression, is unaffected by the loss of DJ-1. All experiments were performed in triplicate, and error bars indicate SEM. (*B*) ARE-regulated luciferase reporter gene activity in Huh7 cells is reduced after siDJ-1 transfection. The firefly luciferase reporter construct is under the control of the NQO1 ARE (224), which is responsive to Nrf2. Cells were treated with 50 μM tBHQ or a DMSO vehicle control. Lysates were assayed for luciferase activity and normalized to crude protein present in the extract. Flag-Nrf2 was transfected as a positive control. Samples with lowered DJ-1 expression contained lower levels of the ARE-regulated luciferase activity and failed to increase luciferase activity after treatment with tBHQ. All experiments were performed in triplicate, and error bars indicate SEM. (*C*) Luciferase activity expressed from a construct under the control of the constitutively active viral SV40 promoter was not affected by siDJ-1. (*D*) Luciferase activity expressed from two mammalian promoters was not affected by siDJ-1. Huh7 cells with siDJ-1 were transfected with luciferase reporter constructs under control of the NQO1 ARE, glucocorticoid response element (GRE), or cAMP response element (CRE). Cultures were treated with the appropriate vehicle control, 50 μM tBHQ, 100 μM dexamethasone (DEX), or 10 μM forskolin (FOR) as indicated. Activation is presented as the percentage induction of control oligomer (siCTL)-transfected cells. All experiments were replicated at least three times.

Figure 4: DJ-1 is required for Nrf2 protein stability

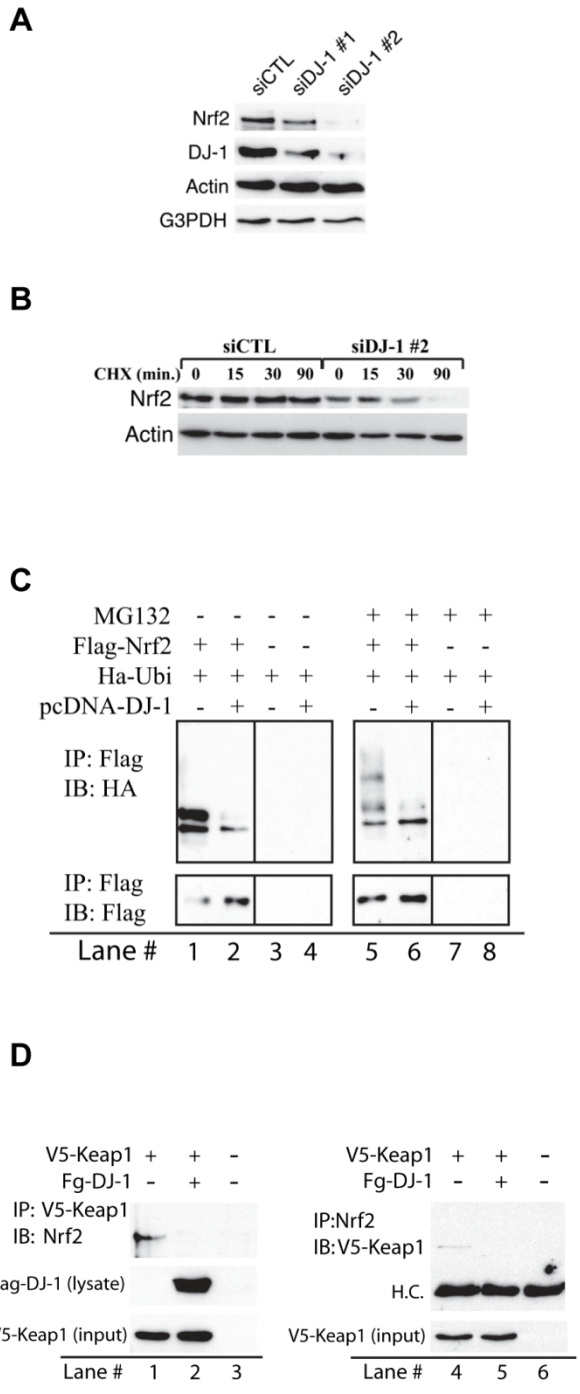

Figure 4. DJ-1 is required for Nrf2 protein stability. (*A*) Western blot analysis of Nrf-2, DJ-1, and control proteins in Huh7 cell lysates after siRNA knockdown of DJ-1. (*B*) Time course of protein expression after cyclohexamide (CHX) treatment. Western blot analysis confirms the presence of Nrf2 at times after CHX treatment in control samples. Actin is used as an unaffected control. (*C*) *In cellulo* assay of Nrf2 ubiquitinylation. Nrf2 and covalently bound ubiquitin were immunoprecipitated from Huh7 extracts and analyzed by SDS/PAGE and Western blot analysis. (*D*) Nrf2/Keap1 co-immunoprecipitation in the presence of DJ-1. V5 epitope-tagged Keap1 was expressed in Huh7 cells with and without overexpressed Flag-DJ-1. Immunoprecipitation using anti-V5 antibody co-immunoprecipitated endogenous Nrf2 protein, and, conversely, immunoprecipitation of endogenous Nrf2 co-isolated V5-Keap1. ‘‘H.C.’’ denotes a cross-reacting band of IgG heavy chain that was present from the immunoprecipitating antibody. Data are representative of at least three independent experiments.

Figure 5: DJ-1 is required for Nrf2 function in MEFs

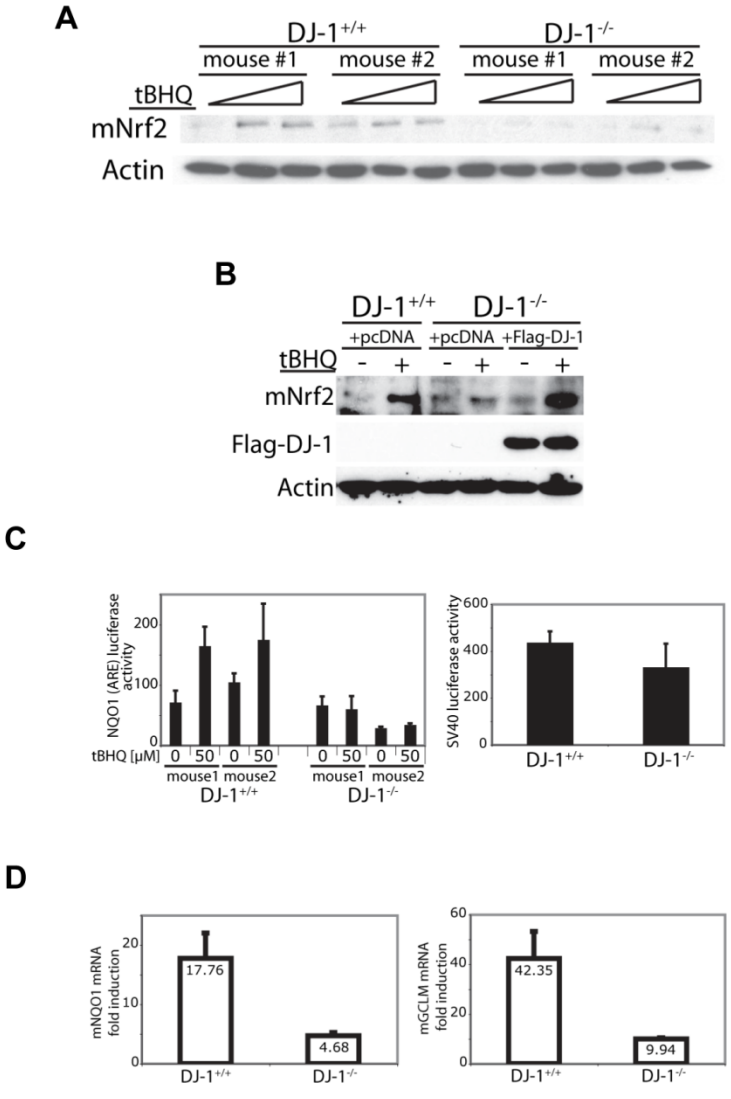

Figure 5. DJ-1 is required for Nrf2 function in MEFs. (*A*) Western blot analysis of mNrf2 protein expression in primary MEFs derived from DJ-1 gene deletion mice and WT littermates. Cultures were treated with tBHQ at 0, 50, and 100 μM. (*B*) Western blot analysis of mNrf2 cultures transfected with either pcDNA or Flag-DJ-1 and treated with 50 μM tBHQ or vehicle control. (*C*) ARE luciferase activity in *DJ-1*$^{+/+}$ and *DJ-1*$^{-/-}$ MEF cultures. Luciferase is under control of the ARE from the human NQO1 gene promoter (*Left*); SV40-luciferase is under control of the constitutively active viral SV40 promoter (*Right*). Luciferase activity is normalized to protein concentration in the extract. (*D*) Real-time quantitative PCR of Nrf2-mediated target gene expression in primary MEFs. NQO1, NAD(P)H quinone oxidoreductase I; GCLM, glutathione cysteine ligase modifier subunit. Data are presented as fold induction after treatment with tBHQ compared with vehicle control. All mRNA measurements are normalized to mouse G3PDH expression. All experiments were performed in triplicate, and error bars indicate SEM. All data are representative of at least three independent experiments.

Figure 6: Characterization of polyclonal rabbit anti-DJ-1 antibody

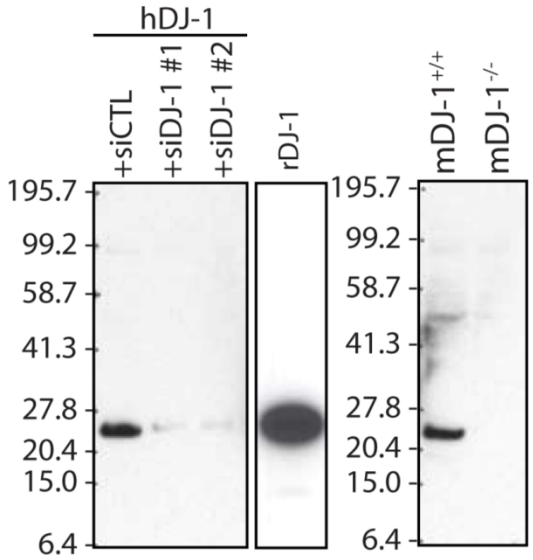

Figure 6. Characterization of polyclonal rabbit anti-DJ-1 antibody. Shown are Western blots of human DJ-1 (hDJ-1), bacterially produced and purified recombinant human DJ-1 protein (rDJ-1), and mouse DJ-1 (mDJ-1). (*Left*) Human DJ-1 from H157 cell lysates transfected with scrambled nonsilencing siRNA (siCTL) or one of two nonoverlapping siRNA oligomers specific to DJ-1 (siDJ-1 #1 and siDJ-1 #2) was immunoblotted with the anti-DJ-1 antibody. The antibody recognized a protein of the predicted mobility in siCTL-treated cells but not cells with the siDJ-1. The antibody also reacted with recombinant DJ-1. (*Right*) Mouse DJ-1 was also recognized by the anti-DJ-1 antibody. Mouse embryonic fibroblast (MEF) cell culture lysates from WT *DJ-1*$^{+/+}$ cells and *DJ-1*$^{-/-}$ genetically ablated knockout mice were prepared. The presence of a single band at 24 kDa that is not present in *DJ-1*$^{-/-}$ cells shows the specificity of this antibody.

Figure 7: Expression profile of known Nrf2-regulated genes with respect to DJ-1 expression

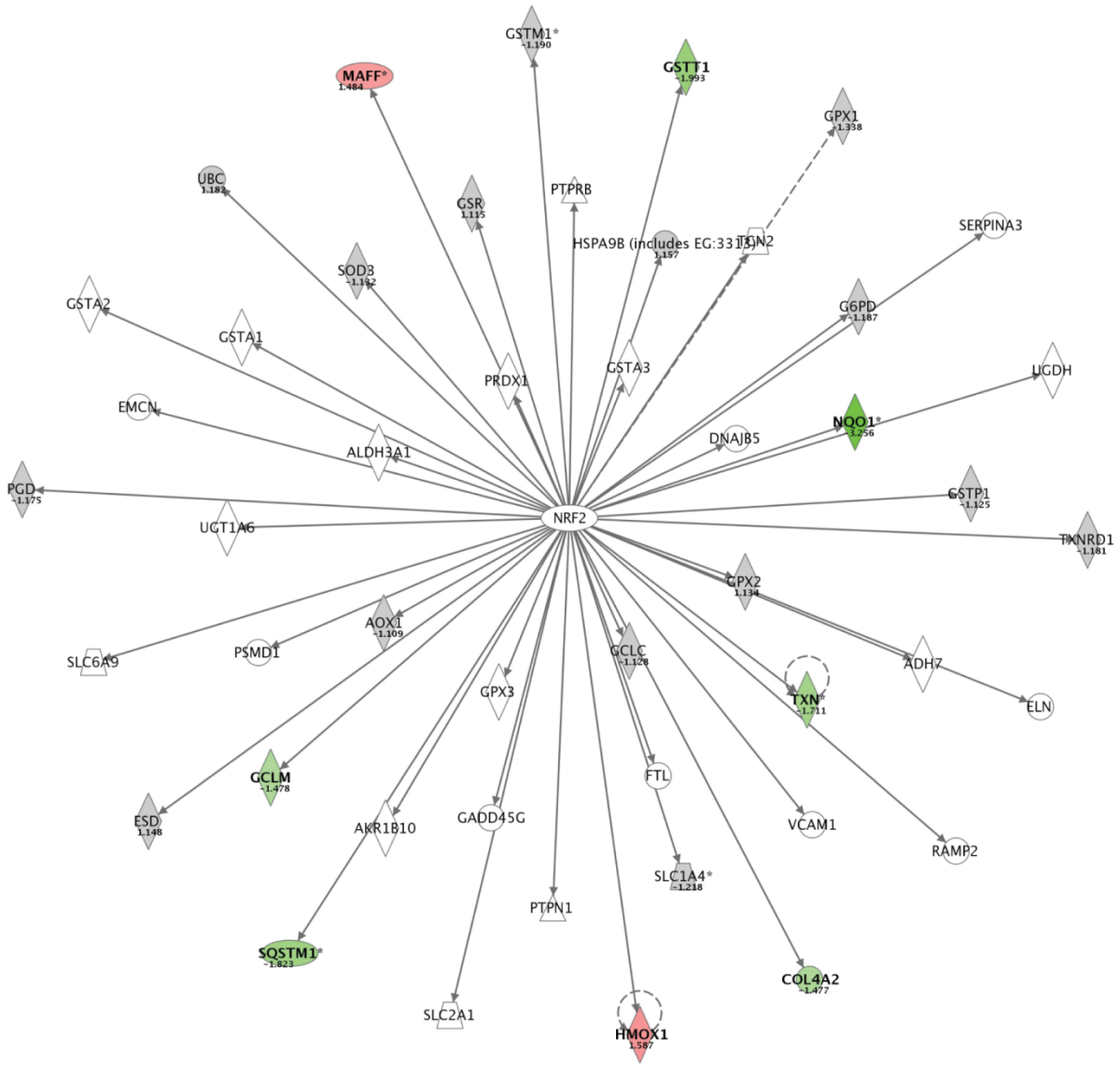

Figure 7. Expression profile of known Nrf2-regulated genes with respect to DJ-1 expression. The Nrf2-regulated gene network was generated by using Ingenuity Pathways Analysis (Ingenuity Systems, Redwood City, CA). A data set containing gene identifiers and corresponding expression values was uploaded in the application. Each gene identifier was mapped to its corresponding gene object in the Ingenuity Pathways Knowledge Base. A fold-change cutoff of 1.4-fold was set to identify genes whose expression was significantly differentially regulated. This diagram is a graphical representation of the genes whose expression is controlled or altered by Nrf2. Gene products are represented as nodes, and the biological relationship (transcription or expression) between two nodes is represented as an edge (line). All edges are supported by at least one reference from the literature, a textbook, or canonical information stored in the Ingenuity Pathways Knowledge Base. The intensity of the node color indicates the degree of up-regulation (red) or down-regulation (green) for changes >1.4-fold. Nodes are displayed by using various shapes that represent the functional class of the gene product. The number under each gene name indicates the fold difference between DJ-1-expressing cells (three arrays) and DJ-1 knockdown cells (two arrays). Nodes without numbers were not present on the array or were excluded from analysis if the raw Affymetrix expression signal was <200 or if the gene was not changed >10% (1.10-fold) between the three DJ-1-expressing arrays and the two DJ-1 knockdown arrays. Among the genes identified, five were increased, and two were decreased. The mechanism by which the presence of DJ-1 causes gene reduction is unclear.

Figure 8: ChIP of the NQO1 promoter

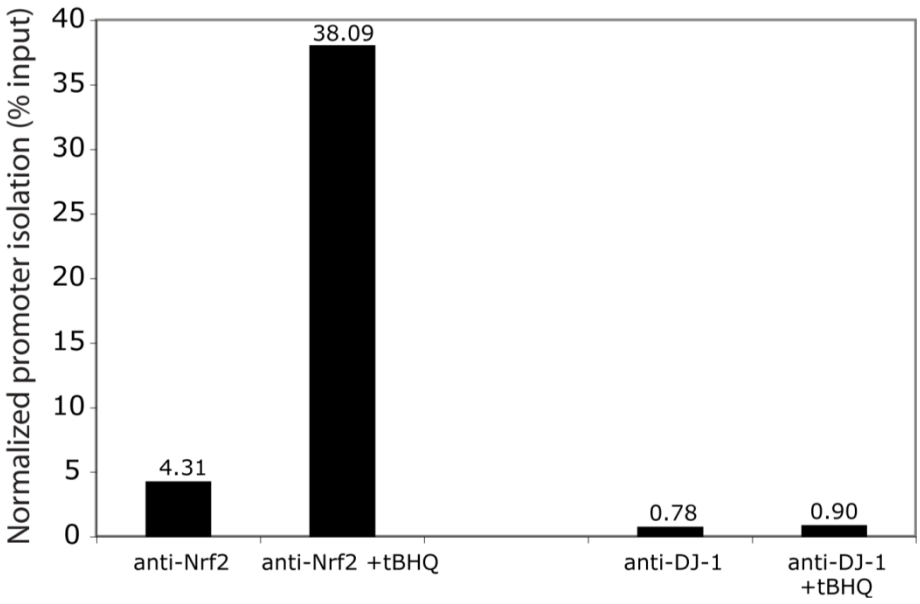

Figure 8. ChIP of the NQO1 promoter. We assayed for the presence of DJ-1 bound to the NQO1 promoter by ChIP using antibodies specific for DJ-1 and Nrf2. In brief, we cross-linked cells by using formaldehyde, lysed the cells, and sheared chromatin by sonication (227). We then immunoprecipitated Nrf2 or DJ-1, digested the protein with proteinase K, and performed SYBR green real-time quantitative PCR with NQO1 promoter-specific primers 5'-CAG GAC TCT CAG CCT TCC AA-3' and 5'-TGG CAC GAA ATG GAG CAG AA-3' that amplify the region of the NQO1 promoter containing the ARE. Data were normalized to the promoter input into the immunoprecipitation. Values given are the quantity of promoter immunoprecipitated as percentage of input. Nrf2 was found bound to the NQO1 promoter, and its binding was enhanced by tBHQ treatment. However, DJ-1 ChIP was not able to enrich for the NQO1 promoter sequence in either treatment, indicating that the association of DJ-1 with this promoter is not detected.

Figure 9: DJ-1 does not alter Keap1 mRNA expression

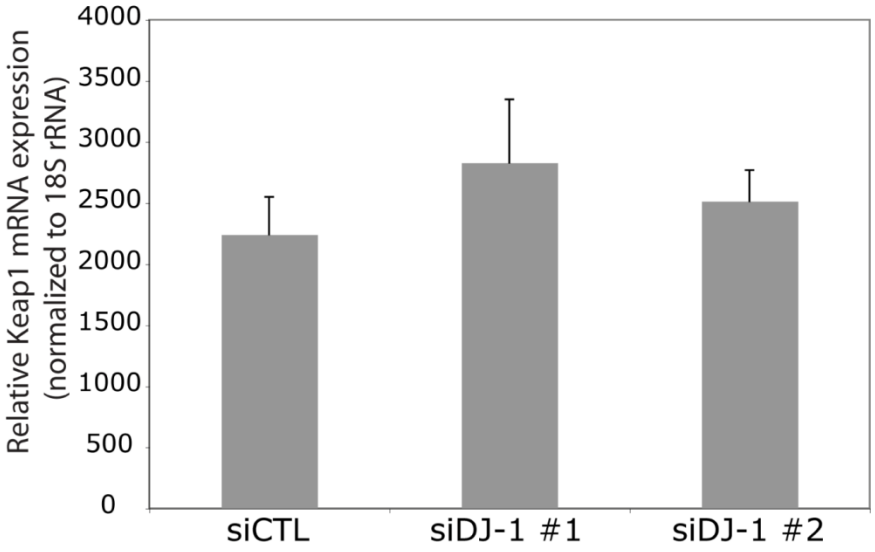

Figure 9. DJ-1 does not alter Keap1 mRNA expression. Keap1 mRNA expression was measured using SYBR green real-time quantitative PCR with the primers 5'-GGC GAA TGA TCA CAG CAA TG-3' and 5'-GCT GGT CCT GAC CAT CAT AG-3', and expression was normalized to 18S rRNA expression. In the main text, the data indicate that siDJ-1 decreased NQO1 transcription and reduced Nrf2 protein stability. However, as this real-time quantitative PCR analysis shows, the effect of DJ-1 is not mediated by differences in Keap1 mRNA expression. All experiments were performed in triplicate, and error bars indicate SEM.

Figure 10: Nrf2 pathway proteins did not co-immunoprecipitate with DJ-1

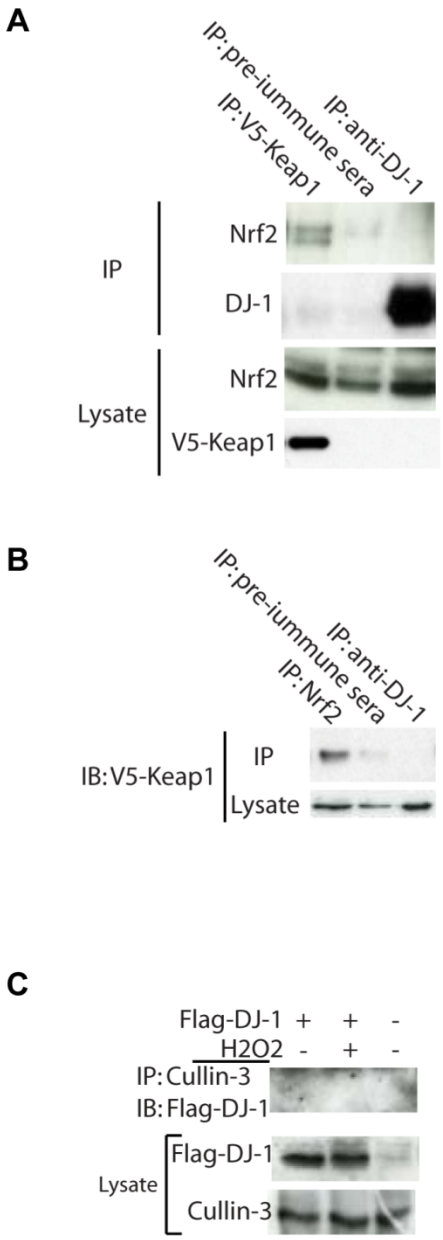

Figure 10. Nrf2 pathway proteins did not co-immunoprecipitate with DJ-1. Using HEK293T cells, we examined DJ-1 protein-protein interactions with Nrf2 and proteins that affect Nrf2 protein stability. V5-Keap1 expression construct was used due to the poor quality of commercially available Keap1 antibodies. (*A*) In contrast to the co-immunoprecipitation of V5-Keap1 and Nrf2, co-immunoprecipitation of DJ-1 with Nrf2 was not detected. Western blot analysis of DJ-1 immunoprecipitation eluates with DJ-1 antibody shows that the anti-DJ-1 antibody is capable of immunoprecipitation. For this DJ-1 blot, TruBlot anti-rabbit-HRP (Insight Biotech, San Diego, CA) was used as a secondary antibody to eliminate any blotting of IgG light chain that would complicate DJ-1 IP/IB blots. (*B*) Similar to *A*, immunoprecipitation of DJ-1 with V5-Keap1 was not detected, and immunoprecipitation of Nrf2 using the H-300 antibody (Santa Cruz Biotechnology, Santa Cruz, CA) does isolate V5-Keap1. (*C*) Keap1 targets Nrf2 for protein degradation by means of Cullin-3-dependent ubiquitination; therefore, we also assayed for DJ-1 protein interaction with Cullin-3. Using rabbit polyclonal anti-Cullin-3 from (204), we immunoprecipitated Cullin-3-containing protein complexes and blotted for Flag-DJ-1. Flag-DJ-1 was used to eliminate background caused by the high expression of endogenous DJ-1. H_2O_2 indicates overnight treatment with 300 M hydrogen peroxide to model oxidative stress. Flag-DJ-1 was not co-immunoprecipitated with Cullin-3 in these cells.

Figure 11: High-dose tBHQ induction of mouse NQO1 and GCLM genes is less dependent on DJ-1

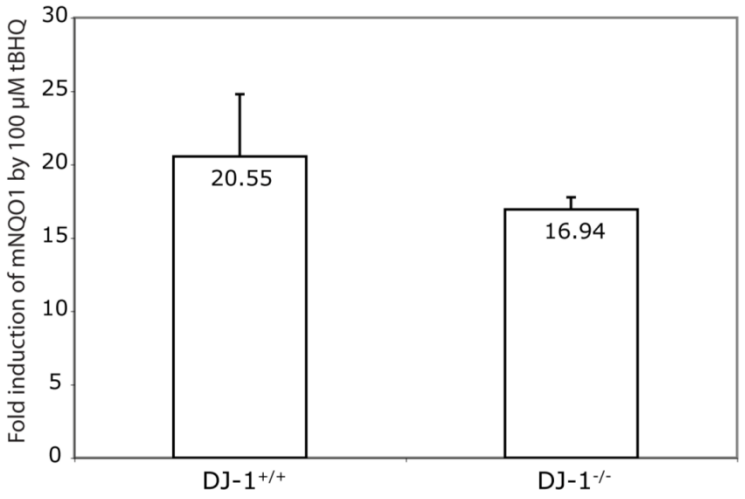

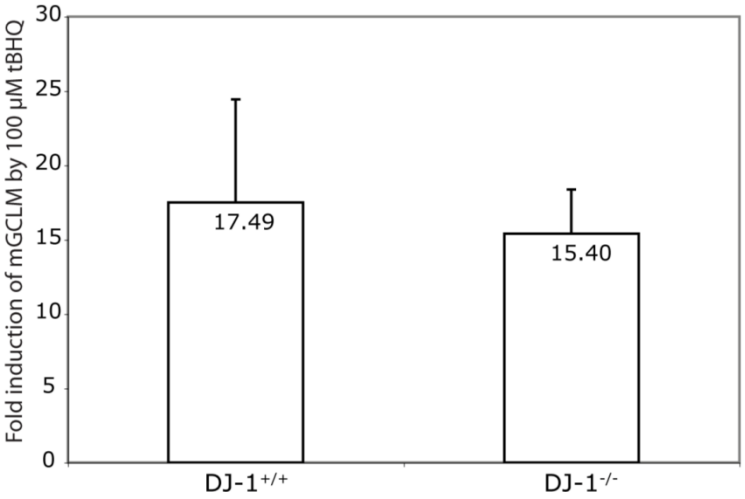

Figure 11. High-dose tBHQ induction of mouse NQO1 and GCLM genes is less dependent on DJ-1. In the main text, we show that MEFs lacking DJ-1 do not induce mNQO1 or mGCLM expression to the same extent as WT MEFs after tBHQ treatment. However, at higher doses (exceeding 100 μM tBHQ), induction of Nrf2-regulated genes approaches levels similar to *DJ-1*$^{+/+}$ cells. All experiments were performed in triplicate in each of two mice, and error bars indicate SEM.

REFERENCES

1. Nagakubo D, et al. (1997) DJ-1, a novel oncogene which transforms mouse NIH3T3 cells in cooperation with ras. *Biochem Biophys Res Commun* 231: 509-513.

2. Taira T, Takahashi K, Kitagawa R, Iguchi-Ariga SM,Ariga H (2001) Molecular cloning of human and mouse DJ-1 genes and identification of Sp1-dependent activation of the human DJ-1 promoter. *Gene* 263: 285-292.

3. MacKeigan JP, et al. (2003) Proteomic profiling drug-induced apoptosis in non-small cell lung carcinoma: identification of RS/DJ-1 and RhoGDIalpha. *Cancer Res* 63: 6928-6934.

4. Davidson B, et al. (2008) Expression and clinical role of DJ-1, a negative regulator of PTEN, in ovarian carcinoma. *Hum Pathol* 39: 87-95.

5. Sitaram RT, et al. (2009) The PTEN regulator DJ-1 is associated with hTERT expression in clear cell renal cell carcinoma. *Int J Cancer* 125: 783-790.

6. Wu F, Liang YQ,Huang ZM (2009) [The expression of DJ-1 gene in human hepatocellular carcinoma and its relationship with tumor invasion and metastasis]. *Zhonghua Gan Zang Bing Za Zhi* 17: 203-206.

7. Le Naour F, et al. (2001) Proteomics-based identification of RS/DJ-1 as a novel circulating tumor antigen in breast cancer. *Clin Cancer Res* 7: 3328-3335.

8. Yuen HF, et al. (2008) DJ-1 could predict worse prognosis in esophageal squamous cell carcinoma. *Cancer Epidemiol Biomarkers Prev* 17: 3593-3602.

9. Jemal A, et al. (2008) Cancer statistics, 2008. *CA Cancer J Clin* 58: 71-96.

10. Sher T, Dy GK,Adjei AA (2008) Small cell lung cancer. *Mayo Clin Proc* 83: 355-367.

11. Pfister DG, et al. (2004) American Society of Clinical Oncology treatment of unresectable non-small-cell lung cancer guideline: update 2003. *J Clin Oncol* 22: 330-353.

12. Lee LF, Haskill JS, Mukaida N, Matsushima K,Ting JP (1997) Identification of tumor-specific paclitaxel (Taxol)-responsive regulatory elements in the interleukin-8 promoter. *Mol Cell Biol* 17: 5097-5105.

13. Collins TS, Lee LF,Ting JP (2000) Paclitaxel up-regulates interleukin-8 synthesis in human lung carcinoma through an NF-kappaB- and AP-1-dependent mechanism. *Cancer Immunol Immunother* 49: 78-84.

14. MacKeigan JP, Collins TS,Ting JP (2000) MEK inhibition enhances paclitaxel-induced tumor apoptosis. *J Biol Chem* 275: 38953-38956.

15. Kim RH, et al. (2005) DJ-1, a novel regulator of the tumor suppressor PTEN. *Cancer Cell* 7: 263-273.

16. Katzenschlager R, et al. (2008) Fourteen-year final report of the randomized PDRG-UK trial comparing three initial treatments in PD. *Neurology* 71: 474-480.

17. Bower JH, Maraganore DM, McDonnell SK,Rocca WA (1999) Incidence and distribution of parkinsonism in Olmsted County, Minnesota, 1976-1990. *Neurology* 52: 1214-1220.

18. Lees AJ, Hardy J,Revesz T (2009) Parkinson's disease. *Lancet* 373: 2055-2066.

19. Spillantini MG, et al. (1997) Alpha-synuclein in Lewy bodies. *Nature* 388: 839-840.

20. Ruottinen HM,Rinne UK (1998) COMT inhibition in the treatment of Parkinson's disease. *J Neurol* 245: P25-34.

21. Lindvall O (1991) Transplants in Parkinson's disease. *Eur Neurol* 31 Suppl 1: 17-27.

22. Kitada T, et al. (1998) Mutations in the parkin gene cause autosomal recessive juvenile parkinsonism. *Nature* 392: 605-608.

23. Valente EM, et al. (2001) Localization of a novel locus for autosomal recessive early-onset parkinsonism, PARK6, on human chromosome 1p35-p36. *Am J Hum Genet* 68: 895-900.

24. Ramirez A, et al. (2006) Hereditary parkinsonism with dementia is caused by mutations in ATP13A2, encoding a lysosomal type 5 P-type ATPase. *Nat Genet* 38: 1184-1191.

25. Polymeropoulos MH, et al. (1997) Mutation in the alpha-synuclein gene identified in families with Parkinson's disease. *Science* 276: 2045-2047.

26. Shen J (2004) Protein kinases linked to the pathogenesis of Parkinson's disease. *Neuron* 44: 575-577.

27. Lwin A, Orvisky E, Goker-Alpan O, LaMarca ME,Sidransky E (2004) Glucocerebrosidase mutations in subjects with parkinsonism. *Mol Genet Metab* 81: 70-73.

28. van Duijn CM, et al. (2001) Park7, a novel locus for autosomal recessive early-onset parkinsonism, on chromosome 1p36. *Am J Hum Genet* 69: 629-634.

29. Bonifati V, et al. (2002) Localization of autosomal recessive early-onset parkinsonism to chromosome 1p36 (PARK7) in an independent dataset. *Ann Neurol* 51: 253-256.

30. Bonifati V, et al. (2003) Mutations in the DJ-1 gene associated with autosomal recessive early-onset parkinsonism. *Science* 299: 256-259.

31. Martinat C, et al. (2004) Sensitivity to oxidative stress in DJ-1-deficient dopamine neurons: an ES- derived cell model of primary Parkinsonism. *PLoS Biol* 2: e327.

32. Goldberg MS, et al. (2005) Nigrostriatal dopaminergic deficits and hypokinesia caused by inactivation of the familial Parkinsonism-linked gene DJ-1. *Neuron* 45: 489-496.

33. Chandran JS, et al. (2008) Progressive behavioral deficits in DJ-1-deficient mice are associated with normal nigrostriatal function. *Neurobiol Dis* 29: 505-514.

34. Chen L, et al. (2005) Age-dependent motor deficits and dopaminergic dysfunction in DJ-1 null mice. *J Biol Chem* 280: 21418-21426.

35. Yamaguchi H,Shen J (2007) Absence of dopaminergic neuronal degeneration and oxidative damage in aged DJ-1-deficient mice. *Mol Neurodegener* 2: 10.

36. Kim RH, et al. (2005) Hypersensitivity of DJ-1-deficient mice to 1-methyl-4-phenyl-1,2,3,6-tetrahydropyrindine (MPTP) and oxidative stress. *Proc Natl Acad Sci U S A* 102: 5215-5220.

37. Inden M, et al. (2006) PARK7 DJ-1 protects against degeneration of nigral dopaminergic neurons in Parkinson's disease rat model. *Neurobiol Dis* 24: 144-158.

38. Aleyasin H, et al. DJ-1 protects the nigrostriatal axis from the neurotoxin MPTP by modulation of the AKT pathway. *Proc Natl Acad Sci U S A* 107: 3186-3191.

39. Xiong H, et al. (2009) Parkin, PINK1, and DJ-1 form a ubiquitin E3 ligase complex promoting unfolded protein degradation. *J Clin Invest* 119: 650-660.

40. Shimura H, et al. (2001) Ubiquitination of a new form of alpha-synuclein by parkin from human brain: implications for Parkinson's disease. *Science* 293: 263-269.

41. Shendelman S, Jonason A, Martinat C, Leete T,Abeliovich A (2004) DJ-1 is a redox-dependent molecular chaperone that inhibits alpha-synuclein aggregate formation. *PLoS Biol* 2: e362.

42. Zhou W, Zhu M, Wilson MA, Petsko GA,Fink AL (2006) The oxidation state of DJ-1 regulates its chaperone activity toward alpha-synuclein. *J Mol Biol* 356: 1036-1048.

43. Mullett SJ,Hinkle DA (2009) DJ-1 knock-down in astrocytes impairs astrocyte-mediated neuroprotection against rotenone. *Neurobiol Dis* 33: 28-36.

44. Lev N, et al. (2009) DJ-1 protects against dopamine toxicity. *J Neural Transm* 116: 151-160.

45. Takahashi K, et al. (2001) DJ-1 positively regulates the androgen receptor by impairing the binding of PIASx alpha to the receptor. *J Biol Chem* 276: 37556-37563.

46. Canet-Aviles RM, et al. (2004) The Parkinson's disease protein DJ-1 is neuroprotective due to cysteine-sulfinic acid-driven mitochondrial localization. *Proc Natl Acad Sci U S A* 101: 9103-9108.

47. Mo JS, Kim MY, Ann EJ, Hong JA,Park HS (2008) DJ-1 modulates UV-induced oxidative stress signaling through the suppression of MEKK1 and cell death. *Cell Death Differ* 15: 1030-1041.

48. Fan J, et al. (2008) DJ-1 decreases Bax expression through repressing p53 transcriptional activity. *J Biol Chem* 283: 4022-4030.

49. Gu L, et al. (2009) Involvement of ERK1/2 signaling pathway in DJ-1-induced neuroprotection against oxidative stress. *Biochem Biophys Res Commun* 383: 469-474.

50. Clements CM, McNally RS, Conti BJ, Mak TW,Ting JP (2006) DJ-1, a cancer- and Parkinson's disease-associated protein, stabilizes the antioxidant transcriptional master regulator Nrf2. *Proc Natl Acad Sci U S A* 103: 15091-15096.

51. Honbou K, et al. (2003) The crystal structure of DJ-1, a protein related to male fertility and Parkinson's disease. *J Biol Chem* 278: 31380-31384.

52. Tao X,Tong L (2003) Crystal structure of human DJ-1, a protein associated with early onset Parkinson's disease. *J Biol Chem* 278: 31372-31379.

53. Wilson MA, Collins JL, Hod Y, Ringe D,Petsko GA (2003) The 1.1-A resolution crystal structure of DJ-1, the protein mutated in autosomal recessive early onset Parkinson's disease. *Proc Natl Acad Sci U S A* 100: 9256-9261.

54. Miller DW, et al. (2003) L166P mutant DJ-1, causative for recessive Parkinson's disease, is degraded through the ubiquitin-proteasome system. *J Biol Chem* 278: 36588-36595.

55. Mitsumoto A,Nakagawa Y (2001) DJ-1 is an indicator for endogenous reactive oxygen species elicited by endotoxin. *Free Radic Res* 35: 885-893.

56. Mitsumoto A, et al. (2001) Oxidized forms of peroxiredoxins and DJ-1 on two-dimensional gels increased in response to sublethal levels of paraquat. *Free Radic Res* 35: 301-310.

57. Kinumi T, Kimata J, Taira T, Ariga H,Niki E (2004) Cysteine-106 of DJ-1 is the most sensitive cysteine residue to hydrogen peroxide-mediated oxidation in vivo in human umbilical vein endothelial cells. *Biochem Biophys Res Commun* 317: 722-728.

58. Taira T, et al. (2004) DJ-1 has a role in antioxidative stress to prevent cell death. *EMBO Rep* 5: 213-218.

59. Duan X, Kelsen SG,Merali S (2008) Proteomic analysis of oxidative stress-responsive proteins in human pneumocytes: insight into the regulation of DJ-1 expression. *J Proteome Res* 7: 4955-4961.

60. Gorner K, et al. (2007) Structural determinants of the C-terminal helix-kink-helix motif essential for protein stability and survival promoting activity of DJ-1. *J Biol Chem* 282: 13680-13691.

61. Waak J, et al. (2009) Oxidizable residues mediating protein stability and cytoprotective interaction of DJ-1 with apoptosis signal-regulating kinase 1. *J Biol Chem* 284: 14245-14257.

62. Niki T, Takahashi-Niki K, Taira T, Iguchi-Ariga SM,Ariga H (2003) DJBP: a novel DJ-1-binding protein, negatively regulates the androgen receptor by recruiting histone

deacetylase complex, and DJ-1 antagonizes this inhibition by abrogation of this complex. *Mol Cancer Res* 1: 247-261.

63. Shinbo Y, et al. (2006) Proper SUMO-1 conjugation is essential to DJ-1 to exert its full activities. *Cell Death Differ* 13: 96-108.

64. Bandyopadhyay S,Cookson MR (2004) Evolutionary and functional relationships within the DJ1 superfamily. *BMC Evol Biol* 4: 6.

65. Lee SJ, et al. (2003) Crystal structures of human DJ-1 and Escherichia coli Hsp31, which share an evolutionarily conserved domain. *J Biol Chem* 278: 44552-44559.

66. Horvath MM,Grishin NV (2001) The C-terminal domain of HPII catalase is a member of the type I glutamine amidotransferase superfamily. *Proteins* 42: 230-236.

67. Du X, et al. (2000) Crystal structure of an intracellular protease from Pyrococcus horikoshii at 2-A resolution. *Proc Natl Acad Sci U S A* 97: 14079-14084.

68. Mizote T, Tsuda M, Nakazawa T,Nakayama H (1996) The thiJ locus and its relation to phosphorylation of hydroxymethylpyrimidine in Escherichia coli. *Microbiology* 142 (Pt 10): 2969-2974.

69. Halio SB, Blumentals, II, Short SA, Merrill BM,Kelly RM (1996) Sequence, expression in Escherichia coli, and analysis of the gene encoding a novel intracellular protease (PfpI) from the hyperthermophilic archaeon Pyrococcus furiosus. *J Bacteriol* 178: 2605-2612.

70. Olzmann JA, et al. (2004) Familial Parkinson's disease-associated L166P mutation disrupts DJ-1 protein folding and function. *J Biol Chem* 279: 8506-8515.

71. Chen J, Li L,Chin LS Parkinson disease protein DJ-1 converts from a zymogen to a protease by carboxyl-terminal cleavage. *Hum Mol Genet*

72. Giaime E, et al. Loss of function of DJ-1 triggered by Parkinson's disease-associated mutation is due to proteolytic resistance to caspase-6. *Cell Death Differ* 17: 158-169.

73. Ooe H, Maita C, Maita H, Iguchi-Ariga SM,Ariga H (2006) Specific cleavage of DJ-1 under an oxidative condition. *Neurosci Lett* 406: 165-168.

74. Zhou W,Freed CR (2005) DJ-1 up-regulates glutathione synthesis during oxidative stress and inhibits A53T alpha-synuclein toxicity. *J Biol Chem* 280: 43150-43158.

75. Sheppard DE,Englesberg E (1967) Further evidence for positive control of the L-arabinose system by gene araC. *J Mol Biol* 25: 443-454.

76. Hod Y, Pentyala SN, Whyard TC,El-Maghrabi MR (1999) Identification and characterization of a novel protein that regulates RNA-protein interaction. *J Cell Biochem* 72: 435-444.

77. Wagenfeld A, Gromoll J,Cooper TG (1998) Molecular cloning and expression of rat contraception associated protein 1 (CAP1), a protein putatively involved in fertilization. *Biochem Biophys Res Commun* 251: 545-549.

78. Okada M, et al. (2002) DJ-1, a target protein for an endocrine disrupter, participates in the fertilization in mice. *Biol Pharm Bull* 25: 853-856.

79. Nachaliel N, Jain D,Hod Y (1993) A cAMP-regulated RNA-binding protein that interacts with phosphoenolpyruvate carboxykinase (GTP) mRNA. *J Biol Chem* 268: 24203-24209.

80. van der Brug MP, et al. (2008) RNA binding activity of the recessive parkinsonism protein DJ-1 supports involvement in multiple cellular pathways. *Proc Natl Acad Sci U S A* 105: 10244-10249.

81. Selvakumaran M, et al. (1994) Immediate early up-regulation of bax expression by p53 but not TGF beta 1: a paradigm for distinct apoptotic pathways. *Oncogene* 9: 1791-1798.

82. Maroney AC, et al. (1998) Motoneuron apoptosis is blocked by CEP-1347 (KT 7515), a novel inhibitor of the JNK signaling pathway. *J Neurosci* 18: 104-111.

83. Saitoh M, et al. (1998) Mammalian thioredoxin is a direct inhibitor of apoptosis signal-regulating kinase (ASK) 1. *Embo J* 17: 2596-2606.

84. Mo JS, et al. DJ-1 modulates the p38 mitogen-activated protein kinase pathway through physical interaction with apoptosis signal-regulating kinase 1. *J Cell Biochem* 110: 229-237.

85. Xu J, et al. (2005) The Parkinson's disease-associated DJ-1 protein is a transcriptional co-activator that protects against neuronal apoptosis. *Hum Mol Genet* 14: 1231-1241.

86. Datta SR, et al. (1997) Akt phosphorylation of BAD couples survival signals to the cell-intrinsic death machinery. *Cell* 91: 231-241.

87. Cardone MH, et al. (1998) Regulation of cell death protease caspase-9 by phosphorylation. *Science* 282: 1318-1321.

88. Brunet A, et al. (1999) Akt promotes cell survival by phosphorylating and inhibiting a Forkhead transcription factor. *Cell* 96: 857-868.

89. Stambolic V, et al. (1998) Negative regulation of PKB/Akt-dependent cell survival by the tumor suppressor PTEN. *Cell* 95: 29-39.

90. Vasseur S, et al. (2009) DJ-1/PARK7 is an important mediator of hypoxia-induced cellular responses. *Proc Natl Acad Sci U S A* 106: 1111-1116.

91. Forsythe JA, et al. (1996) Activation of vascular endothelial growth factor gene transcription by hypoxia-inducible factor 1. *Mol Cell Biol* 16: 4604-4613.

92. Itoh K, et al. (1999) Keap1 represses nuclear activation of antioxidant responsive elements by Nrf2 through binding to the amino-terminal Neh2 domain. *Genes Dev* 13: 76-86.

93. McMahon M, Itoh K, Yamamoto M,Hayes JD (2003) Keap1-dependent proteasomal degradation of transcription factor Nrf2 contributes to the negative regulation of antioxidant response element-driven gene expression. *J Biol Chem* 278: 21592-21600.

94. Kobayashi A, et al. (2004) Oxidative stress sensor Keap1 functions as an adaptor for Cul3-based E3 ligase to regulate proteasomal degradation of Nrf2. *Mol Cell Biol* 24: 7130-7139.

95. Marini MG, et al. (1997) hMAF, a small human transcription factor that heterodimerizes specifically with Nrf1 and Nrf2. *J Biol Chem* 272: 16490-16497.

96. Katoh Y, et al. (2001) Two domains of Nrf2 cooperatively bind CBP, a CREB binding protein, and synergistically activate transcription. *Genes Cells* 6: 857-868.

97. Itoh K, et al. (1997) An Nrf2/small Maf heterodimer mediates the induction of phase II detoxifying enzyme genes through antioxidant response elements. *Biochem Biophys Res Commun* 236: 313-322.

98. Venugopal R,Jaiswal AK (1996) Nrf1 and Nrf2 positively and c-Fos and Fra1 negatively regulate the human antioxidant response element-mediated expression of NAD(P)H:quinone oxidoreductase1 gene. *Proc Natl Acad Sci U S A* 93: 14960-14965.

99. Hayden MS,Ghosh S (2008) Shared principles in NF-kappaB signaling. *Cell* 132: 344-362.

100. Hoffmann A,Baltimore D (2006) Circuitry of nuclear factor kappaB signaling. *Immunol Rev* 210: 171-186.

101. Fan CM,Maniatis T (1991) Generation of p50 subunit of NF-kappa B by processing of p105 through an ATP-dependent pathway. *Nature* 354: 395-398.

102. Beg AA,Baldwin AS, Jr. (1993) The I kappa B proteins: multifunctional regulators of Rel/NF-kappa B transcription factors. *Genes Dev* 7: 2064-2070.

103. Ishida T, et al. (1996) Identification of TRAF6, a novel tumor necrosis factor receptor-associated factor protein that mediates signaling from an amino-terminal domain of the CD40 cytoplasmic region. *J Biol Chem* 271: 28745-28748.

104. Hsu H, Huang J, Shu HB, Baichwal V,Goeddel DV (1996) TNF-dependent recruitment of the protein kinase RIP to the TNF receptor-1 signaling complex. *Immunity* 4: 387-396.

105. DiDonato JA, Hayakawa M, Rothwarf DM, Zandi E,Karin M (1997) A cytokine-responsive IkappaB kinase that activates the transcription factor NF-kappaB. *Nature* 388: 548-554.

106. Woronicz JD, Gao X, Cao Z, Rothe M,Goeddel DV (1997) IkappaB kinase-beta: NF-kappaB activation and complex formation with IkappaB kinase-alpha and NIK. *Science* 278: 866-869.

107. Heusch M, Lin L, Geleziunas R,Greene WC (1999) The generation of nfkb2 p52: mechanism and efficiency. *Oncogene* 18: 6201-6208.

108. Ouyang W, Li J, Ma Q,Huang C (2006) Essential roles of PI-3K/Akt/IKKbeta/NFkappaB pathway in cyclin D1 induction by arsenite in JB6 Cl41 cells. *Carcinogenesis* 27: 864-873.

109. Zong WX, Edelstein LC, Chen C, Bash J,Gelinas C (1999) The prosurvival Bcl-2 homolog Bfl-1/A1 is a direct transcriptional target of NF-kappaB that blocks TNFalpha-induced apoptosis. *Genes Dev* 13: 382-387.

110. Chu ZL, et al. (1997) Suppression of tumor necrosis factor-induced cell death by inhibitor of apoptosis c-IAP2 is under NF-kappaB control. *Proc Natl Acad Sci U S A* 94: 10057-10062.

111. Stephens RM, Rice NR, Hiebsch RR, Bose HR, Jr.,Gilden RV (1983) Nucleotide sequence of v-rel: the oncogene of reticuloendotheliosis virus. *Proc Natl Acad Sci U S A* 80: 6229-6233.

112. Van Waes C (2007) Nuclear factor-kappaB in development, prevention, and therapy of cancer. *Clin Cancer Res* 13: 1076-1082.

113. Brown M, Cohen J, Arun P, Chen Z,Van Waes C (2008) NF-kappaB in carcinoma therapy and prevention. *Expert Opin Ther Targets* 12: 1109-1122.

114. Wood KM, Roff M,Hay RT (1998) Defective IkappaBalpha in Hodgkin cell lines with constitutively active NF-kappaB. *Oncogene* 16: 2131-2139.

115. Mukaida N, Mahe Y,Matsushima K (1990) Cooperative interaction of nuclear factor-kappa B- and cis-regulatory enhancer binding protein-like factor binding elements in activating the interleukin-8 gene by pro-inflammatory cytokines. *J Biol Chem* 265: 21128-21133.

116. Stade BG, Messer G, Riethmuller G,Johnson JP (1990) Structural characteristics of the 5' region of the human ICAM-1 gene. *Immunobiology* 182: 79-87.

117. Strieter RM, et al. (1992) Interleukin-8. A corneal factor that induces neovascularization. *Am J Pathol* 141: 1279-1284.

118. Dustin ML, Rothlein R, Bhan AK, Dinarello CA,Springer TA (1986) Induction by IL 1 and interferon-gamma: tissue distribution, biochemistry, and function of a natural adherence molecule (ICAM-1). *J Immunol* 137: 245-254.

119. Orr TS, Elliott EV, Altounyan RE,Stern MA (1980) Modulation of release of neutrophil chemotactic factor (NCF). *Clin Allergy* 10 Suppl: 491-496.

120. Smith CW,Anderson DC (1991) PMN adhesion and extravasation as a paradigm for tumor cell dissemination. *Cancer Metastasis Rev* 10: 61-78.

121. Rubie C, et al. (2007) Correlation of IL-8 with induction, progression and metastatic potential of colorectal cancer. *World J Gastroenterol* 13: 4996-5002.

122. Chavey C, et al. (2008) Interleukin-8 expression is regulated by histone deacetylases through the nuclear factor-kappaB pathway in breast cancer. *Mol Pharmacol* 74: 1359-1366.

123. Masuya D, et al. (2001) The intratumoral expression of vascular endothelial growth factor and interleukin-8 associated with angiogenesis in nonsmall cell lung carcinoma patients. *Cancer* 92: 2628-2638.

124. Karashima T, et al. (2003) Nuclear factor-kappaB mediates angiogenesis and metastasis of human bladder cancer through the regulation of interleukin-8. *Clin Cancer Res* 9: 2786-2797.

125. Millar HJ, Nemeth JA, McCabe FL, Pikounis B,Wickstrom E (2008) Circulating human interleukin-8 as an indicator of cancer progression in a nude rat orthotopic human non-small cell lung carcinoma model. *Cancer Epidemiol Biomarkers Prev* 17: 2180-2187.

126. Singh RK,Lokeshwar BL (2009) Depletion of intrinsic expression of Interleukin-8 in prostate cancer cells causes cell cycle arrest, spontaneous apoptosis and increases the efficacy of chemotherapeutic drugs. *Mol Cancer* 8: 57.

127. Dong C, Slattery MJ, Liang S,Peng HH (2005) Melanoma cell extravasation under flow conditions is modulated by leukocytes and endogenously produced interleukin 8. *Mol Cell Biomech* 2: 145-159.

128. Samanta AK, Oppenheim JJ,Matsushima K (1989) Identification and characterization of specific receptors for monocyte-derived neutrophil chemotactic factor (MDNCF) on human neutrophils. *J Exp Med* 169: 1185-1189.

129. Ginestier C, et al. CXCR1 blockade selectively targets human breast cancer stem cells in vitro and in xenografts. *J Clin Invest*

130. Huang S, et al. (2002) Fully humanized neutralizing antibodies to interleukin-8 (ABX-IL8) inhibit angiogenesis, tumor growth, and metastasis of human melanoma. *Am J Pathol* 161: 125-134.

131. Ke JJ, Shao QS,Ling ZQ (2006) Expression of E-selectin, integrin beta1 and immunoglobulin superfamily member in human gastric carcinoma cells and its clinicopathologic significance. *World J Gastroenterol* 12: 3609-3611.

132. Kammerer S, et al. (2004) Large-scale association study identifies ICAM gene region as breast and prostate cancer susceptibility locus. *Cancer Res* 64: 8906-8910.

133. Torii A, et al. (1993) Expression of intercellular adhesion molecule-1 in hepatocellular carcinoma. *J Surg Oncol* 53: 239-242.

134. Lin YC, Shun CT, Wu MS,Chen CC (2006) A novel anticancer effect of thalidomide: inhibition of intercellular adhesion molecule-1-mediated cell invasion and metastasis through suppression of nuclear factor-kappaB. *Clin Cancer Res* 12: 7165-7173.

135. Rosette C, et al. (2005) Role of ICAM1 in invasion of human breast cancer cells. *Carcinogenesis* 26: 943-950.

136. Dixit VM, et al. (1990) Tumor necrosis factor-alpha induction of novel gene products in human endothelial cells including a macrophage-specific chemotaxin. *J Biol Chem* 265: 2973-2978.

137. Krikos A, Laherty CD,Dixit VM (1992) Transcriptional activation of the tumor necrosis factor alpha-inducible zinc finger protein, A20, is mediated by kappa B elements. *J Biol Chem* 267: 17971-17976.

138. Jaattela M, Mouritzen H, Elling F,Bastholm L (1996) A20 zinc finger protein inhibits TNF and IL-1 signaling. *J Immunol* 156: 1166-1173.

139. Song HY, Rothe M,Goeddel DV (1996) The tumor necrosis factor-inducible zinc finger protein A20 interacts with TRAF1/TRAF2 and inhibits NF-kappaB activation. *Proc Natl Acad Sci U S A* 93: 6721-6725.

140. Heyninck K,Beyaert R (1999) The cytokine-inducible zinc finger protein A20 inhibits IL-1-induced NF-kappaB activation at the level of TRAF6. *FEBS Lett* 442: 147-150.

141. Wertz IE, et al. (2004) De-ubiquitination and ubiquitin ligase domains of A20 downregulate NF-kappaB signalling. *Nature* 430: 694-699.

142. Lin SC, et al. (2008) Molecular basis for the unique deubiquitinating activity of the NF-kappaB inhibitor A20. *J Mol Biol* 376: 526-540.

143. Novak U, et al. (2009) The NF-{kappa}B negative regulator TNFAIP3 (A20) is inactivated by somatic mutations and genomic deletions in marginal zone lymphomas. *Blood* 113: 4918-4921.

144. Chanudet E, et al. A20 is targeted by promoter methylation, deletion and inactivating mutation in MALT lymphoma. *Leukemia* 24: 483-487.

145. Honma K, et al. (2009) TNFAIP3/A20 functions as a novel tumor suppressor gene in several subtypes of non-Hodgkin lymphomas. *Blood* 114: 2467-2475.

146. Schmitz R, et al. (2009) TNFAIP3 (A20) is a tumor suppressor gene in Hodgkin lymphoma and primary mediastinal B cell lymphoma. *J Exp Med* 206: 981-989.

147. Evans PC, et al. (2001) Isolation and characterization of two novel A20-like proteins. *Biochem J* 357: 617-623.

148. Evans PC, et al. (2003) A novel type of deubiquitinating enzyme. *J Biol Chem* 278: 23180-23186.

149. Enesa K, et al. (2008) NF-kappaB suppression by the deubiquitinating enzyme Cezanne: a novel negative feedback loop in pro-inflammatory signaling. *J Biol Chem* 283: 7036-7045.

150. La Starza R, et al. (2007) A common 93-kb duplicated DNA sequence at 1q21.2 in acute lymphoblastic leukemia and Burkitt lymphoma. *Cancer Genet Cytogenet* 175: 73-76.

151. Guo Q, et al. (2009) A20 is overexpressed in glioma cells and may serve as a potential therapeutic target. *Expert Opin Ther Targets* 13: 733-741.

152. Ahn KS,Aggarwal BB (2005) Transcription factor NF-kappaB: a sensor for smoke and stress signals. *Ann N Y Acad Sci* 1056: 218-233.

153. Carayol N, et al. (2006) A dominant function of IKK/NF-kappaB signaling in global lipopolysaccharide-induced gene expression. *J Biol Chem* 281: 31142-31151.

154. Rushworth SA, Chen XL, Mackman N, Ogborne RM,O'Connell MA (2005) Lipopolysaccharide-induced heme oxygenase-1 expression in human monocytic cells is mediated via Nrf2 and protein kinase C. *J Immunol* 175: 4408-4415.

155. Knorr-Wittmann C, Hengstermann A, Gebel S, Alam J,Muller T (2005) Characterization of Nrf2 activation and heme oxygenase-1 expression in NIH3T3 cells exposed to aqueous extracts of cigarette smoke. *Free Radic Biol Med* 39: 1438-1448.

156. Rushworth SA, MacEwan DJ,O'Connell MA (2008) Lipopolysaccharide-induced expression of NAD(P)H:quinone oxidoreductase 1 and heme oxygenase-1 protects against excessive inflammatory responses in human monocytes. *J Immunol* 181: 6730-6737.

157. Alam J, et al. (1999) Nrf2, a Cap'n'Collar transcription factor, regulates induction of the heme oxygenase-1 gene. *J Biol Chem* 274: 26071-26078.

158. Jun CD, et al. (2006) Gliotoxin reduces the severity of trinitrobenzene sulfonic acid-induced colitis in mice: evidence of the connection between heme oxygenase-1 and the nuclear factor-kappaB pathway in vitro and in vivo. *Inflamm Bowel Dis* 12: 619-629.

159. Kimura T, et al. (2009) Ethanol-induced expression of glutamate-cysteine ligase catalytic subunit gene is mediated by NF-kappaB. *Toxicol Lett* 185: 110-115.

160. Go YM, Gipp JJ, Mulcahy RT,Jones DP (2004) H2O2-dependent activation of GCLC-ARE4 reporter occurs by mitogen-activated protein kinase pathways without oxidation of cellular glutathione or thioredoxin-1. *J Biol Chem* 279: 5837-5845.

161. Lavrovsky Y, Schwartzman ML, Levere RD, Kappas A,Abraham NG (1994) Identification of binding sites for transcription factors NF-kappa B and AP-2 in the promoter region of the human heme oxygenase 1 gene. *Proc Natl Acad Sci U S A* 91: 5987-5991.

162. Yang H, et al. (2005) Nrf1 and Nrf2 regulate rat glutamate-cysteine ligase catalytic subunit transcription indirectly via NF-kappaB and AP-1. *Mol Cell Biol* 25: 5933-5946.

163. Arinze IJ,Kawai Y (2005) Transcriptional activation of the human Galphai2 gene promoter through nuclear factor-kappaB and antioxidant response elements. *J Biol Chem* 280: 9786-9795.

164. Rangasamy T, et al. (2005) Disruption of Nrf2 enhances susceptibility to severe airway inflammation and asthma in mice. *J Exp Med* 202: 47-59.

165. Fan J, Frey RS, Rahman A,Malik AB (2002) Role of neutrophil NADPH oxidase in the mechanism of tumor necrosis factor-alpha -induced NF-kappa B activation and intercellular adhesion molecule-1 expression in endothelial cells. *J Biol Chem* 277: 3404-3411.

166. Hirota K, et al. (1999) Distinct roles of thioredoxin in the cytoplasm and in the nucleus. A two-step mechanism of redox regulation of transcription factor NF-kappaB. *J Biol Chem* 274: 27891-27897.

167. Seldon MP, et al. (2007) Heme oxygenase-1 inhibits the expression of adhesion molecules associated with endothelial cell activation via inhibition of NF-kappaB RelA phosphorylation at serine 276. *J Immunol* 179: 7840-7851.

168. Lee DF, et al. (2009) KEAP1 E3 ligase-mediated downregulation of NF-kappaB signaling by targeting IKKbeta. *Mol Cell* 36: 131-140.

169. Liu GH, Qu J,Shen X (2008) NF-kappaB/p65 antagonizes Nrf2-ARE pathway by depriving CBP from Nrf2 and facilitating recruitment of HDAC3 to MafK. *Biochim Biophys Acta* 1783: 713-727.

170. Healy ZR, et al. (2005) Divergent responses of chondrocytes and endothelial cells to shear stress: cross-talk among COX-2, the phase 2 response, and apoptosis. *Proc Natl Acad Sci U S A* 102: 14010-14015.

171. Liu H, et al. (2008) Expression and role of DJ-1 in leukemia. *Biochem Biophys Res Commun* 375: 477-483.

172. Hod Y (2004) Differential control of apoptosis by DJ-1 in prostate benign and cancer cells. *J Cell Biochem* 92: 1221-1233.

173. Zhang HY, Wang HQ, Liu HM, Guan Y,Du ZX (2008) Regulation of tumor necrosis factor-related apoptosis-inducing ligand-induced apoptosis by DJ-1 in thyroid cancer cells. *Endocr Relat Cancer* 15: 535-544.

174. Yokota T, et al. (2003) Down regulation of DJ-1 enhances cell death by oxidative stress, ER stress, and proteasome inhibition. *Biochem Biophys Res Commun* 312: 1342-1348.

175. Bargou RC, et al. (1997) Constitutive nuclear factor-kappaB-RelA activation is required for proliferation and survival of Hodgkin's disease tumor cells. *J Clin Invest* 100: 2961-2969.

176. Sovak MA, et al. (1997) Aberrant nuclear factor-kappaB/Rel expression and the pathogenesis of breast cancer. *J Clin Invest* 100: 2952-2960.

177. Blackinton J, et al. (2009) Formation of a stabilized cysteine sulfinic acid is critical for the mitochondrial function of the parkinsonism protein DJ-1. *J Biol Chem* 284: 6476-6485.

178. Anderson PC,Daggett V (2008) Molecular basis for the structural instability of human DJ-1 induced by the L166P mutation associated with Parkinson's disease. *Biochemistry* 47: 9380-9393.

179. Mukhopadhyay T, Roth JA,Maxwell SA (1995) Altered expression of the p50 subunit of the NF-kappa B transcription factor complex in non-small cell lung carcinoma. *Oncogene* 11: 999-1003.

180. Qin XF, An DS, Chen IS,Baltimore D (2003) Inhibiting HIV-1 infection in human T cells by lentiviral-mediated delivery of small interfering RNA against CCR5. *Proc Natl Acad Sci U S A* 100: 183-188.

181. Taxman DJ, et al. (2006) Criteria for effective design, construction, and gene knockdown by shRNA vectors. *BMC Biotechnol* 6: 7.

182. Moi P, Chan K, Asunis I, Cao A,Kan YW (1994) Isolation of NF-E2-related factor 2 (Nrf2), a NF-E2-like basic leucine zipper transcriptional activator that binds to the tandem NF-E2/AP1 repeat of the beta-globin locus control region. *Proc Natl Acad Sci U S A* 91: 9926-9930.

183. auf dem Keller U, et al. (2006) Nrf transcription factors in keratinocytes are essential for skin tumor prevention but not for wound healing. *Mol Cell Biol* 26: 3773-3784.

184. Khor TO, et al. (2008) Increased susceptibility of Nrf2 knockout mice to colitis-associated colorectal cancer. *Cancer Prev Res (Phila Pa)* 1: 187-191.

185. Stacy DR, et al. (2006) Increased expression of nuclear factor E2 p45-related factor 2 (NRF2) in head and neck squamous cell carcinomas. *Head Neck* 28: 813-818.

186. Hong YB, et al. Nuclear factor (erythroid-derived 2)-like 2 regulates drug resistance in pancreatic cancer cells. *Pancreas* 39: 463-472.

187. Kim SK, et al. (2008) Increased expression of Nrf2/ARE-dependent anti-oxidant proteins in tamoxifen-resistant breast cancer cells. *Free Radic Biol Med* 45: 537-546.

188. Mahaffey CM, et al. (2009) Multidrug-resistant protein-3 gene regulation by the transcription factor Nrf2 in human bronchial epithelial and non-small-cell lung carcinoma. *Free Radic Biol Med* 46: 1650-1657.

189. Akhdar H, et al. (2009) Involvement of Nrf2 activation in resistance to 5-fluorouracil in human colon cancer HT-29 cells. *Eur J Cancer* 45: 2219-2227.

190. Wang XJ, et al. (2008) Nrf2 enhances resistance of cancer cells to chemotherapeutic drugs, the dark side of Nrf2. *Carcinogenesis* 29: 1235-1243.

191. Kim HR, et al. (2008) Suppression of Nrf2-driven heme oxygenase-1 enhances the chemosensitivity of lung cancer A549 cells toward cisplatin. *Lung Cancer* 60: 47-56.

192. Maher JM, et al. (2007) Oxidative and electrophilic stress induces multidrug resistance-associated protein transporters via the nuclear factor-E2-related factor-2 transcriptional pathway. *Hepatology* 46: 1597-1610.

193. Kim YR, et al. Oncogenic NRF2 mutations in squamous cell carcinomas of oesophagus and skin. *J Pathol* 220: 446-451.

194. Shibata T, et al. (2008) Cancer related mutations in NRF2 impair its recognition by Keap1-Cul3 E3 ligase and promote malignancy. *Proc Natl Acad Sci U S A* 105: 13568-13573.

195. Nioi P,Nguyen T (2007) A mutation of Keap1 found in breast cancer impairs its ability to repress Nrf2 activity. *Biochem Biophys Res Commun* 362: 816-821.

196. Oeffner F, et al. (2008) Novel interaction partners of Bardet-Biedl syndrome proteins. *Cell Motil Cytoskeleton* 65: 143-155.

197. Beckman JS, Carson M, Smith CD,Koppenol WH (1993) ALS, SOD and peroxynitrite. *Nature* 364: 584.

198. Bonifati V, et al. (2003) DJ-1(PARK7), a novel gene for autosomal recessive, early onset parkinsonism. *Neurol Sci* 24: 159-160.

199. Shinbo Y, Taira T, Niki T, Iguchi-Ariga SM,Ariga H (2005) DJ-1 restores p53 transcription activity inhibited by Topors/p53BP3. *Int J Oncol* 26: 641-648.

200. Cho HY, Reddy SP,Kleeberger SR (2006) Nrf2 defends the lung from oxidative stress. *Antioxid Redox Signal* 8: 76-87.

201. Dhakshinamoorthy S,Jaiswal AK (2001) Functional characterization and role of INrf2 in antioxidant response element-mediated expression and antioxidant induction of NAD(P)H:quinone oxidoreductase1 gene. *Oncogene* 20: 3906-3917.

202. Cullinan SB, Gordan JD, Jin J, Harper JW,Diehl JA (2004) The Keap1-BTB protein is an adaptor that bridges Nrf2 to a Cul3-based E3 ligase: oxidative stress sensing by a Cul3-Keap1 ligase. *Mol Cell Biol* 24: 8477-8486.

203. Zhang DD, Lo SC, Cross JV, Templeton DJ,Hannink M (2004) Keap1 is a redox-regulated substrate adaptor protein for a Cul3-dependent ubiquitin ligase complex. *Mol Cell Biol* 24: 10941-10953.

204. Furukawa M,Xiong Y (2005) BTB protein Keap1 targets antioxidant transcription factor Nrf2 for ubiquitination by the Cullin 3-Roc1 ligase. *Mol Cell Biol* 25: 162-171.

205. Wild AC, Moinova HR,Mulcahy RT (1999) Regulation of gamma-glutamylcysteine synthetase subunit gene expression by the transcription factor Nrf2. *J Biol Chem* 274: 33627-33636.

206. Ramos-Gomez M, et al. (2001) Sensitivity to carcinogenesis is increased and chemoprotective efficacy of enzyme inducers is lost in nrf2 transcription factor-deficient mice. *Proc Natl Acad Sci U S A* 98: 3410-3415.

207. Kwak MK, et al. (2003) Modulation of gene expression by cancer chemopreventive dithiolethiones through the Keap1-Nrf2 pathway. Identification of novel gene clusters for cell survival. *J Biol Chem* 278: 8135-8145.

208. Fahey JW, et al. (2002) Sulforaphane inhibits extracellular, intracellular, and antibiotic-resistant strains of Helicobacter pylori and prevents benzo[a]pyrene-induced stomach tumors. *Proc Natl Acad Sci U S A* 99: 7610-7615.

209. Cao TT, et al. (2005) Increased nuclear factor-erythroid 2 p45-related factor 2 activity protects SH-SY5Y cells against oxidative damage. *J Neurochem* 95: 406-417.

210. Nakaso K, et al. (2006) Novel cytoprotective mechanism of anti-parkinsonian drug deprenyl: PI3K and Nrf2-derived induction of antioxidative proteins. *Biochem Biophys Res Commun* 339: 915-922.

211. Satoh T, et al. (2006) Activation of the Keap1/Nrf2 pathway for neuroprotection by electrophilic [correction of electrophillic] phase II inducers. *Proc Natl Acad Sci U S A* 103: 768-773.

212. Iyanagi T,Yamazaki I (1970) One-electron-transfer reactions in biochemical systems. V. Difference in the mechanism of quinone reduction by the NADH dehydrogenase and the NAD(P)H dehydrogenase (DT-diaphorase). *Biochim Biophys Acta* 216: 282-294.

213. Cresteil T,Jaiswal AK (1991) High levels of expression of the NAD(P)H:quinone oxidoreductase (NQO1) gene in tumor cells compared to normal cells of the same origin. *Biochem Pharmacol* 42: 1021-1027.

214. Kolesar JM, Kuhn JG,Burris HA, 3rd (1995) Detection of a point mutation in NQO1 (DT-diaphorase) in a patient with colon cancer. *J Natl Cancer Inst* 87: 1022-1024.

215. Hara H, Ohta M, Ohta K, Kuno S,Adachi T (2003) Increase of antioxidative potential by tert-butylhydroquinone protects against cell death associated with 6-hydroxydopamine-induced oxidative stress in neuroblastoma SH-SY5Y cells. *Brain Res Mol Brain Res* 119: 125-131.

216. van Muiswinkel FL, et al. (2004) Expression of NAD(P)H:quinone oxidoreductase in the normal and Parkinsonian substantia nigra. *Neurobiol Aging* 25: 1253-1262.

217. Jaiswal AK (2000) Regulation of genes encoding NAD(P)H:quinone oxidoreductases. *Free Radic Biol Med* 29: 254-262.

218. Kast C, Wang M,Whiteway M (2003) The ERK/MAPK pathway regulates the activity of the human tissue factor pathway inhibitor-2 promoter. *J Biol Chem* 278: 6787-6794.

219. Huang HC, Nguyen T,Pickett CB (2000) Regulation of the antioxidant response element by protein kinase C-mediated phosphorylation of NF-E2-related factor 2. *Proc Natl Acad Sci U S A* 97: 12475-12480.

220. Dhakshinamoorthy S,Jaiswal AK (2002) c-Maf negatively regulates ARE-mediated detoxifying enzyme genes expression and anti-oxidant induction. *Oncogene* 21: 5301-5312.

221. Stewart D, Killeen E, Naquin R, Alam S,Alam J (2003) Degradation of transcription factor Nrf2 via the ubiquitin-proteasome pathway and stabilization by cadmium. *J Biol Chem* 278: 2396-2402.

222. Kish SJ, Shannak K,Hornykiewicz O (1988) Uneven pattern of dopamine loss in the striatum of patients with idiopathic Parkinson's disease. Pathophysiologic and clinical implications. *N Engl J Med* 318: 876-880.

223. Begleiter A, Leith MK, Thliveris JA,Digby T (2004) Dietary induction of NQO1 increases the antitumour activity of mitomycin C in human colon tumours in vivo. *Br J Cancer* 91: 1624-1631.

224. Dhakshinamoorthy S,Jaiswal AK (2000) Small maf (MafG and MafK) proteins negatively regulate antioxidant response element-mediated expression and antioxidant induction of the NAD(P)H:Quinone oxidoreductase1 gene. *J Biol Chem* 275: 40134-40141.

225. Engelbrecht Y, et al. (2003) Glucocorticoids induce rapid up-regulation of mitogen-activated protein kinase phosphatase-1 and dephosphorylation of extracellular signal-regulated kinase and impair proliferation in human and mouse osteoblast cell lines. *Endocrinology* 144: 412-422.

226. Piskurich JF, Linhoff MW, Wang Y,Ting JP (1999) Two distinct gamma interferon-inducible promoters of the major histocompatibility complex class II transactivator gene are differentially regulated by STAT1, interferon regulatory factor 1, and transforming growth factor beta. *Mol Cell Biol* 19: 431-440.

227. Greer SF, Zika E, Conti B, Zhu XS,Ting JP (2003) Enhancement of CIITA transcriptional function by ubiquitin. *Nat Immunol* 4: 1074-1082.